The structural connectivity of the human angular gyrus as revealed by microdissection and diffusion tractography

Laurent Petit, Kariem Mahdy Ali, François Rheault, Arnaud Boré, Sandrine Cremona, Francesco Corsini, Alessandro de Benedictis, Maxime Descoteaux, Silvio Sarubbo

The structural connectivity of the human angular gyrus as revealed by microdissection and diffusion tractography

Laurent Petit[1], Kariem Mahdy Ali[2], François Rheault[3],Arnaud Boré[4], Sandrine Cremona[1], Francesco Corsini[5], Alessandro De Benedictis[6], Maxime Descoteaux[4], Silvio Sarubbo[5]

[1] Université Bordeaux, CNRS, CEA, IMN, GIN, UMR 5293, F-33000 Bordeaux, France

[2] Department of Neurosurgery, Medical University of Graz, Austria

[3] Electrical and Computer Engineering, Vanderbilt University, Nashville, USA

[4] Sherbrooke Connectivity Imaging Lab (SCIL), Université de Sherbrooke, Canada

[5] Department of Neurosurgery, Azienda Provinciale per i Servizi Sanitari, "S. Chiara" Hospital, Trento, Italy

[6]Neurosurgery Unit, Department of Neurosciences, Bambino Gesù Children's Hospital, IRCCS, Rome, Italy

Corresponding author:

Laurent PETIT, Groupe d'Imagerie Neurofonctionnelle
Institut des Maladies Neurodégénératives CNRS UMR 5293
Université de Bordeaux
Centre Broca Nouvelle-Aquitaine - 3ème étage
146 rue Léo Saignat - CS 61292 - Case 28
33076 Bordeaux Cedex, France
Email: laurent.petit@u-bordeaux.fr

Authors' emails and ORCID:

Laurent Petit	laurent.petit@u-bordeaux.fr	0000-0003-2499-5367
Kariem Mahdy Ali	kariem.mahdy-ali@medunigraz.at	
François Rheault	francois.rheault@vanderbilt.edu	0000-0002-0097-8004
Arnaud Boré	Arnaud.Bore@usherbrooke.ca	0000-0002-4822-1211
Sandrine Cremona	sandrine.cremona@u-bordeaux.fr	0000-0002-2294-8199
Francesco Corsini	francesco.corsini@apss.tn.it	
Alessandro De Benedictis	alessandro.debenedictis@opbg.net	0000-0002-5414-198X
Maxime Descoteaux	Maxime.Descoteaux@usherbrooke.ca	0000-0002-8191-2129
Silvio Sarubbo	srbslv@unife.it	0000-0003-1113-3717

Abstract (249 words)

The angular gyrus (AG) has been described in numerous studies to be consistently activated in various functional tasks. The angular gyrus is a critical connector epicenter linking multiple functional networks due to its location in the posterior part of the inferior parietal cortex, namely at the junction between the parietal, temporal, and occipital lobes. It is thus crucial to identify the different pathways that anatomically connect this high-order association region to the rest of the brain. Our study revisits the three-dimensional architecture of the structural AG connectivity by combining state-of-the-art postmortem blunt microdissection with advanced in vivo diffusion tractography to comprehensively describe the association, projection, and commissural fibers that connect the human angular gyrus. AG appears as a posterior "angular stone" of associative connections belonging to mid- and long-range dorsal and ventral fibers of the superior and inferior longitudinal systems, respectively, to short-range parietal, occipital, and temporal fibers, including U-shaped fibers in the posterior transverse system. Thus, AG is at a pivotal dorso-ventral position reflecting its critical role in the different functional networks, particularly in language elaboration and spatial attention and awareness in the left and right hemispheres, respectively. We also reveal striatal, thalamic, and brainstem connections and a typical inter-hemispheric homotopic callosal connectivity supporting the suggested AG role in the integration of sensory input for modulating motor control and planning. The present description of AG's highly distributed wiring diagram may drastically improve intraoperative subcortical testing and post-operative neurologic outcomes related to surgery in and around the angular gyrus.

Introduction

With its location in the postero-dorsal portion of the inferior parietal cortex, namely at the junction between the parietal, temporal, and occipital lobes, the angular gyrus (AG) is a critical connector epicenter linking numerous functional networks involved in semantic processing, word reading and comprehension, number processing, default mode network, memory retrieval, attention and spatial cognition, reasoning, and social cognition (Seghier 2013). It is thus crucial to identify the different tracts anatomically connecting this high-order association region to the rest of the brain.

From the most fundamental point of view, the white matter is organized in fiber tracts, aggregating axons in close apposition to each other and sharing cortical and/or subcortical origins and destinations. The complex connections and pathways arising from the brain can be reduced to a series of organizational principles (Schmahmann and Pandya 2006; Nieuwenhuys et al. 2008). Every cortical area is linked with other cortical and subcortical regions by pathways grouped into three distinct categories initially defined by Meynert (Meynert 1885): association, commissural, and projection fibers. The complexity of connections and pathways arising from AG can thus be reduced to a relatively simple schema. The angular gyrus would be therefore linked with other cortical and subcortical areas by pathways grouped into (1) association fibers traveling to other ipsilateral cortical areas from the shortest U-shaped fibers connecting the neighborhood cortical areas to the long-range pathways, (2) commissural fibers passing to the contralateral hemisphere, (3) projection fibers coursing to the basal ganglia, thalamus, and brainstem structures.

Our study describes the angular gyrus's comprehensive clinically actionable structural connectivity by utilizing diffusion magnetic resonance imaging (dMRI)-based tractography and validation with modified Klingler-based anatomical microdissection as ground truth. The dMRI-based tractography includes 411 healthy participants of the BIL&GIN database, balanced for both sex (53% women) and handedness (49% left-handers) (Mazoyer et al. 2016). The BIL&GIN database was designed to answer the question of organizational rules of the hemispheric specialization by increasing the variability while including a population balanced in gender and handedness. Its set of diffusion MRI data allows an in-

depth exploration of the hemispheric asymmetries of the white matter pathways, currently those of angular gyrus connectivity.

Materials and methods

MRI acquisitions and whole-brain tractography

Diffusion-weighted (DWI) and T1-weighted images of 411 healthy participants from the BIL&GIN database were used (mean age of 29.9 ± 7.9 years; 53% women; 49% left-handers stated by self-reported handedness) (Mazoyer et al. 2016). All participants gave written consent before participating in the study, approved by the local ethics committee (CCPRB Basse-Normandie). High-resolution 3D T1 weighted images were obtained using a 3D-FFE-TFE sequence (TR, 20 ms; TE, 4.6 ms; flip angle, 10°; inversion time, 800 ms; turbo field echo factor, 65; Sense factor, 2; field of view, 256 × 256 × 180 mm; isotropic voxel, 1x1x1 mm^3). DWI data were acquired using a single-shot spin-echo echo-planar sequence composed of one b_0 map (b = 0 s/mm^2) followed by 21 diffusion gradient maps (b = 1000 s/mm^2) homogeneously spread over a half-sphere and the 21 opposite directions spread over the opposite half-sphere. A second series with the same features was acquired to increase the signal-to-noise ratio. Seventy axial slices parallel to the AC-PC plane were acquired from the bottom of the cerebellum to the vertex with the following imaging parameters: TR = 8500 ms; TE = 81 ms; angle = 90°; SENSE reduction factor = 2.5; a field of view 224 mm; acquisition matrix 112 × 112, 2 mm isotropic voxels.

A whole-brain tractogram was built for each participant by using the TractoFlow diffusion MRI processing pipeline (Theaud et al. 2020), based on Nextflow (Di Tommaso et al. 2017) and Singularity (Kurtzer et al. 2017) or Docker (link) containers. It consists of 15 tasks, from the basic preprocessing steps on diffusion-weighted and T1-weighted images to build a whole-brain tractogram. This later was built using the fODF image, inclusion and exclusion maps, and the whole WM as a seeding mask. We used the default parameters: ten seeds per voxel in the WM mask, a step size of 0.5 mm, a maximum angle of 20°, and a streamline length between 10 and 250 mm.

Each T1-weighted image was normalized to the MNI space using ANTS (Avants et al. 2009). Therefore, the affine transformation and nonlinear deformation were applied to warp the whole-brain tractogram to the MNI space.

Automatic extraction of whole-brain anatomically-plausible streamlines

We split the WM fibers included in a whole-brain tractogram into anatomically plausible or implausible fibers using ExTractorflow (Petit et al. 2019). ExTractorflow is a rule-based automatic pipeline that filters out false-positive streamlines from tractograms by following brain neuroanatomy organizational principles (Meynert 1885; Dejerine and Dejerine-Klumpke 1895, 1901; Ludwig and Klingler 1956; Crosby et al. 1962; Schmahmann and Pandya 2006; Nieuwenhuys et al. 2008). First, every cortical area is linked with other cortical and subcortical regions by pathways grouped into three distinct categories: association, commissural, and projection fibers. Second, the commissural, projection, and long-range association fibers travel within the central WM part of the core of a gyrus, namely the gyral stem, and therefore never from the side of a gyrus by crossing a sulcus. Third, the shorter U-shaped association fibers connect adjacent gyri by running in a thin band immediately beneath the GM, constituting the most external part of the gyral stem. Following these anatomical principles, regions of interest (ROIs) from the Johns Hopkins University (JHU) template (Oishi et al. 2009) are used to define ROI-based sequential filtering conditions. ExTractor starts, therefore, by considering a streamline as anatomically-implausible either when shorter than 20 mm, making a 360° loop, terminating along the ventricles, or even being broken within the deep WM structures as defined in (Oishi et al. 2009), *e.g.*, the streamlines ending within the corpus callosum, corona radiata, internal capsule, external capsule, parts of association bundles, etc.

Interestingly, the JHU template includes both cortical gray matter and underlying superficial white matter parts for each gyrus. By manipulating these different ROIs, it is possible to create additional ROIs that optimize the filtering of anatomically plausible fibers while applying the principles of WM fiber organization emanating from a given gyrus. Two additional ROIs were thus used for each gyrus and each hemisphere. The first one corresponds to the outermost part of the gyrus, namely its GM shell (AG_{shell}, Figure 1B). The second corresponds to the "entrance/exit door" of the gyrus, namely its WM stem (AG_{stem}), which was manually drawn between the shell boundaries corresponding to the fundus of the sulci delimiting the gyrus. An essential step in ExTractorflow is to consider as plausible fibers only those ending in a gyrus while having passed through the stem and not crossing the shell. Anatomically

unplausible streamlines were then filtered out when shorter than 20 mm, or making a loop with an angle of more than 360° or was broken with at least one termination within the deep WM structures as well as those terminating along the ventricles. A second stage of anatomical Boolean rules uses the JHU template ROIs to keep anatomically plausible streamlines strictly. For example, the streamlines connecting the frontal cortex to the parietal cortex via the external capsule cannot cross the adjacent putamen or insula. Still, they must pass strictly through the external capsule. Another example, the streamlines connecting AG with the thalamus have to pass through the posterior part of the corona radiata (corresponding to the posterior thalamic radiation (PTR) in the JHU template) and not through the superior part of the corona radiata (SCR).

The remaining commissural, projection, and association (including U-shaped) streamlines thus compose a final anatomically-plausible whole-brain tractogram (Figure 1A).

Virtual dissection of WM connections of the angular gyrus

The virtual dissection of the structural AG connectivity was performed on the 411 anatomically-plausible whole-brain tractograms using the regions of interest (ROIs) from the JHU template. We first considered only streamlines with one cortical termination in the left and right angular gyri, passing through the AG_{stem} and not crossing the AG_{shell} (Figure 1B). Association angular fibers comprised the streamlines with the other termination in any other ipsilateral gyrus, passing through its stem and not crossing its shell. Projection angular fibers were composed of the streamlines with the other termination either in the putamen, caudate nucleus, thalamus, or the brain stem. Homotopic commissural angular fibers were composed of the streamlines ending in left and right AG.

AG tractography data analysis

Averaged MNI coordinates of the center of gravity of the fibers termination of each AG pair were computed in each subject, therefore reported (mean ± standard deviation) over the total number of participants in Table 1. Similarly, averaged length, area, volume, and shape descriptors of each AG pair were also computed in each participant using the shape analysis method (Yeh 2020) and are reported in

Supplementary Table 1. This describes the between-subject variations of macroscopic structural features of the multiple types of angular fiber pathways. Note that a given tract is considered present in a subject if at least 5 streamlines compose it. Thus, a tract observed in a smaller number of participants can be regarded as "hard-to-tract" because of anatomical constraints that are pitfalls for the tractography algorithms, *e.g.*, high rate of fiber crossings and bottlenecks (Rheault et al. 2020; Schilling et al. 2022).

Postmortem dissection of AG

We included pictures of micro-dissections of 8 hemispheres (5 left and 3 right) included in the Brain Anatomy Data Bank (BADaBank) of the Structural and Functional Connectivity Lab Project, performed at the Department of Neurosurgery of the "S. Chiara" Hospital (Azienda Provinciale per i Servizi Sanitari, Trento, Italy). According to the protocols approved by the Ethical Committee of the APSS (N° 06/2018), after extraction of the brain hemispheres, the specimens were arranged with injection in carotids and vertebral arteries with immersion in formalin 10% for 40 days. The formalin immersion was followed by gently removing vessels and arachnoids and a first freezing process at -80 °C for at least 20 days (maximum 30 days). After a cautious decortication according to the cortex sparing technique (Martino et al. 2010), the specimens were submitted to re-immersions in formalin 10% and frost-defrost cycles following the different layer-by-layer dissection techniques. This modified Klingler's preparation was developed to improve the penetration of the formalin in the deep layers and improve the visualization and separation of the deeper fibers (Sarubbo et al. 2016; Maffei et al. 2019). Finally, the results of the micro-dissections were confirmed by the 3D exploration of photogrammetric step-by-step multilayer dissection in eleven 3D-hemispheres models (5 left and 6 right), according to the previous technique described by our group (De Benedictis et al. 2018; Mahdy Ali and Avesani 2021).

The identification of the tracts during micro-dissection and the confirmation in the three-dimensional photogrammetric models were performed by two neurosurgeons with several years of experience in anatomical micro-dissection. The best available models for the respective tracts were then chosen, and images showing the respective tracts were edited at the highest possible resolution. The respective tracts were highlighted at maximum magnification for graphical purposes using a

commercially available photo editing software (Adobe Photoshop, Adobe Inc., Delaware, USA). Due to the destructive nature of microdissection, a certain number of fibers are inevitably lost, especially at the cortical origin and termination sites. Thus, the highlighted tracts resemble the vast majority of the fibers of the respective tract but not the complete tract itself.

Statistical analysis of the hemispheric asymmetry of each AG tract

Statistical analyses were performed with R 4.0.0 (https://www.r-project.org/). We tested the hemispheric asymmetry of each of the association and projection tracts. Raw values were normalized for each participant per 1000 mm^3 of the left and right angular gyrus volume, respectively, to account for the original volume difference between the left and right AG ROI in the JHU template (GM + superficial WM; left = 2639 mm^3; right = 3218 mm^3). We ran a mixed-effect linear regression model for each AG tract with random effects fitted at the participant level, the cerebral hemisphere (left vs. right) as the fixed effect predictor, and the tract's volume as the dependent variable. The statistical significance of hemisphere difference was assessed through an ANOVA component with a Bonferroni corrected alpha threshold of 0.0011 (for 44 tests). All models were adjusted on Manual Preference (Left vs. Right), Gender (Men vs. Women), age, education, and cerebral volume as fixed effect covariates. Note that to correct for non-linearity and heteroscedasticity of residuals, we reproduced the same analyses following a boxcox transformation of the dependent variables (Box and Cox 1964). The significant differences between hemispheres were identical.

Results

The AG is structurally connected to distinct cortical and subcortical areas in the human brain. We have identified 22 different bilateral AG tracts to which we must add homotopic callosal fibers connecting both left and right angular gyri (Figures 2). The AG is connected with the frontal lobe through dorsal and ventral long-range association fibers, the parietal, occipital, and temporal lobes through an abundance of short-range (including U-shaped) association fibers, and with the thalamus, putamen, midbrain, and pons through projection fibers. Figure 3 highlights the connectivity pattern of the fibers association tracts terminating in AG. The shape of the colored lines represents the general path morphology of these long- and short-range association tracts. It corresponds to the centroid of the concatenated WM fibers extracted over the 411 participants for each AG tract. The thickness of the colored lines corresponds to the averaged diameter of each AG tract estimated with the shape analysis (Suppl. Table 1). Figures 4 to 10 (except figure 9) show both tractography- and dissection-based representation of the different AG tracts except for the homotopic callosal, midbrain, and pons fibers that require a particular dissection approach envisaged in further studies. Figure 9 highlights the tripartite organization of the termination of the short-range fibers in AG.

Long-range association angular fibers (Figures 3, 4, and 5)

Regarding the long-range association pathways, the angular gyrus is predominantly connected to the frontal cortex via the dorsal pathway of the superior longitudinal system (SLS, (Mandonnet et al. 2018). Fronto-dorsal AG connections were identified with the inferior frontal (IFG), middle frontal (MFG), and precentral (PrCG) gyri in the 411 subjects for both hemispheres (Figures 3 and 4). They correspond to the most extensive AG tracts in volume, whole areas, and diameter (Suppl. Table 1). The three fronto-dorsal AG tracts lie between the superior convexity of the frontal cortex, run above the superior limiting sulcus of the insula, and terminate in the superior part of AG (Figure 3). They follow a medio-lateral distribution, from the most medial route for the AG-MFG tract to the most lateral one for the AG-IFG tract. AG-MFG corresponds to the SLF-II sub-component of SLS, while AG-PrCG and AG-IFG belong to the SLF-III sub-component, as previously described (Wang et al. 2016). We recently

reviewed the hodology of the SLS of the human brain (Vavassori et al. 2021) and found the involvement of the angular gyrus as part of the definition of the SLS (*i.e.*, SLF/AF complex) since Dejerine (Dejerine and Dejerine-Klumpke 1895). Whatever the nomenclature of SLF sub-components used for more than a century, the angular gyrus has been consistently described as connecting MFG, PrCG, and IFG via the dorsal pathway (Cf. figures 5,7 and 8 in (Vavassori et al. 2021)).

The angular gyrus is also connected, but to a lesser extent, to the frontal cortex via the ventral pathway of the inferior longitudinal system (ILS, (Mandonnet et al. 2018). Fronto-ventral AG connections were identified with the anterior part of the superior frontal gyrus (SFG), and the ventral parts of MFG and IFG, up to the fronto-orbital gyri (FrOrbG) (Figures 3 and 5). They run under the anterior limiting sulcus of the insula in the external capsule, and continue under the inferior limiting sulcus of the insula before turning within the anterior part of the *stratum sagittale* (SS) and terminate in the inferior part of AG. It corresponds to the inferior fronto occipital fascicle (IFOF), namely the deepest layer of the ILS, as previously described in tractography and dissection (Wu et al. 2016a; Wang et al. 2013; Palejwala et al. 2020; Di Carlo et al. 2019) (see also a recent review (De Benedictis et al. 2021). Figure 3 also shows that the main route of the fronto-ventral AG tracts runs deeper than the main route of the short-range temporo-AG tracts that belong to the middle longitudinal fascicle (MdLF), whose lateromedial orientation is known to pass superficially to the IFOF at the level of the anterior *stratum sagittale* (Makris et al. 2017; Latini et al. 2020; Di Carlo et al. 2019; Wu et al. 2016b; Bullock et al. 2019).

A last long-range association AG tract was consistently observed with the insula. It also includes some projection fibers terminating in the claustrum (Figures 3 and 10) that remain to be undoubtedly demonstrated with a dedicated combined tractography/microdissection study. This AG-Ins tract leaves the angular gyrus by the dorsal pathway and then goes towards the insula at the level of the postcentral gyrus.

Short-range association angular fibers (Figures 3 and 6 to 9)

We identified a dense network of short-range association AG tracts with the neighboring parietal, occipital and temporal gyri. The closest to the angular gyrus constitute the so-called U-shaped fibers, namely the supramarginal (SMG), superior parietal (SPG), superior and middle occipital (SOG, MOG), and superior and middle temporal (STG, MTG) gyri (Guevara et al. 2020). Except for SOG, these U-shaped AG fibers were observed in almost all 411 subjects (Suppl. Table 1). Interestingly, these short-range fibers project into the angular gyrus in a tripartite lobar organization (Figure 9). The short-range parietal terminations are grouped in the superior part of AG along the intraparietal sulcus. The occipital short-range AG tracts project to the posterior part of AG along the anterior occipital sulcus. The short-range temporal terminations are located in the inferior part of AG around the vertical ramus of the superior temporal sulcus. Figure 3 and the 3D-scatter plots in Figure 9 show that, beyond this tripartite organization, the short-range fiber terminations in AG obey a symmetrical topology depending on the neighboring gyrus in each lobe. The endings of SMG-AG, PoCG-AG, SPG-AG, and PrCu-AG follow an anterior-to-superior distribution in AG similar to the location of the adjacent parietal gyri around AG (Figures 3 and 6). Following the intergyral parietal nomenclature proposed by Catani et al. (2017), the current AG-SMG corresponds to a parietal angular-to-supramarginal (PAS) tract, AG-PoCG to a parietal inferior-to-postcentral (PIP) tract, and AG-SPG and AG-PrCu to parietal inferior-to-superior (PIS) tracts (Catani et al. 2017). Contrary to this previous study, which could not visualize connections between AG and the precuneus, we consistently observed it bilaterally in each of the 411 participants and in microdissection, confirming what was earlier described in non-human primates (Rozzi et al. 2006). The termination of AG-SOG, AG-MOG, and AG-IOG are distributed in the posterior part of AG with respect to the respective occipital gyri (Figures 3 and 7), and the termination AG-STG, AG-MTG, and AG-ITG with the respective temporal gyri (Figures 3 and 8). These short-range parieto-occipital tracts belong to the inferior parietal portion of the vertical occipital fascicle (VOF) (Bullock et al. 2019; Mahdy Ali and Avesani 2021). We observe that these AG fibers of the VOF terminate in the posterior part of AG as initially described (Yeatman et al. 2014).

Projection angular fibers (Figures 2 and 10)

We identified two types of bilateral projection fibers connecting the angular gyrus (Figure 2). Cortico-thalamic and cortico-striatal tracts were consistently extracted, running from the angular gyrus through the retro-lenticular portion of the internal capsule to the thalamus and the putamen, respectively. Interestingly, the thalamic fibers enter the thalamus at the level of the pulvinar, while the cortico-striatal fibers terminate in the tail of the putamen (Figure 10). The second type of angular projection fibers deals with the brainstem and corresponds to cortico-tectal and cortico-pontine fibers (Figure 2). Both run medio-posteriorly to the cortico-thalamic and cortico-striatal angular tracts.

Commissural angular fibers (Figure 2)

In addition to the association and projection angular tracts described above, the left and right AG are interconnected via a dense callosal fiber bundle. These homotopic callosal fibers project through the splenium of the corpus callosum to connect the angular gyri bilaterally (Figure 2).

Asymmetrical connectivity of AG (Figure 11)

The statistical analysis of individual hemispheric volumes of each of the 22 tracts (with left and right representation) revealed significant rightward or leftward asymmetries depending on the tract (Bonferroni corrected alpha threshold of 0.0011) without any effect of Manual Preference or Gender after correction for age, education and the cerebral volume (Figure 11). A strong rightward asymmetry was first observed for the three fronto-dorsal AG tracts. In contrast, the short-range AG connectivity showed alternatively rightward (PoCG, SMG, IOG) or leftward (PrCu, SPG, MOG, ITG) asymmetries. AG-putamen and cortico-tectal AG connectivity were leftward asymmetrical, while the cortico-pontine AG asymmetry was rightward. No asymmetries were observed for the tracts that were present in less than 50% of the 411 participants.

Discussion

AG, as the postero-dorsal portion of the inferior parietal cortex, together with the supramarginal gyrus (SMG), constitute the so-called Geschwind's territories. These cortical territories, and in particular the AG, were demonstrated to be critical for different brain functions in both hemispheres, such as, among others, language (*i.e.*, semantic control and phonological/articulatory encoding), spatial attention and awareness, working memory, calculation, and social cognition (Sarubbo et al. 2015; Zaca et al. 2018; Sarubbo et al. 2016; Thiebaut de Schotten et al. 2005; Seghier 2013). Our macrostructural analysis, integrating multimodal anatomical data provided by high-resolution tractography and microdissection, reveals a highly distributed wiring diagram of WM fibers with AG as a cortical hub. It supports AG's multimodal and pivotal functional roles as an integration area, an epicenter in the sense of (Mesulam 2008), between different sensory inputs (visual, auditory, and somato-sensorial) cortices and the temporal and frontal associative and effector areas.

Considering its sulco-gyral anatomy, AG is split into two parts by the elongation of the superior temporal sulcus within the parietal lobe (Kiriyama et al. 2009). The anterior part of AG faces the temporal border of the posterior third of the superior temporal sulcus (STS), and the posterior one faces the occipital side. Even with possible anatomical variations, we demonstrate that this sulco-gyral structure reflects the first level of short-range connection throughout continuous and homogeneous layers of U-fibers, allowing a tripodal inter-lobar connection of AG (Sarubbo et al. 2016) with the superior temporal gyrus (STG), the superior and middle occipital gyri (SOG/MOG), and in the parietal lobe, the supramarginal (SMG) and superior parietal (SPG) gyri (Figure 9). Note that we restricted the current analysis of the AG connectivity with its neighboring gyri at the short-range streamlines with a U-shaped arrangement. It explains why the present AG-STG connectivity does not travel anteriorly toward the temporal pole. Further investigations are requested to study lengthier AG-STG fibers belonging to the MdLF as previously described (Makris et al. 2013; Makris et al. 2017; Bullock et al. 2019).

These local (short-range) cortical connections (involving both Wernicke and Geschwind territories and the convexity of the occipital cortex) play a role in the integration of visual stimuli in the verbal

semantic processing and could play a role in the local plasticity phenomena supporting language recovery after restricted damage at the temporo-parieto-occipital junction in the left hemisphere (Sarubbo et al. 2012; Jiao et al. 2020).

Beyond this short-range associative connection, we identified mid- and long-range associative connections, belonging mainly to the SLS but also the ILS (Mandonnet et al. 2018). On the dorsal side, the angular gyrus is predominantly connected with the postcentral gyrus, the precentral gyrus (i.e., the ventral premotor cortex, VPMC), and the posterior portion of the IFG, as part of the classical description of the superior longitudinal fascicles, namely SLF-II and SLF-III. We also observed that these fronto-dorsal tracts are rightward asymmetrical as the SLF-II and SLF-III (Thiebaut de Schotten et al. 2011).

The strong and dense connectivity throughout the whole precentral gyrus encompassing both primary (M1) and premotor (PM) cortices suggests that the angular gyrus plays a role in voluntary movement. For a long time restricted only to the superior parietal lobule (for a review, (Gallivan and Culham 2015), such a role has recently been extended to the angular gyrus with evidence of direct connectivity between AG and M1/PM. Ipsilateral AG-M1/PM connections have been observed non-invasively by dual-coil TMS in awake patients (Cattaneo and Barchiesi 2011; Koch et al. 2010). Interestingly, Koch et al. (2010) used tensor-based tractography in combination with their TMS approach and described that AG was strongly connected with M1 and PM. More recently, direct parietal-motor functional connections in humans, including AG-M1, have been demonstrated with intraoperative direct dual cortical stimulation (Cattaneo et al. 2020). Our results in tractography and microdissection confirm that AG is strongly connected with M1/PM within the precentral gyrus. Figure 4 and the corresponding probabilistic map of the AG-PrCG connectivity (Cf. Supplementary figure) show a large fanning along the convexity of the precentral gyrus, which suggests a mototopic representation of the connections between AG and PrCG. Our microdissection data preferentially observed AG fibers projecting to the ventral third of the precentral gyrus. Our microdissection data preferentially described a connection of the angular gyrus with the ventral third of the precentral gyrus. Further microdissections are requested to validate whether this connectivity extends to the whole precentral gyrus.

As opposed to the apparent spread of AG-PrCG connectivity, the projection between AG and PoCG appears to be limited to the mid-PoCG in tractography and microdissection. It may correspond to the somatosensory region of the proximal arm/trunk. Sparse direct connections between AG and the primary somatosensory areas have been previously described (Koch et al. 2010; Richard et al. 2021) without a clear somatotopic organization. Complementary functional connectivity studies are needed to understand this connectivity and its role better.

The angular gyrus is also strongly connected with the posterior portion of the MFG, close to the classical description of the frontal eye fields (FEF, for a review (Petit and Pouget 2019)). These connections were also previously demonstrated with the cortico-cortical evoked potentials technique (Matsumoto et al. 2012), highlighting a symmetrical dorso-ventral organization between frontal and parietal cortical territories. In particular, the AG-MFG fibers are part of the classical description of the SLF-II (mid-dorsal component of the SLS, (Vavassori et al. 2021). They constitute the structural background for the known involvement of the dorsal portion of AG facing the intra-parietal sulcus in the fronto-parietal network, which is crucial for spatial attention and awareness (Thiebaut de Schotten et al. 2005; Sarubbo et al. 2020). The present rightward asymmetry of the AG-MFG connectivity is also consistent with the previously described more extensive rightward parieto-frontal network involved in visuospatial attention (Thiebaut de Schotten et al. 2011). This pattern of dorsal connectivity of the AG supports its role in integrating sensory input for motor planning and output.

On the ventral side, both tractography and microdissection confirm the existence of a mid- and long-range AG connectivity with the mid-dorsal cortices of the frontal lobe throughout the IFOF (the deepest component of the ILS) (Sarubbo et al. 2013; Caverzasi et al. 2014; Hau et al. 2016; Wu et al. 2016a), and the temporal lobe throughout the superficial and deep components of the posterior transverse system, namely the vertical portion of the SLF and middle longitudinal fascicle (MdLF), respectively (Mahdy Ali and Avesani 2021).

The cross-connection pattern between dorsal and ventral language streams supports the multimodal function role of the AG cortex as revealed by fMRI studies showing functional nodes for semantic and phonological/syntactic elaboration (Vigneau et al. 2006). Different direct electrical stimulation (DES)

evidences also demonstrated a high probability of evoking anomia during object naming while deactivating these cortical territories (Sarubbo et al. 2015; Sarubbo et al. 2020), supporting a role of AG in the integration between the semantic elaboration of sensory input and speech encoding. In the left hemisphere, this fronto-parietal network (including AG) plays a crucial role in semantic control (Xu et al. 2017).

Our results about AG connections with striatal, thalamic, and brainstem structures support different and growing pieces of evidence coming from neurophysiological and neuroimaging studies. A cortico-striatal circuitry, including the cortical territories of the fronto-parietal network (AG-MFG), described above and dedicated to spatial attention, awareness, and the integration of sensory input for motor control (including gait, ocular movements, etc.), was hypothesized since the 1990s on the background of neurophysiological evidence. This cortical-subcortical circuitry includes different deep nuclei and brainstem regions, segregated in direct and indirect pathways (between others, the pulvinar thalami, intralaminar nuclei, mesopontine tegmentum, basal forebrain, globus pallidus, subthalamic nucleus, substantia nigra, and caudate nucleus) (LaBerge 1995; Kinomura et al. 1996). More recently, a functional imbalance (hypo- vs. hyper-activation) between the functional connectivity of certain cortical territories of the fronto-parietal network involved in oculomotor control (notably, the frontal and parietal eyes fields) and the striatal structures (putamen and caudate) was demonstrated as a pathological substrate in Parkinson Disease (Rebelo et al. 2021).

Finally, the bilateral homotopic connectivity between left and right AG reflects the most common pattern of inter-hemispheric connection provided by the corpus callosum (De Benedictis et al. 2016). This pattern of inter-hemispheric connection constitutes the essential structural background for balancing functional activity (*i.e.*, inhibitory/excitatory) between left and right homologous cortices. It was demonstrated that direct current stimulation of the posterior cortices of the IPL, *i.e.* AG, induced modulation of interhemispheric parietal balance, improving visuospatial attention deficits in neglect patients (Sparing et al. 2009).

Nowadays, it is accepted that the macaque brain does not present *stricto sensu*, an angular gyrus. Still, the parietal areas Opt and PG are considered the homologs of the human AG. We refer the reader

to the review of Niu and Palomero-Gallagher in this special issue for a detailed description of the connectivity of the Opt and PG regions, revealing remarkable comparability of connectivity features between AG in humans and Opt/PG in macaques (Niu and Palomero-Gallagher 2022).

Strengths and limitations

From the tractography point of view, one may first consider that the number of directions and b values in the present diffusion MRI data would be far from optimal for the original ODF estimation. We previously demonstrated in (Chenot et al. 2019) that, albeit acquired more than ten years ago, BIL&GIN diffusion MRI data were acquired with an excellent signal-to-noise ratio allowing us to apply cutting-edge tractography algorithm on such 'old' data. Nevertheless, this does not prevent these data from suffering from the same problem as any other diffusion MRI data, namely the reconstruction of many false-positive fibers (Maier-Hein et al. 2017). Nevertheless, this does not prevent these data from suffering from the same problem as any other type of diffusion MRI data, namely the reconstruction of many false-positive fibers. We then used ExTractorflow to keep only the anatomically plausible fibers before extracting, more specifically, the whole connectivity of the angular gyrus. To ensure this anatomical plausibility, ExTractorflow applies quite strict rules that may lead to consider some fibers as implausible. It explains why we did not observe heterotopic callosal connectivity of the angular gyrus. This heterotopic commissural connectivity is not well known in humans beyond the frontal cortex (De Benedictis et al. 2016) and is not included in the plausible fiber dataset proposed by ExTractorflow. On the other hand, we could not describe the connections between the angular gyrus and the caudate nucleus because the latter is not entirely represented in the JHU template. In particular, the tail of the caudate nucleus is absent from the 176 ROIs of this atlas, whereas it is known that the AG connects the tail of the caudate nucleus (Yeterian and Pandya 1993).

Anatomical microdissection offers the possibility to study the subcortical wiring of the brain itself by directly visualizing the tracts. It has been shown that the Klingler dissection technique using formalin fixation and freezing of the specimen preserves the structure of myelinated axons while extra-axonal structures were mostly destroyed (Zemmoura et al. 2016). It is therefore well suited to study the course

of the fiber tracts and their spatial relation to each other. However, this technique requires the availability of specimens and time for specimen preparation and dissection. It also requires experience when performing the dissection. Due to its destructive nature, anatomical microdissection is an irreversible process. Thus, not all fiber tracts can be visualized at the same time. Also, the presence and size of certain fiber tracts are subject to individual variability.

Conclusion

To conclude, our combined tractography and microdissection study of the AG wiring diagram reveals its highly distributed connected structure with a central representation between the human brain's main associative layers of WM. The angular gyrus is thus a posterior "angular stone" of associative connections belonging to the mid- and long-range dorsal fibers of the SLS and ventral fibers of the ILS, and short-range fibers, namely U-shaped fibers, and the posterior transverse system, locally connecting all the cortical territories of the temporo-parieto-occipital junction. This dorso-ventral pivotal position reflects the critical role of AG in different networks, particularly in language elaboration and spatial attention and awareness in the left and right hemispheres, respectively. Moreover, we reveal deep nuclei and brainstem connections and a typical inter-hemispheric homotopic connectivity supporting the suggested role, in the context of the fronto-parietal network, in the integration of sensory input for modulating motor control and planning. These structural pieces of evidence all together match the critical and multimodal functional roles attributed to these cortical territories in both hemispheres on the background of brain mapping data from clinical, neuroimaging, and neurophysiological studies.

Figure Captions

Figure 1. A. Diagram summarizing the main steps of ExTractorflow to filter out false-positive streamlines from a whole-brain tractogram by following brain neuroanatomy organizational principles. In this example, an original tractogram of a single subject initially composed of more than 3.5 million streamlines provides a final whole-brain tractogram of around 590 000 anatomically plausible streamlines once a series of filters (anatomical rules schematically represented with yellow lines) are applied. B. Example of the application of stem/shell fibers extraction. To be considered to belong to a given tract that may connect the angular gyrus (AG) and the middle frontal gyrus (MFG), the anatomically plausible streamlines have to end in AG and MFG and pass through the AG and MFG stems and not through the AG and MFG shells. L: left; R: right; A: anterior; P: posterior

Figure 2. Overview of the different bilateral AG tracts identified in tractography in 411 healthy participants. At the top, short-, mid-, and long-range association tracts connecting AG in the left hemisphere. At the bottom the homotopic callosal AG fibers and the striatal, thalamic, and brainstem tracts. For illustrative purposes, each represented tract is the concatenation of all the streamlines identified over 411 subjects limited to a maximum of 10 000 streamlines when the total exceeds this value. A: anterior; P: posterior

Figure 3. Schematic overview of the AG connectivity for the short-, mid-, and long-range association fibers (see text for details). In light blue, the fronto-dorsal pathway with the dorsal middle frontal (dMFG), precentral (dPrCG), and inferior (dIFG) gyri. In yellow, the fronto-ventral pathway with the ventral superior frontal (vSFG), middle frontal (vMFG), inferior frontal (vIFG), and fronto-orbital (vFrOrbG) gyri. In orange, the AG connectivity with the insula (Ins). In red, the intra-lobar AG connectivity with the supramarginal (SMG), postcentral (PoCG), and superior parietal (SPG) gyri and the precuneus (PrCu). In dark blue, the short inter-lobar AG connectivity with the superior occipital (SOG), middle occipital (MOG), and inferior occipital (IOG) gyri. In green, the short inter-lobar AG connectivity with the superior temporal (STG), middle temporal (MTG), and inferior temporal (ITG)

gyri. Each line corresponds to the centroid of the concatenated WM fibers extracted over the 411 participants for each AG tract. Its diameter represents the averaged diameter of each AG tract estimated with the shape analysis (Suppl. Table 1).

Figure 4. Tractography (top) and dissection (bottom) of the fronto-dorsal AG tracts. For the illustrative purpose of the tractography results, each represented tract is the concatenation of all the streamlines identified over 411 subjects limited to a maximum of 5000 streamlines when the total exceeds this value. A: anterior; P: posterior; S: Superior; I: Inferior; see figure 3 caption for acronyms' labeling.

Figure 5. Tractography (top) and dissection (bottom) of the fronto-ventral AG tracts. See Figure 3 caption and text for details and acronyms' labeling.

Figure 6. Tractography (top) and dissection (bottom) of the short-range parietal AG tracts. See Figure 3 caption and text for details and acronyms' labeling.

Figure 7. Tractography (top) and dissection (bottom) of the short-range occipital AG tracts. See Figure 4 caption and text for details and acronyms' labeling.

Figure 8. Tractography (top) and dissection (bottom) of the short-range temporal AG tracts. See Figure 3 caption and text for details and acronyms' labeling.

Figure 9. The tripartite lobar organization of AG's mid- and short-range fibers with its neighboring gyri. The short-range parietal terminations (in red) are grouped in the superior part of AG along the intraparietal sulcus. The occipital short-range AG tracts (in dark blue) project to the posterior part of AG along the anterior occipital sulcus. The short-range temporal terminations (in green) are located in the inferior part of AG around the vertical ramus of the superior temporal sulcus. At the bottom, 3D-

scatter plots show that, beyond this tripartite organization, the fiber terminations in AG obey a symmetrical topology depending on the neighboring gyrus in each lobe.

Figure 10. Tractography (top) and dissection (bottom) of the association (Insula/Claustrum, left part), and projection AG-Putamen (middle part) and AG-Thalamus (right part) tracts. See Figure 4 caption and text for details and acronyms' labeling.

Figure 11. Summary of the statistical analysis of the hemispheric asymmetry of each AG tract. Emmeans volume values are expressed in mm^3 with a 95% confidence interval. For each participant, left and right raw values were normalized per 1000 mm^3 of the left and right angular gyrus volume, respectively. L: left; R: right; ***: Bonferroni corrected alpha threshold of 0.0011; Put: putamen; Thal: thalamus; MB: cortico-tectal connectivity; Pons: cortico-pontine connectivity; other labels see Figure 3 caption for acronyms' labeling.

Supplementary figure. Axial, sagittal and coronal sections of the 23 probabilistic maps of the present AG connectivity in MNI space. For a given tract, the color bar indicates the frequency of voxels containing the tract from 50 to 100% of the participants where the tract was frequently observed (close to the total of 411 participants, *actc* color scale) or from 10 to 100% of the participants where the tract was less frequently observed (*plasma* color scale). For example, for a tract observed in all participants, a value of 80 in a voxel means that 329 out of 411 individual tracts are passing through this voxel. L left, R right. Displays made with MRIcroGL (http://www.nitrc.org/projects/mricrogl/).

Statements & Declarations

Funding: No particular funding was received for conducting this study.

Conflicts of interest/Competing interests: No conflict of interest for any authors.

Ethics approval :

- The present manuscript is not submitted elsewhere for simultaneous consideration;
- The submitted work is original and has not been published elsewhere in any form or language (partially or in whole);
- No re-use of material to avoid the concerns about text-recycling (self-plagiarism) in the present manuscript;
- The part of the study, including in-vivo diffusion MRI data, was approved by the local ethics committee (CCPRB Basse-Normandie, France).
- The part of the study, including postmortem dissection data, was approved by the Ethical Committee of the Azienda Provinciale per i Servizi Sanitari, Trento, Italy (N° 06/2018).

Consent to participate and for publication: For the part of the study involving *in vivo* diffusion MRI data, all participants gave written consent prior to participation in the study and no opposition to the publication of any type of results generated with their data.

Availability of data and material: The *in vivo* diffusion MRI dataset analyzed in the current study belongs to the BIL&GIN database. The BIL&GIN is not freely available, but a data-sharing model based on collaborative research agreements has been implemented. Request for joint research projects can be made through the BIL&GIN website or by email to the corresponding author of the present paper.

Code availability (software application or custom code): no specific code developed, not applicable.

References

Avants BB, Tustison NJ, Song G (2009) Advanced normalization tools (ANTS). Insight Journal 2:1-35

Box GEP, Cox DR (1964) An Analysis of Transformations. Journal of the Royal Statistical Society Series B (Methodological) 26 (2):211-252

Bullock D, Takemura H, Caiafa CF, Kitchell L, McPherson B, Caron B, Pestilli F (2019) Associative white matter connecting the dorsal and ventral posterior human cortex. Brain Structure and Function 224 (8):2631-2660. doi:10.1007/s00429-019-01907-8

Catani M, Robertsson N, Beyh A, Huynh V, de Santiago Requejo F, Howells H, Barrett RLC, Aiello M, Cavaliere C, Dyrby TB, Krug K, Ptito M, D'Arceuil H, Forkel SJ, Dell'Acqua F (2017) Short parietal lobe connections of the human and monkey brain. Cortex 97:339-357. doi:10.1016/j.cortex.2017.10.022

Cattaneo L, Barchiesi G (2011) Transcranial Magnetic Mapping of the Short-Latency Modulations of Corticospinal Activity from the Ipsilateral Hemisphere during Rest. Front Neural Circuits 5:14. doi:10.3389/fncir.2011.00014

Cattaneo L, Giampiccolo D, Meneghelli P, Tramontano V, Sala F (2020) Cortico-cortical connectivity between the superior and inferior parietal lobules and the motor cortex assessed by intraoperative dual cortical stimulation. Brain Stimulation 13 (3):819-831. doi:https://doi.org/10.1016/j.brs.2020.02.023

Caverzasi E, Papinutto N, Amirbekian B, Berger MS, Henry RG (2014) Q-Ball of Inferior Fronto-Occipital Fasciculus and Beyond. PLoS ONE 9 (6):e100274. doi:10.1371/journal.pone.0100274

Chenot Q, Tzourio-Mazoyer N, Rheault F, Descoteaux M, Crivello F, Zago L, Mellet E, Jobard G, Joliot M, Mazoyer B, Petit L (2019) A population-based atlas of the human pyramidal tract in 410 healthy participants. Brain Struct Funct 224 (2):599-612. doi:http://dx.doi.org/10.1007/s00429-018-1798-7

Crosby E, Humphrey T, Lauer EW (1962) Correlative anatomy of the nervous system. The MacMillan Company, New York

De Benedictis A, Marras CE, Petit L, Sarubbo S (2021) The inferior fronto-occipital fascicle: a century of controversies from anatomy theaters to operative neurosurgery. J Neurosurg Sci 65 (6):605-615. doi:10.23736/S0390-5616.21.05360-1

De Benedictis A, Nocerino E, Menna F, Remondino F, Barbareschi M, Rozzanigo U, Corsini F, Olivetti E, Marras CE, Chioffi F, Avesani P, Sarubbo S (2018) Photogrammetry of the Human Brain: A Novel Method for Three-Dimensional Quantitative Exploration of the Structural Connectivity in Neurosurgery and Neurosciences. World Neurosurg 115:e279-e291. doi:10.1016/j.wneu.2018.04.036

De Benedictis A, Petit L, Descoteaux M, Marras CE, Barbareschi M, Corsini F, Dallabona M, Chioffi F, Sarubbo S (2016) New insights in the homotopic and heterotopic connectivity of the frontal portion of the human corpus callosum revealed by microdissection and diffusion tractography. Hum Brain Mapp 37 (12):4718-4735. doi:http://dx.doi.org/10.1002/hbm.23339

Dejerine J, Dejerine-Klumpke A (1895) Anatomie des centres nerveux. Tome 1. Rueff et Cie, Paris

Dejerine J, Dejerine-Klumpke A (1901) Anatomie des centres nerveux. Tome 2. Rueff et Cie, Paris

Di Carlo DT, Benedetto N, Duffau H, Cagnazzo F, Weiss A, Castagna M, Cosottini M, Perrini P (2019) Microsurgical anatomy of the sagittal stratum. Acta Neurochir (Wien) 161 (11):2319-2327. doi:10.1007/s00701-019-04019-8

Di Tommaso P, Chatzou M, Floden EW, Barja PP, Palumbo E, Notredame C (2017) Nextflow enables reproducible computational workflows. Nat Biotechnol 35 (4):316-319. doi:10.1038/nbt.3820

Gallivan JP, Culham JC (2015) Neural coding within human brain areas involved in actions. Curr Opin Neurobiol 33:141-149. doi:10.1016/j.conb.2015.03.012

Guevara M, Guevara P, Román C, Mangin J-F (2020) Superficial white matter: A review on the dMRI analysis methods and applications. NeuroImage 212:116673. doi:10.1016/j.neuroimage.2020.116673

Hau J, Sarubbo S, Perchey G, Crivello F, Zago L, Mellet E, Jobard G, Joliot M, Mazoyer BM, Tzourio-Mazoyer N, Petit L (2016) Cortical Terminations of the Inferior Fronto-Occipital and Uncinate

Fasciculi: Anatomical Stem-Based Virtual Dissection. Front Neuroanat 10:58. doi:10.3389/fnana.2016.00058
Jiao Y, Lin F, Wu J, Li H, Fu W, Huo R, Cao Y, Wang S, Zhao J (2020) Plasticity in language cortex and white matter tracts after resection of dominant inferior parietal lobule arteriovenous malformations: a combined fMRI and DTI study. J Neurosurg 134 (3):953-960. doi:10.3171/2019.12.JNS191987
Kinomura S, Larsson J, Gulyas B, Roland PE (1996) Activation by attention of the human reticular formation and thalamic intralaminar nuclei. Science 271:512-515
Kiriyama I, Miki H, Kikuchi K, Ohue S, Matsuda S, Mochizuki T (2009) Topographic analysis of the inferior parietal lobule in high-resolution 3D MR imaging. AJNR Am J Neuroradiol 30 (3):520-524. doi:10.3174/ajnr.A1417
Koch G, Cercignani M, Pecchioli C, Versace V, Oliveri M, Caltagirone C, Rothwell J, Bozzali M (2010) In vivo definition of parieto-motor connections involved in planning of grasping movements. NeuroImage 51 (1):300-312. doi:http://dx.doi.org/10.1016/j.neuroimage.2010.02.022
Kurtzer GM, Sochat V, Bauer MW (2017) Singularity: Scientific containers for mobility of compute. PLoS One 12 (5):e0177459. doi:10.1371/journal.pone.0177459
LaBerge D (1995) Computational and anatomical models of selective attention in object identification. In: Gazzaniga MS (ed) The cognitive neurosciences. vol 41. MIT Press, Cambridge, pp 649-663
Latini F, Trevisi G, Fahlstrom M, Jemstedt M, Alberius Munkhammar A, Zetterling M, Hesselager G, Ryttlefors M (2020) New Insights Into the Anatomy, Connectivity and Clinical Implications of the Middle Longitudinal Fasciculus. Front Neuroanat 14 (106):610324. doi:10.3389/fnana.2020.610324
Ludwig E, Klingler J (1956) Atlas cerebri humani. S. Karger, Basel
Maffei C, Sarubbo S, Jovicich J (2019) Diffusion-based tractography atlas of the human acoustic radiation. Scientific Reports 9 (1):4046. doi:10.1038/s41598-019-40666-8
Mahdy Ali K, Avesani P (2021) The vertical superior longitudinal fascicle and the vertical occipital fascicle. J Neurosurg Sci 65 (6):581-589. doi:10.23736/S0390-5616.21.05368-6
Maier-Hein KH, Neher PF, Houde JC, Cote MA, Garyfallidis E, Zhong J, Chamberland M, Yeh FC, Lin YC, Ji Q, Reddick WE, Glass JO, Chen DQ, Feng Y, Gao C, Wu Y, Ma J, He R, Li Q, Westin CF, Deslauriers-Gauthier S, Gonzalez JOO, Paquette M, St-Jean S, Girard G, Rheault F, Sidhu J, Tax CMW, Guo F, Mesri HY, David S, Froeling M, Heemskerk AM, Leemans A, Bore A, Pinsard B, Bedetti C, Desrosiers M, Brambati S, Doyon J, Sarica A, Vasta R, Cerasa A, Quattrone A, Yeatman J, Khan AR, Hodges W, Alexander S, Romascano D, Barakovic M, Auria A, Esteban O, Lemkaddem A, Thiran JP, Cetingul HE, Odry BL, Mailhe B, Nadar MS, Pizzagalli F, Prasad G, Villalon-Reina JE, Galvis J, Thompson PM, Requejo FS, Laguna PL, Lacerda LM, Barrett R, Dell'Acqua F, Catani M, Petit L, Caruyer E, Daducci A, Dyrby TB, Holland-Letz T, Hilgetag CC, Stieltjes B, Descoteaux M (2017) The challenge of mapping the human connectome based on diffusion tractography. Nat Commun 8 (1):1349. doi:http://dx.doi.org/10.1038/s41467-017-01285-x
Makris N, Preti MG, Wassermann D, Rathi Y, Papadimitriou GM, Yergatian C, Dickerson BC, Shenton ME, Kubicki M (2013) Human middle longitudinal fascicle: segregation and behavioral-clinical implications of two distinct fiber connections linking temporal pole and superior temporal gyrus with the angular gyrus or superior parietal lobule using multi-tensor tractography. Brain Imaging Behav 7 (3):335-352. doi:10.1007/s11682-013-9235-2
Makris N, Zhu A, Papadimitriou GM, Mouradian P, Ng I, Scaccianoce E, Baselli G, Baglio F, Shenton ME, Rathi Y, Dickerson B, Yeterian E, Kubicki M (2017) Mapping temporo-parietal and temporo-occipital cortico-cortical connections of the human middle longitudinal fascicle in subject-specific, probabilistic, and stereotaxic Talairach spaces. Brain Imaging Behav 11 (5):1258-1277. doi:10.1007/s11682-016-9589-3
Mandonnet E, Sarubbo S, Petit L (2018) The Nomenclature of Human White Matter Association Pathways: Proposal for a Systematic Taxonomic Anatomical Classification. Front Neuroanat 12:94. doi:http://dx.doi.org/10.3389/fnana.2018.00094

Martino J, Brogna C, Robles SG, Vergani F, Duffau H (2010) Anatomic dissection of the inferior fronto-occipital fasciculus revisited in the lights of brain stimulation data. Cortex 46 (5):691-699. doi:10.1016/j.cortex.2009.07.015

Matsumoto R, Nair DR, Ikeda A, Fumuro T, LaPresto E, Mikuni N, Bingaman W, Miyamoto S, Fukuyama H, Takahashi R, Najm I, Shibasaki H, Lüders HO (2012) Parieto-frontal network in humans studied by cortico-cortical evoked potential. Human Brain Mapping 33 (12):2856-2872. doi:10.1002/hbm.21407

Mazoyer B, Mellet E, Perchey G, Zago L, Crivello F, Jobard G, Delcroix N, Vigneau M, Leroux G, Petit L, Joliot M, Tzourio-Mazoyer N (2016) BIL&GIN: A neuroimaging, cognitive, behavioral, and genetic database for the study of human brain lateralization. Neuroimage 124 Part B:1225-1231. doi:10.1016/j.neuroimage.2015.02.071

Mesulam M-M (2008) Representation, inference, and transcendent encoding in neurocognitive networks of the human brain. Annals of Neurology 64 (4):367-378

Meynert T (1885) Psychiatry: Clinical Treatise on the Diseases of the Fore-Brain, trans. B. Sachs. GP Putnam, New York & London

Nieuwenhuys R, Voogd J, van Huijzen C (2008) The human central nervous system. 4th edn. Springer-Verlag, Berlin

Niu M, Palomero-Gallagher N (2022) Architecture and connectivity of the human angular gyrus and of its homolog region in the macaque brain. Brain Struct Funct. doi:10.1007/s00429-022-02509-7

Oishi K, Faria A, Jiang H, Li X, Akhter K, Zhang J, Hsu JT, Miller MI, van Zijl PCM, Albert M, Lyketsos CG, Woods R, Toga AW, Pike GB, Rosa-Neto P, Evans A, Mazziotta J, Mori S (2009) Atlas-based whole brain white matter analysis using large deformation diffeomorphic metric mapping: Application to normal elderly and Alzheimer's disease participants. NeuroImage 46 (2):486-499

Palejwala AH, O'Connor KP, Pelargos P, Briggs RG, Milton CK, Conner AK, Milligan TM, O'Donoghue DL, Glenn CA, Sughrue ME (2020) Anatomy and white matter connections of the lateral occipital cortex. Surg Radiol Anat 42 (3):315-328. doi:10.1007/s00276-019-02371-z

Petit L, Pouget P (2019) The comparative anatomy of frontal eye fields in primates. Cortex 118:51-64. doi:10.1016/j.cortex.2019.02.023

Petit L, Rheault F, Descoteaux M, Tzourio-Mazoyer N Half of the streamlines built in a whole human brain tractogram is anatomically uninterpretable. In: 25th Conference of the Organization for Human Brain Mapping, Roma, 2019.

Rebelo D, Oliveira F, Abrunhosa A, Januario C, Lemos J, Castelo-Branco M (2021) A link between synaptic plasticity and reorganization of brain activity in Parkinson's disease. Proc Natl Acad Sci U S A 118 (3):e2013962118. doi:10.1073/pnas.2013962118

Rheault F, Poulin P, Valcourt Caron A, St-Onge E, Descoteaux M (2020) Common misconceptions, hidden biases and modern challenges of dMRI tractography. J Neural Eng 17 (1):011001. doi:10.1088/1741-2552/ab6aad

Richard N, Desmurget M, Teillac A, Beuriat PA, Bardi L, Coude G, Szathmari A, Mottolese C, Sirigu A, Hiba B (2021) Anatomical bases of fast parietal grasp control in humans: A diffusion-MRI tractography study. Neuroimage 235:118002. doi:10.1016/j.neuroimage.2021.118002

Rozzi S, Calzavara R, Belmalih A, Borra E, Gregoriou GG, Matelli M, Luppino G (2006) Cortical Connections of the Inferior Parietal Cortical Convexity of the Macaque Monkey. Cerebral Cortex 16 (10):1389-1417. doi:10.1093/cercor/bhj076

Sarubbo S, De Benedictis A, Maldonado IL, Basso G, Duffau H (2013) Frontal terminations for the inferior fronto-occipital fascicle: anatomical dissection, DTI study and functional considerations on a multi-component bundle. Brain structure & function 218:21-37. doi:10.1007/s00429-011-0372-3

Sarubbo S, De Benedictis A, Merler S, Mandonnet E, Balbi S, Granieri E, Duffau H (2015) Towards a functional atlas of human white matter. Hum Brain Mapp 36 (8):3117-3136. doi:10.1002/hbm.22832

Sarubbo S, De Benedictis A, Merler S, Mandonnet E, Barbareschi M, Dallabona M, Chioffi F, Duffau H (2016) Structural and functional integration between dorsal and ventral language streams as

revealed by blunt dissection and direct electrical stimulation. Hum Brain Mapp 37 (11):3858-3872. doi:10.1002/hbm.23281
Sarubbo S, Le Bars E, Moritz-Gasser S, Duffau H (2012) Complete recovery after surgical resection of left Wernicke's area in awake patient: a brain stimulation and functional MRI study. Neurosurg Rev 35 (2):287-292; discussion 292. doi:10.1007/s10143-011-0351-4
Sarubbo S, Tate M, De Benedictis A, Merler S, Moritz-Gasser S, Herbet G, Duffau H (2020) Mapping critical cortical hubs and white matter pathways by direct electrical stimulation: an original functional atlas of the human brain. NeuroImage 205:116237. doi:10.1016/j.neuroimage.2019.116237
Schilling KG, Tax CMW, Rheault F, Landman BA, Anderson AW, Descoteaux M, Petit L (2022) Prevalence of white matter pathways coming into a single white matter voxel orientation: The bottleneck issue in tractography. Hum Brain Mapp 43 (4):1196-1213. doi:http://dx.doi.org/10.1002/hbm.25697
Schmahmann JD, Pandya DN (2006) Fiber pathways of the brain. Oxford University Press, New York
Seghier ML (2013) The angular gyrus: multiple functions and multiple subdivisions. The Neuroscientist 19 (1):43-61. doi:10.1177/1073858412440596
Sparing R, Thimm M, Hesse MD, Kust J, Karbe H, Fink GR (2009) Bidirectional alterations of interhemispheric parietal balance by non-invasive cortical stimulation. Brain 132 (Pt 11):3011-3020. doi:10.1093/brain/awp154
Theaud G, Houde JC, Bore A, Rheault F, Morency F, Descoteaux M (2020) TractoFlow: A robust, efficient and reproducible diffusion MRI pipeline leveraging Nextflow & Singularity. Neuroimage 218:116889. doi:http://dx.doi.org/10.1016/j.neuroimage.2020.116889
Thiebaut de Schotten M, Dell'Acqua F, Forkel SJ, Simmons A, Vergani F, Murphy DGM, Catani M (2011) A lateralized brain network for visuospatial attention. Nat Neurosci 14 (10):1245-1246. doi:http://www.nature.com/neuro/journal/v14/n10/abs/nn.2905.html#supplementary-information
Thiebaut de Schotten M, Urbanski M, Duffau H, Volle E, Levy R, Dubois B, Bartolomeo P (2005) Direct evidence for a parietal-frontal pathway subserving spatial awareness in humans. Science 309 (5744):2226-2228
Vavassori L, Sarubbo S, Petit L (2021) Hodology of the superior longitudinal system of the human brain: a historical perspective, the current controversies, and a proposal. Brain Struct Funct 226 (5):1363-1384. doi:10.1007/s00429-021-02265-0
Vigneau M, Beaucousin V, Hervé P-Y, Duffau H, Crivello F, Houde O, Mazoyer B, Tzourio-Mazoyer N (2006) Meta-analyzing left hemisphere language areas: phonology, semantics, and sentence processing. Neuroimage 30 (4):1414-1432
Wang X, Pathak S, Stefaneanu L, Yeh FC, Li S, Fernandez-Miranda JC (2016) Subcomponents and connectivity of the superior longitudinal fasciculus in the human brain. Brain Struct Funct 221 (4):2075-2092. doi:10.1007/s00429-015-1028-5
Wang Y, Fernandez-Miranda JC, Verstynen T, Pathak S, Schneider W, Yeh F-C (2013) Rethinking the Role of the Middle Longitudinal Fascicle in Language and Auditory Pathways. Cerebral Cortex 23 (10):2347-2356. doi:10.1093/cercor/bhs225
Wu Y, Sun D, Wang Y, Wang Y (2016a) Subcomponents and connectivity of the inferior fronto-occipital fasciculus revealed by diffusion spectrum imaging fiber tracking. Frontiers in Neuroanatomy 10:88. doi:10.3389/fnana.2016.00088
Wu Y, Sun D, Wang Y, Wang Y, Wang Y (2016b) Tracing short connections of the temporo-parieto-occipital region in the human brain using diffusion spectrum imaging and fiber dissection. Brain Research 1646:152-159. doi:10.1016/j.brainres.2016.05.046
Xu Y, He Y, Bi Y (2017) A Tri-network Model of Human Semantic Processing. Frontiers in Psychology 8:1538. doi:10.3389/fpsyg.2017.01538
Yeatman JD, Weiner KS, Pestilli F, Rokem A, Mezer A, Wandell BA (2014) The vertical occipital fasciculus: a century of controversy resolved by in vivo measurements. Proc Natl Acad Sci U S A 111 (48):E5214-5223. doi:10.1073/pnas.1418503111
Yeh FC (2020) Shape analysis of the human association pathways. Neuroimage 223:117329. doi:10.1016/j.neuroimage.2020.117329

Yeterian EH, Pandya DN (1993) Striatal connections of the parietal assoiation cortices in rhesus monkey. JCompNeurol 332:175-197

Zaca D, Corsini F, Rozzanigo U, Dallabona M, Avesani P, Annicchiarico L, Zigiotto L, Faraca G, Chioffi F, Jovicich J, Sarubbo S (2018) Whole-Brain Network Connectivity Underlying the Human Speech Articulation as Emerged Integrating Direct Electric Stimulation, Resting State fMRI and Tractography. Front Hum Neurosci 12:405. doi:10.3389/fnhum.2018.00405

Zemmoura I, Blanchard E, Raynal PI, Rousselot-Denis C, Destrieux C, Velut S (2016) How Klingler's dissection permits exploration of brain structural connectivity? An electron microscopy study of human white matter. Brain Struct Funct 221 (5):2477-2486. doi:10.1007/s00429-015-1050-7

A. Extraction of whole-brain anatomically-plausible streamlines

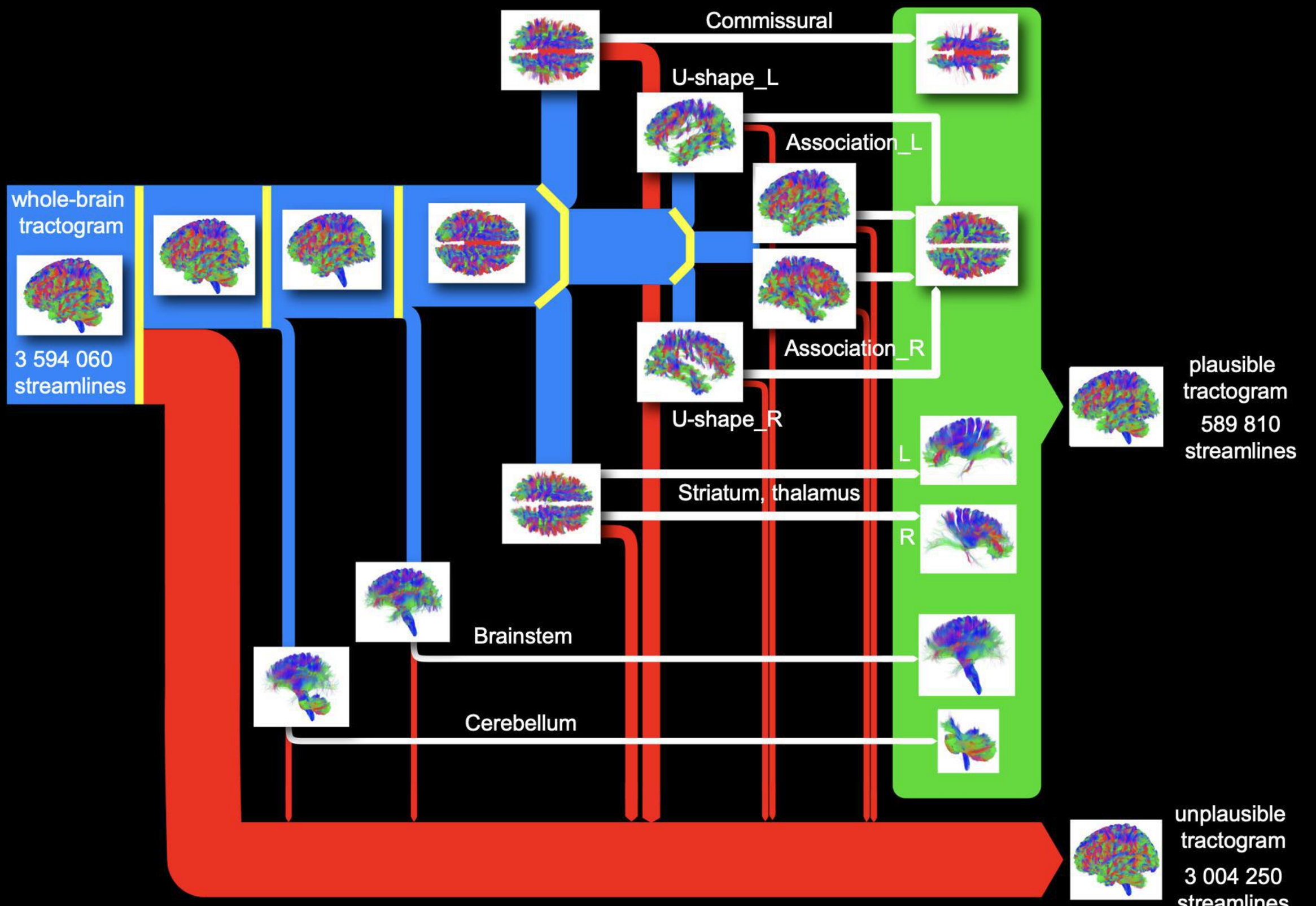

B. Stem/shell AG fibers extraction

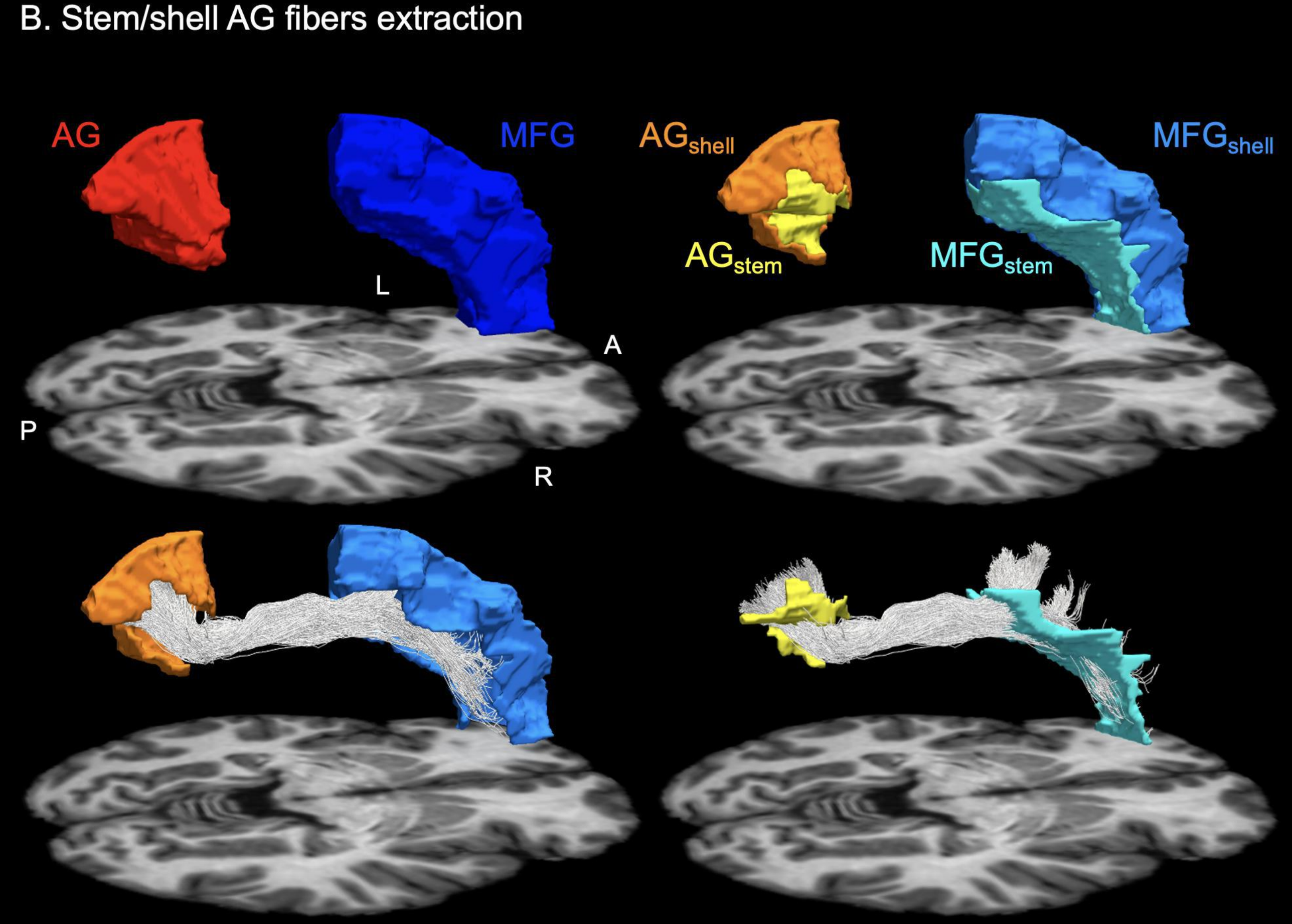

Lateral view

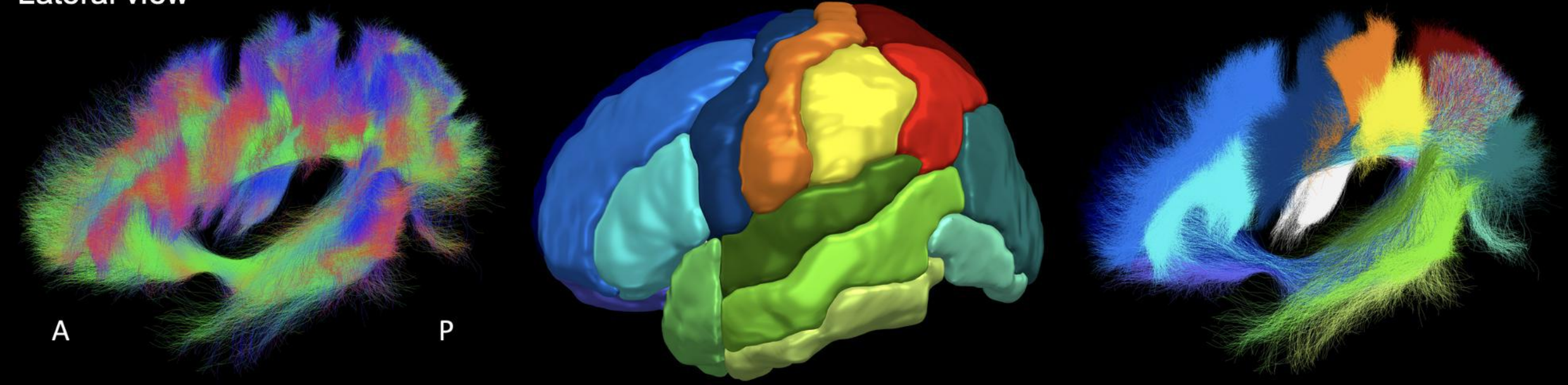

Medial view

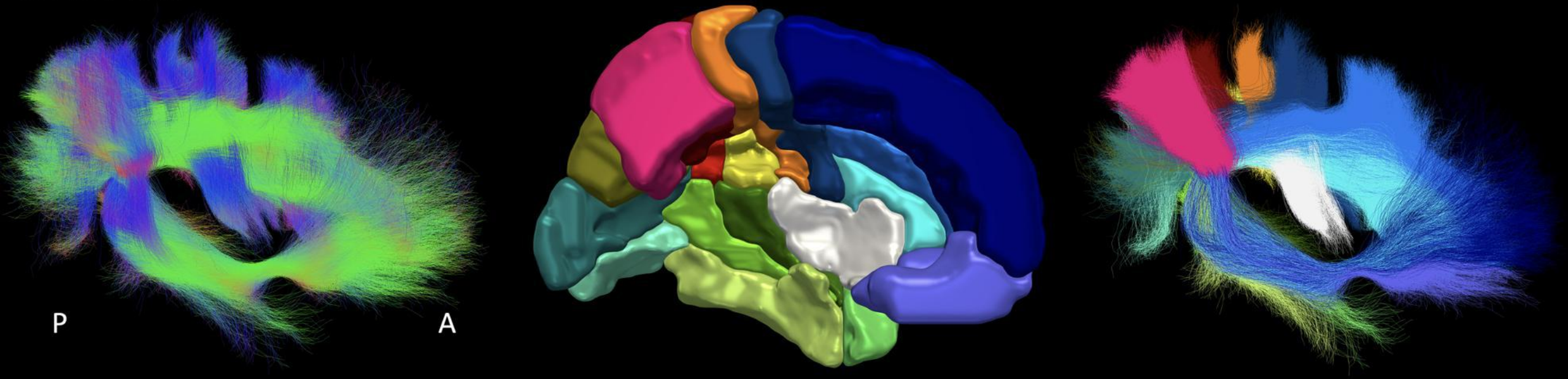

Angular G. *Supramarginal G.* *Sup. Par. G.* *Precuneus* *Postcentral G.*
Sup. Occ. G. *Mid. Occ. G.* *Inf. Occ. G.* *Sup. Temp. G.* *Mid. Temp. G.*
Inf. Temp. G. *Sup. Front. G.* *Mid. Front. G.* *Inf. Front. G.* *Fronto-Orbital G.*
Precentral G. *Insula*

Homotopic callosal AG

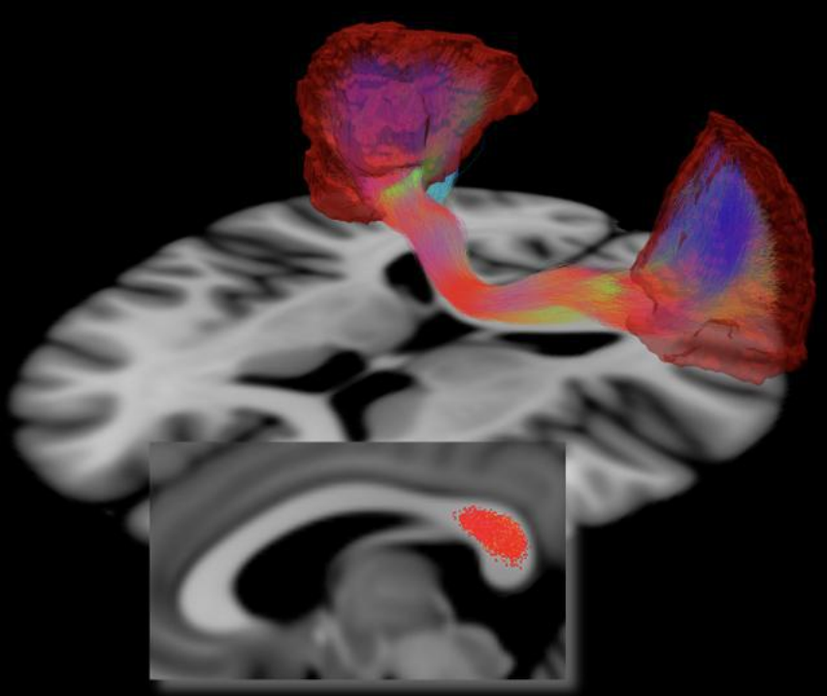

AG-Putamen

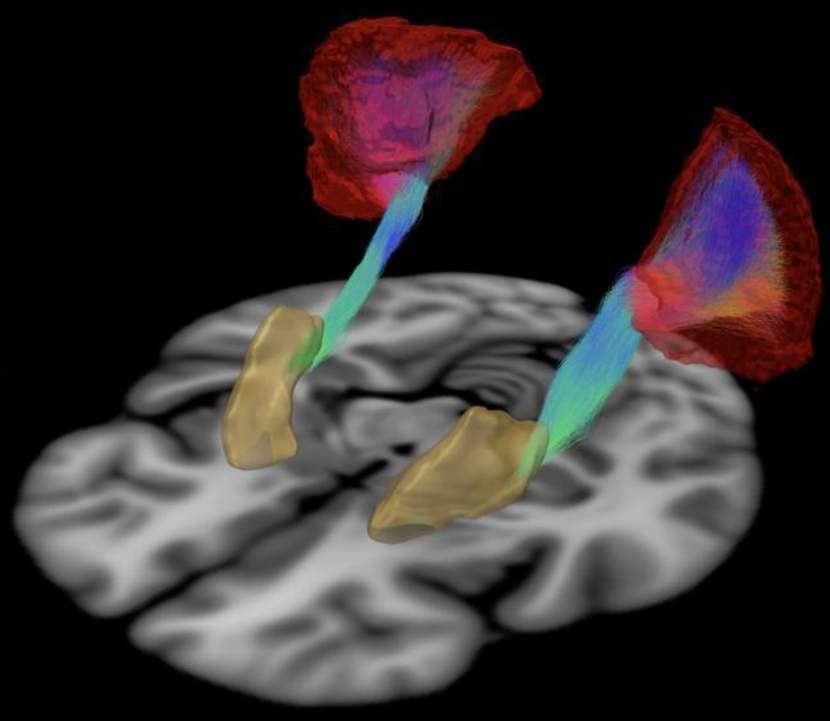

AG-Thalamus

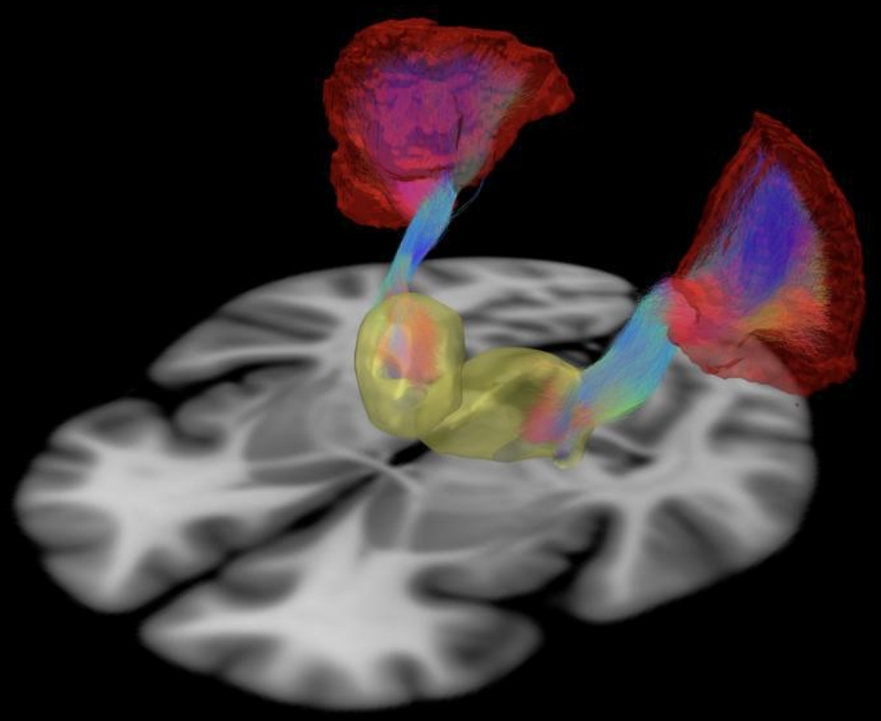

AG-Midbrain

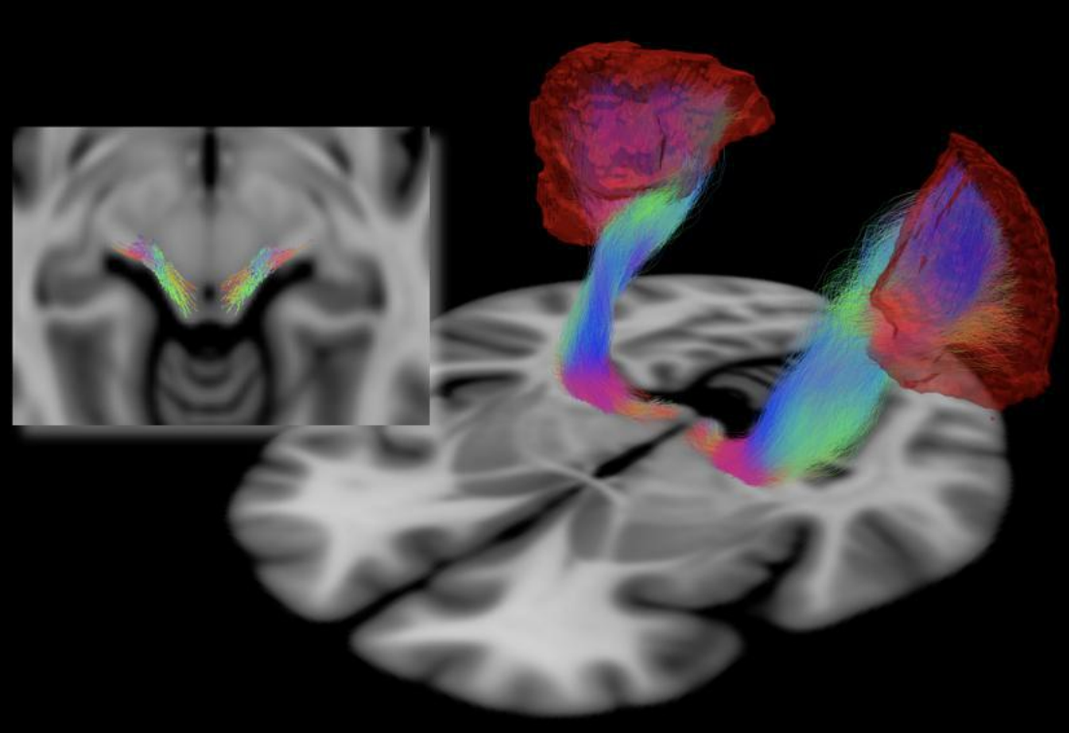

AG-Pons

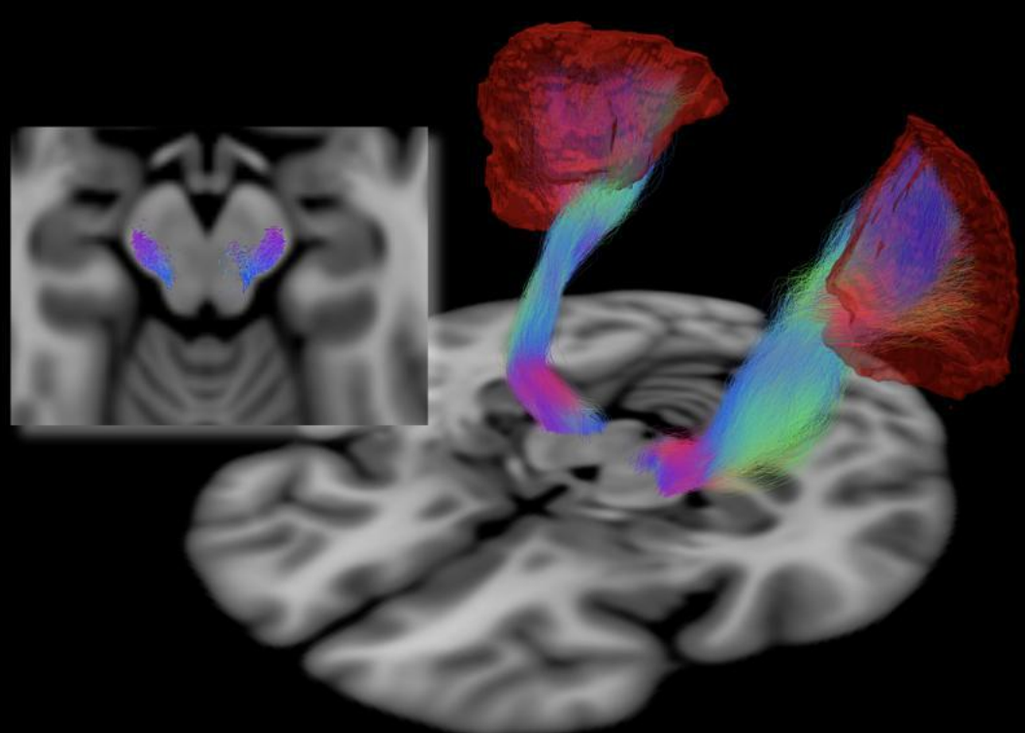

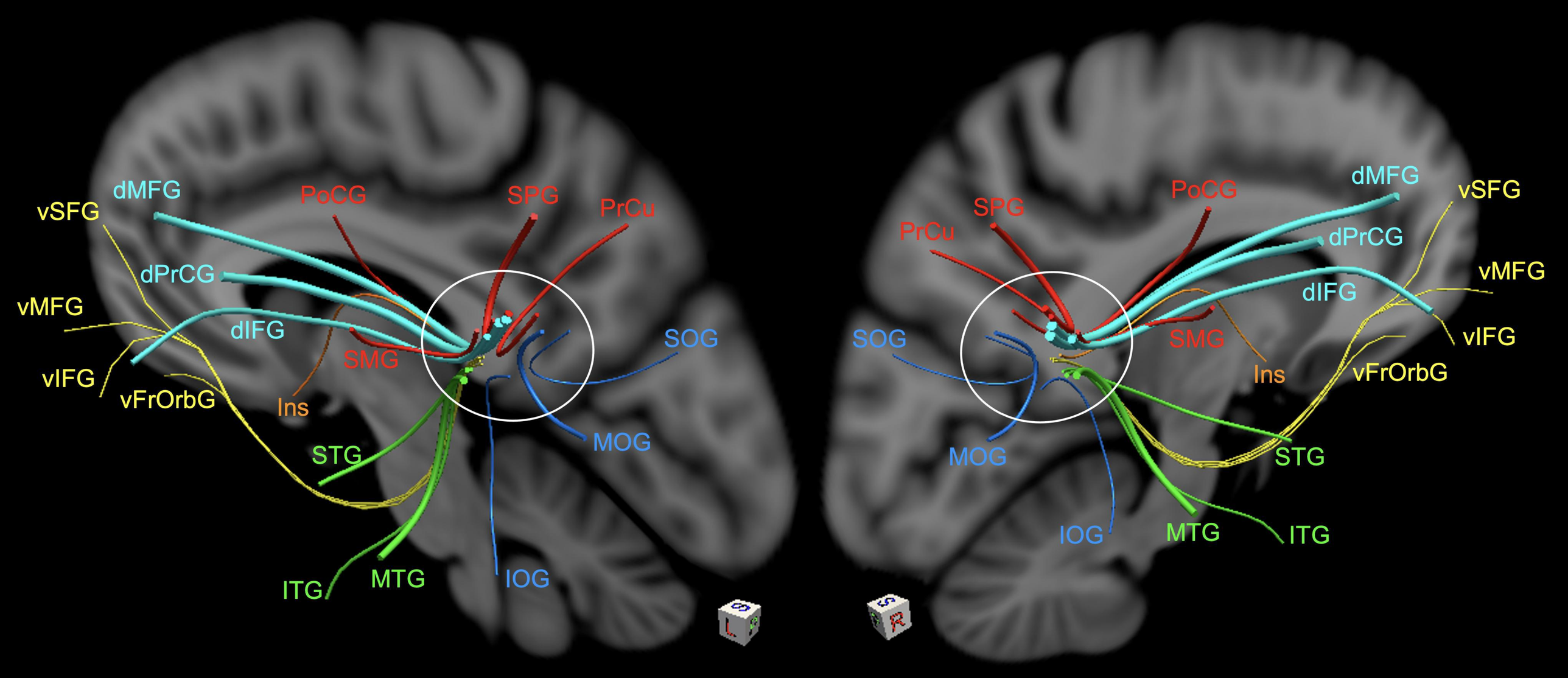
vSFG
dMFG
PoCG
SPG
PrCu
dPrCG
vMFG
dIFG
SMG
SOG
vIFG
vFrOrbG
Ins
MOG
STG
ITG
MTG
IOG
L
PrCu
SPG
PoCG
dMFG
vSFG
dPrCG
vMFG
dIFG
vIFG
SOG
SMG
Ins
vFrOrbG
MOG
STG
IOG
MTG
ITG
R

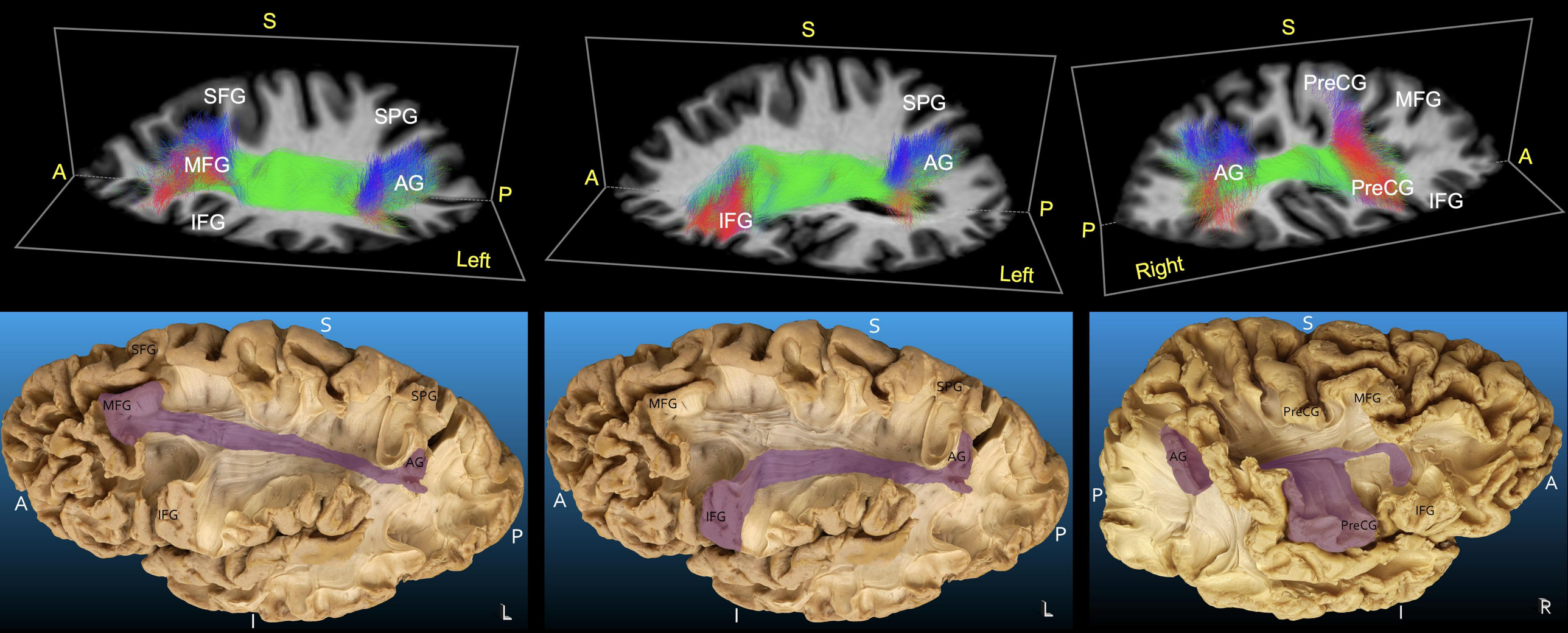
S
SFG
SPG
MFG
AG
A
P
IFG
Left
S
SPG
AG
A
P
IFG
Left
S
PreCG
MFG
AG
A
PreCG
IFG
P
Right
S
SFG
SPG
MFG
AG
A
IFG
P
I
L
S
MFG
SPG
AG
A
IFG
P
I
L
S
PreCG
MFG
AG
A
P
IFG
PreCG
I
R

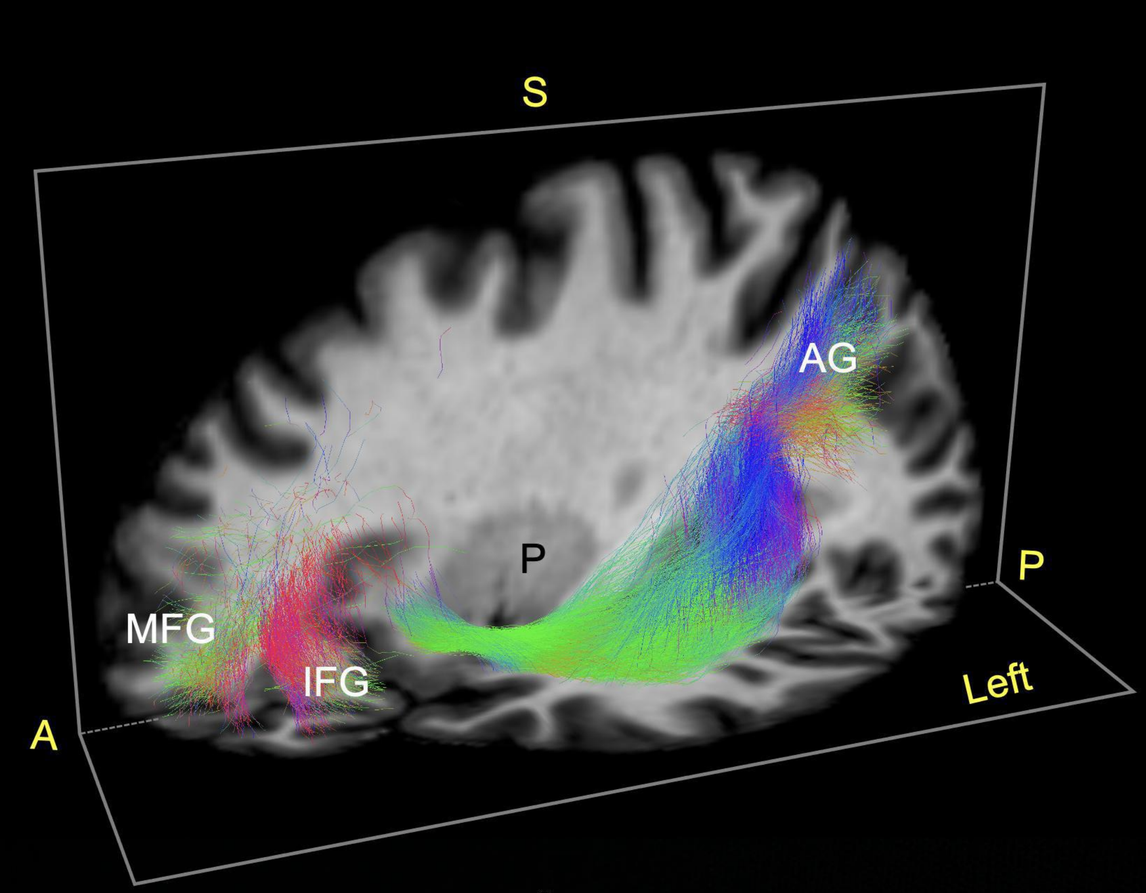
S
AG
P
MFG
IFG
P
Left
A

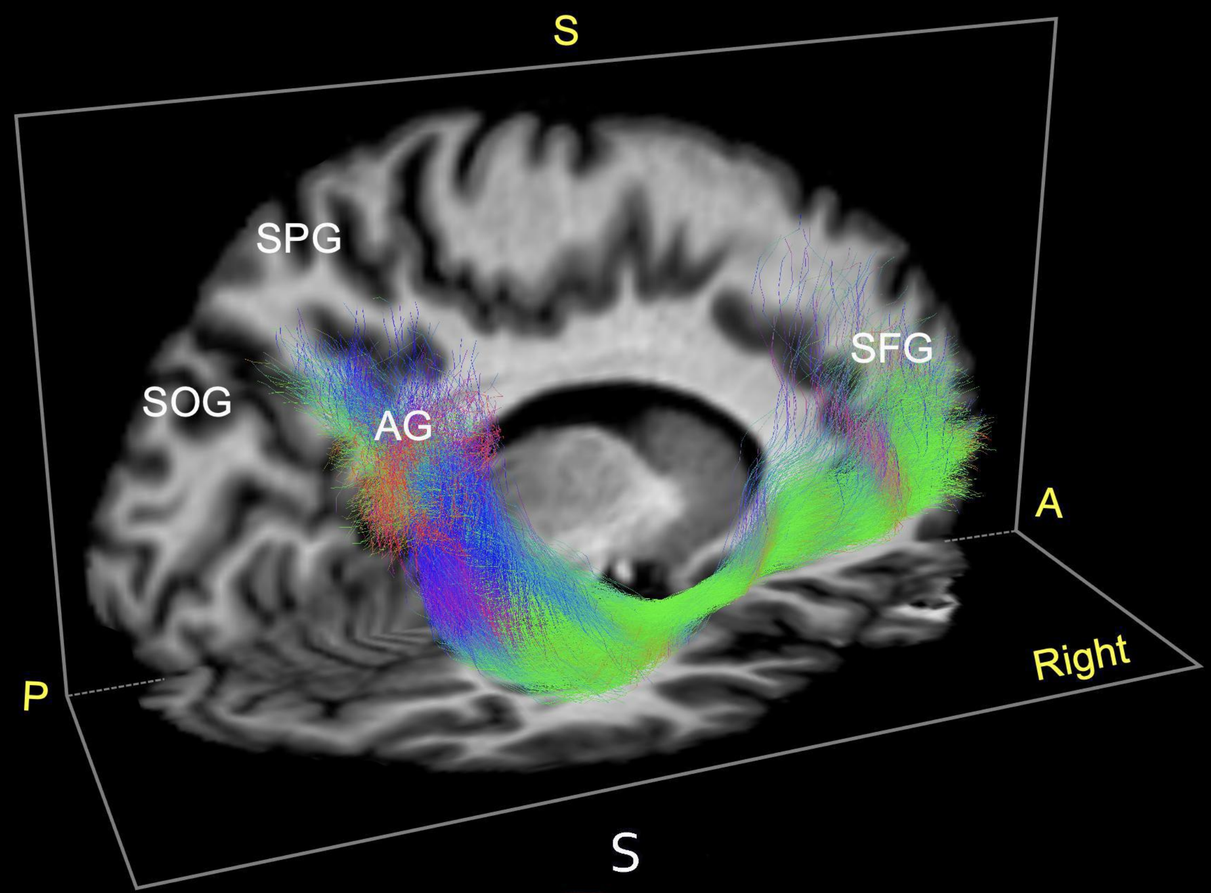
S
SPG
SOG
AG
SFG
A
P
Right
S

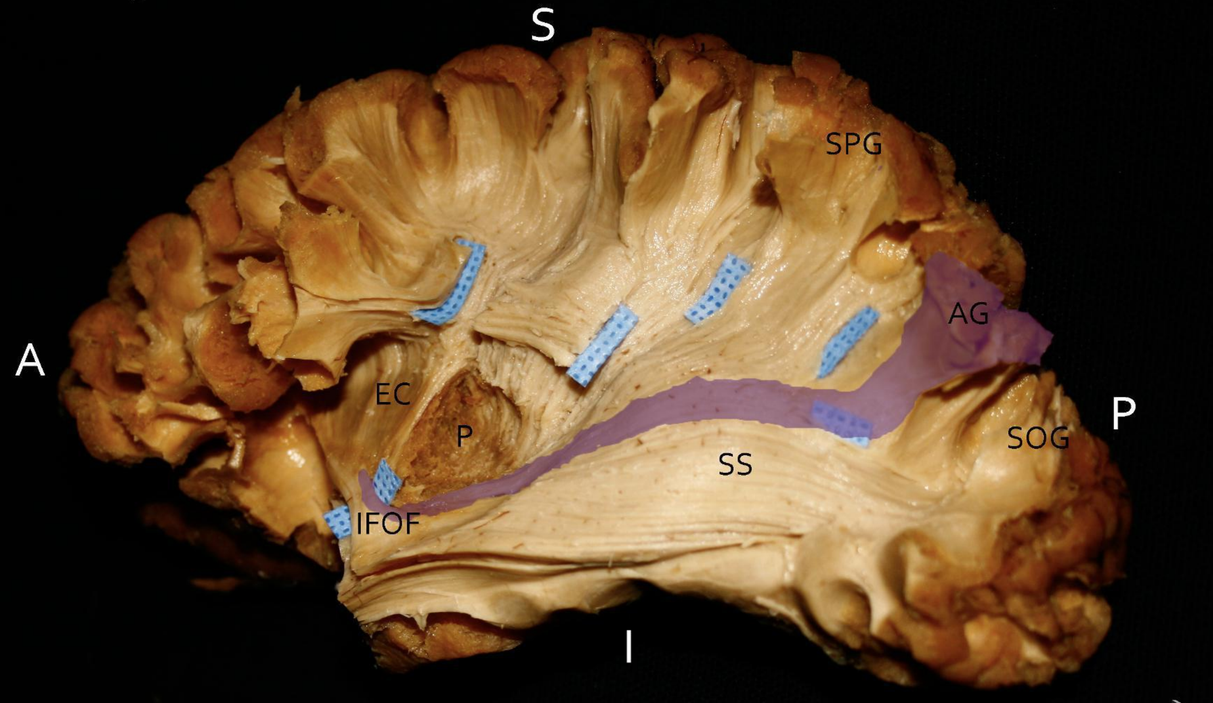
S
SPG
AG
A
EC
P
SS
SOG
P
IFOF
I
L

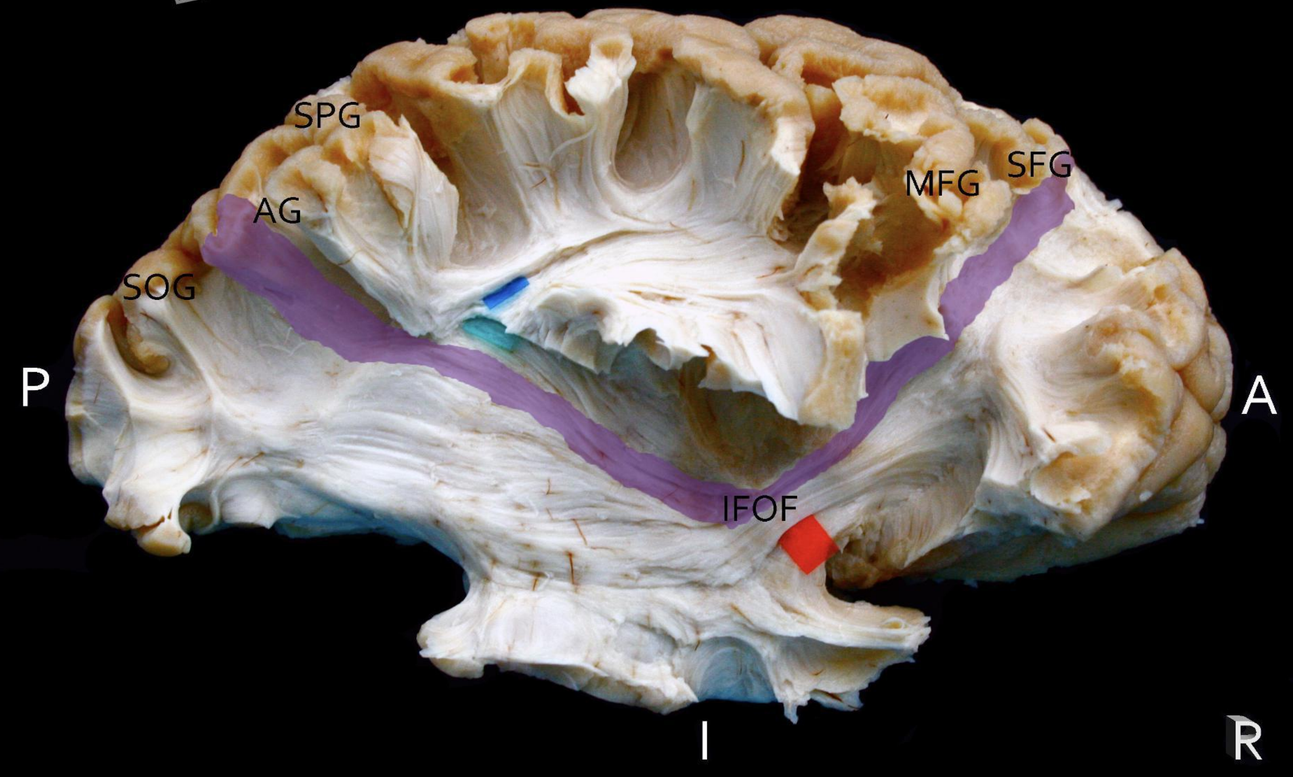
SPG
MFG
SFG
AG
SOG
P
A
IFOF
I
R

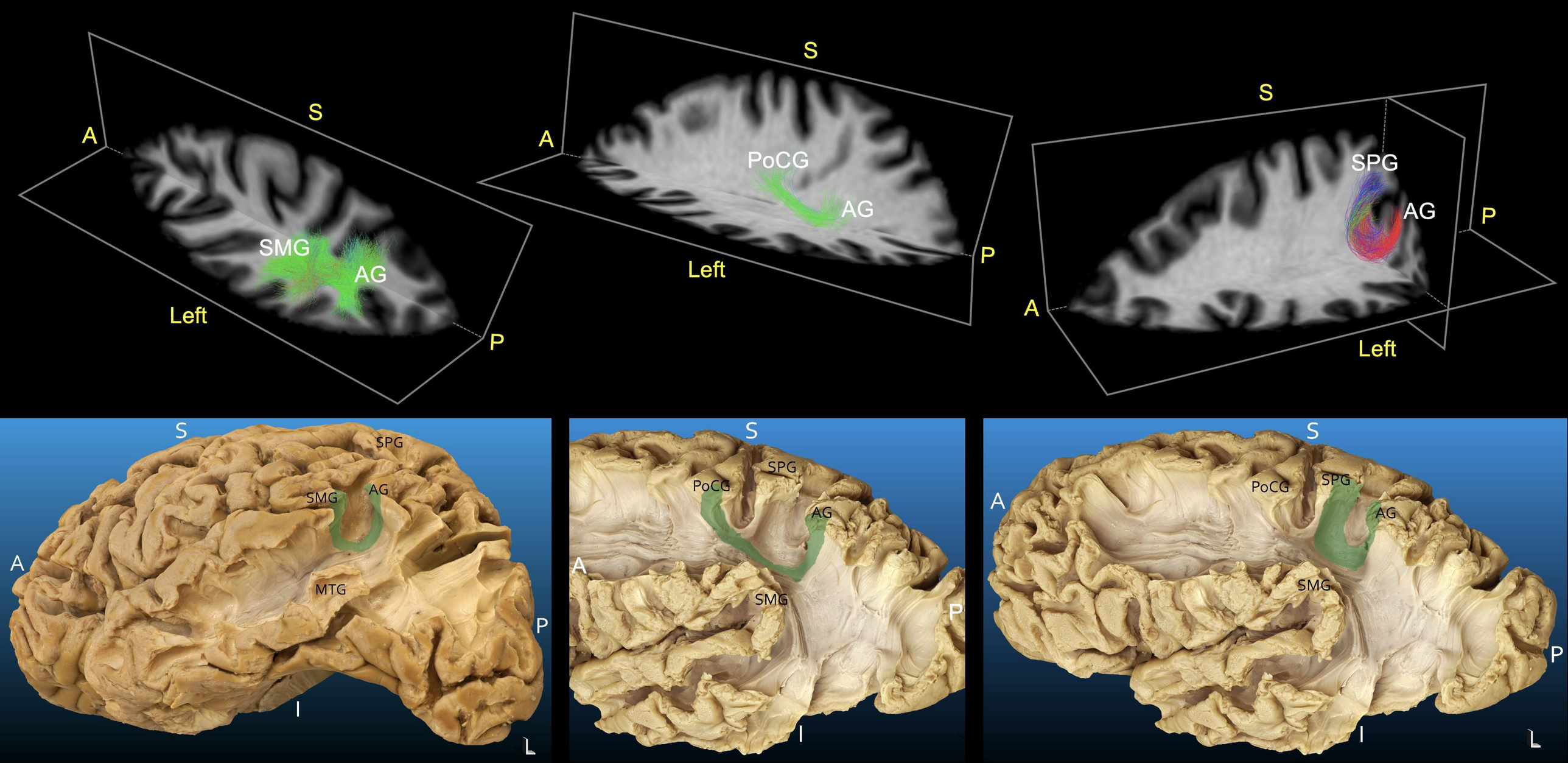
S
A
SMG
AG
Left
P
S
A
PoCG
AG
Left
P
S
SPG
AG
P
A
Left
S
SPG
SMG
AG
A
MTG
P
I
L
S
SPG
PoCG
AG
A
SMG
P
I
S
PoCG
SPG
AG
A
SMG
P
I
L

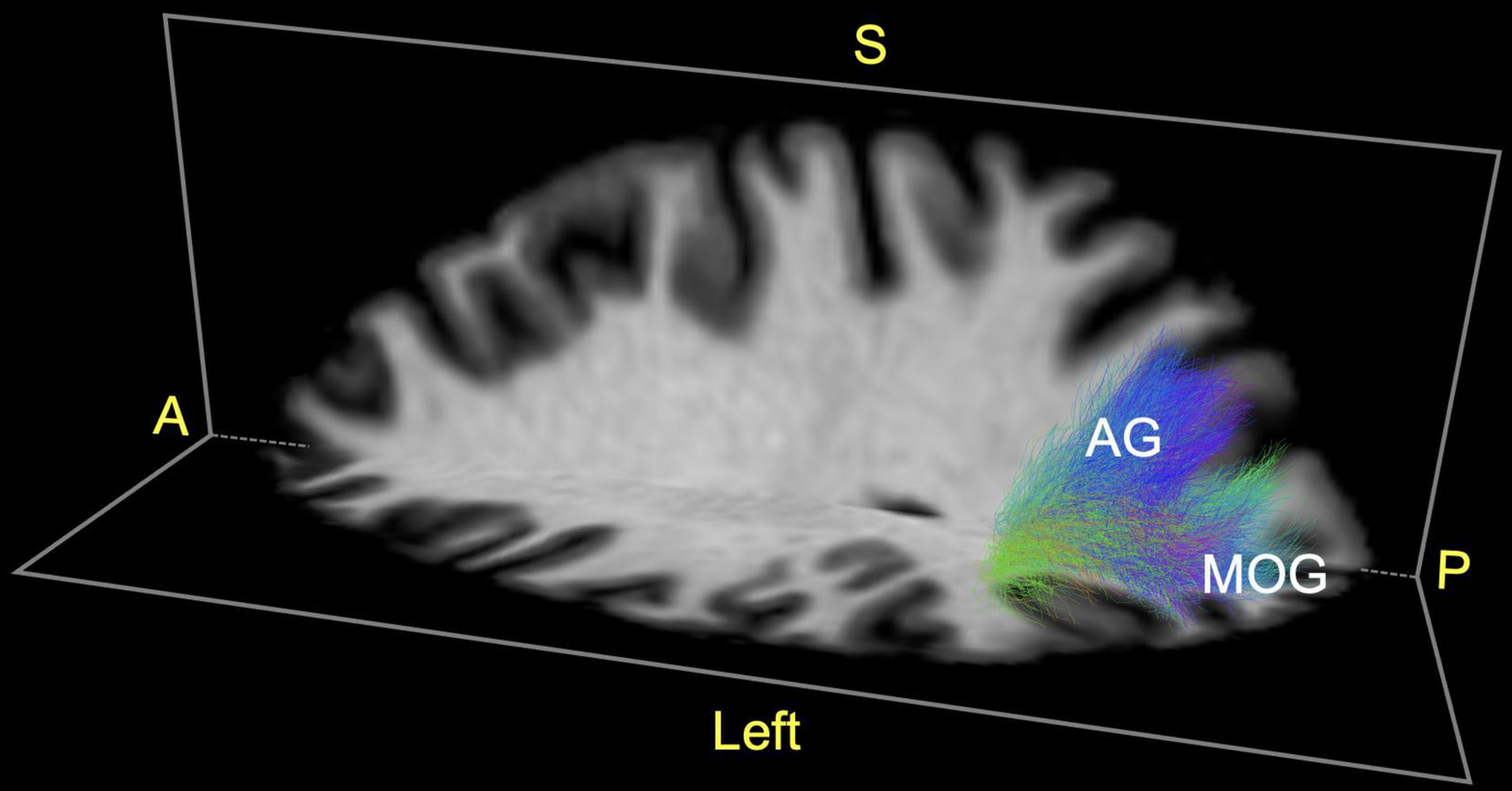
S
A
AG
MOG
P
Left

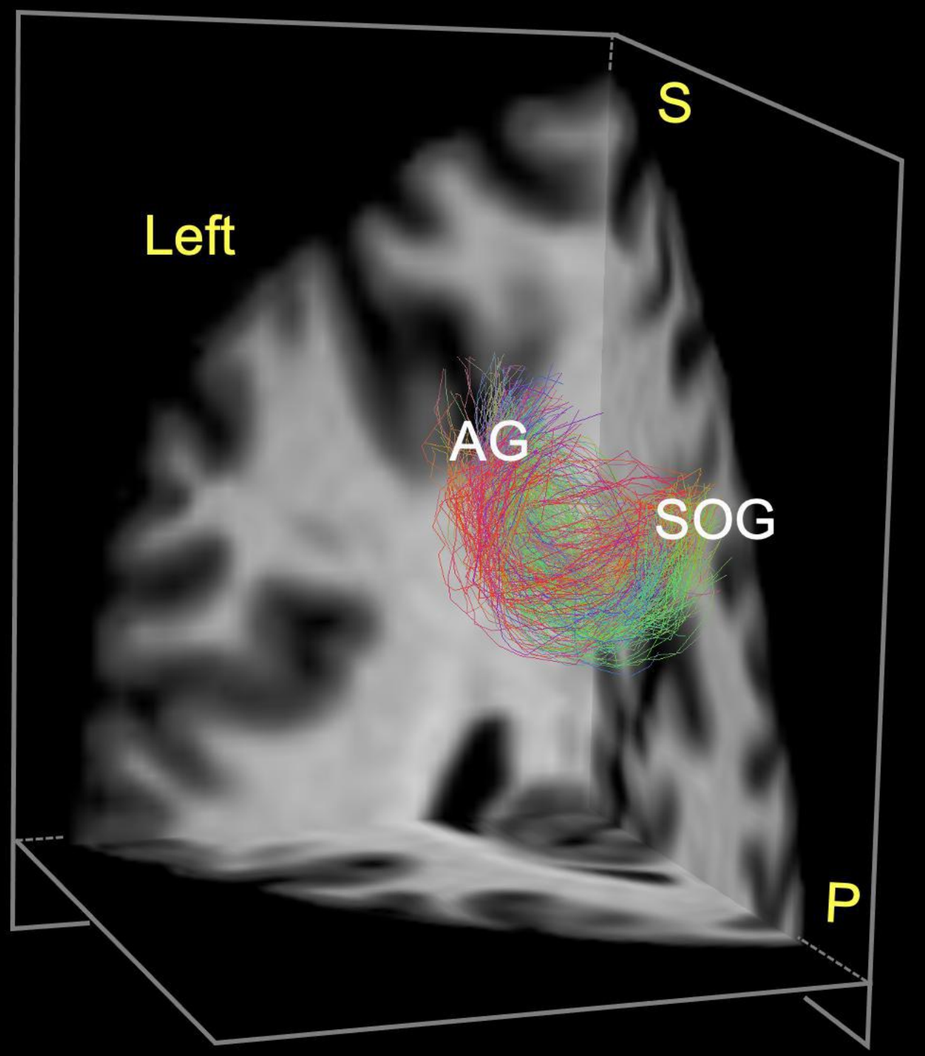
S
Left
AG
SOG
P

S
SPG
A
AG
SOG
SMG
MOG
IOG
P
I
L

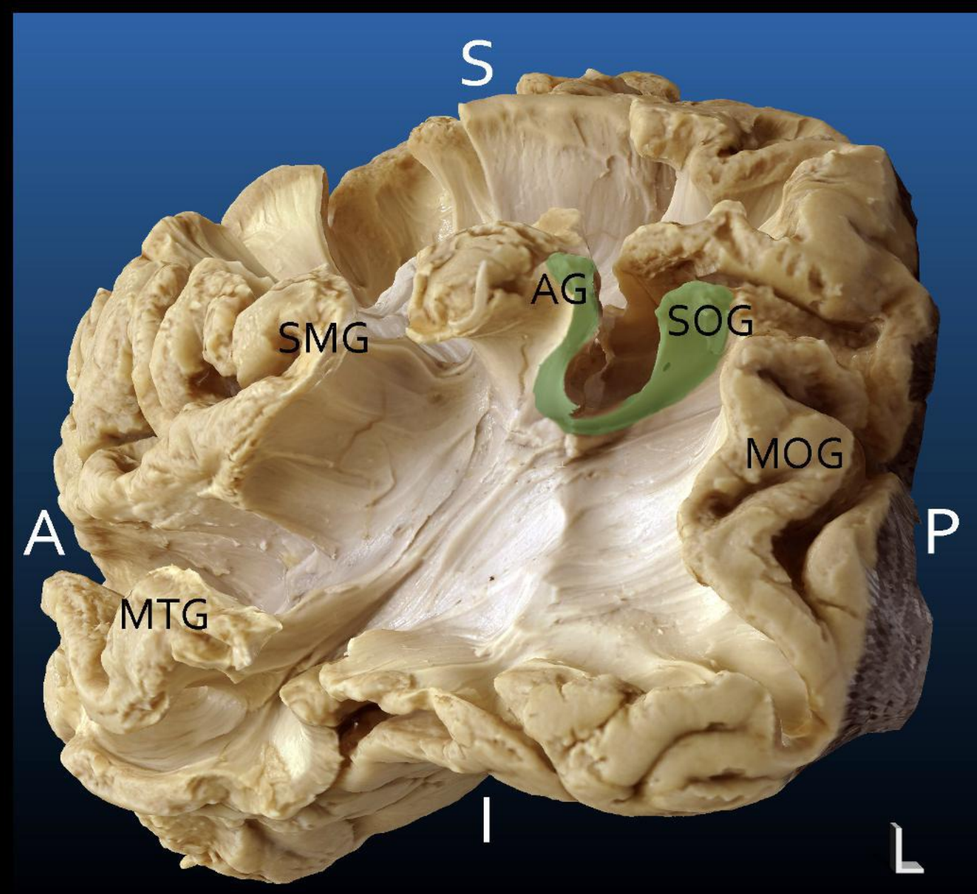
S
AG
SMG
SOG
MOG
A
P
MTG
I
L

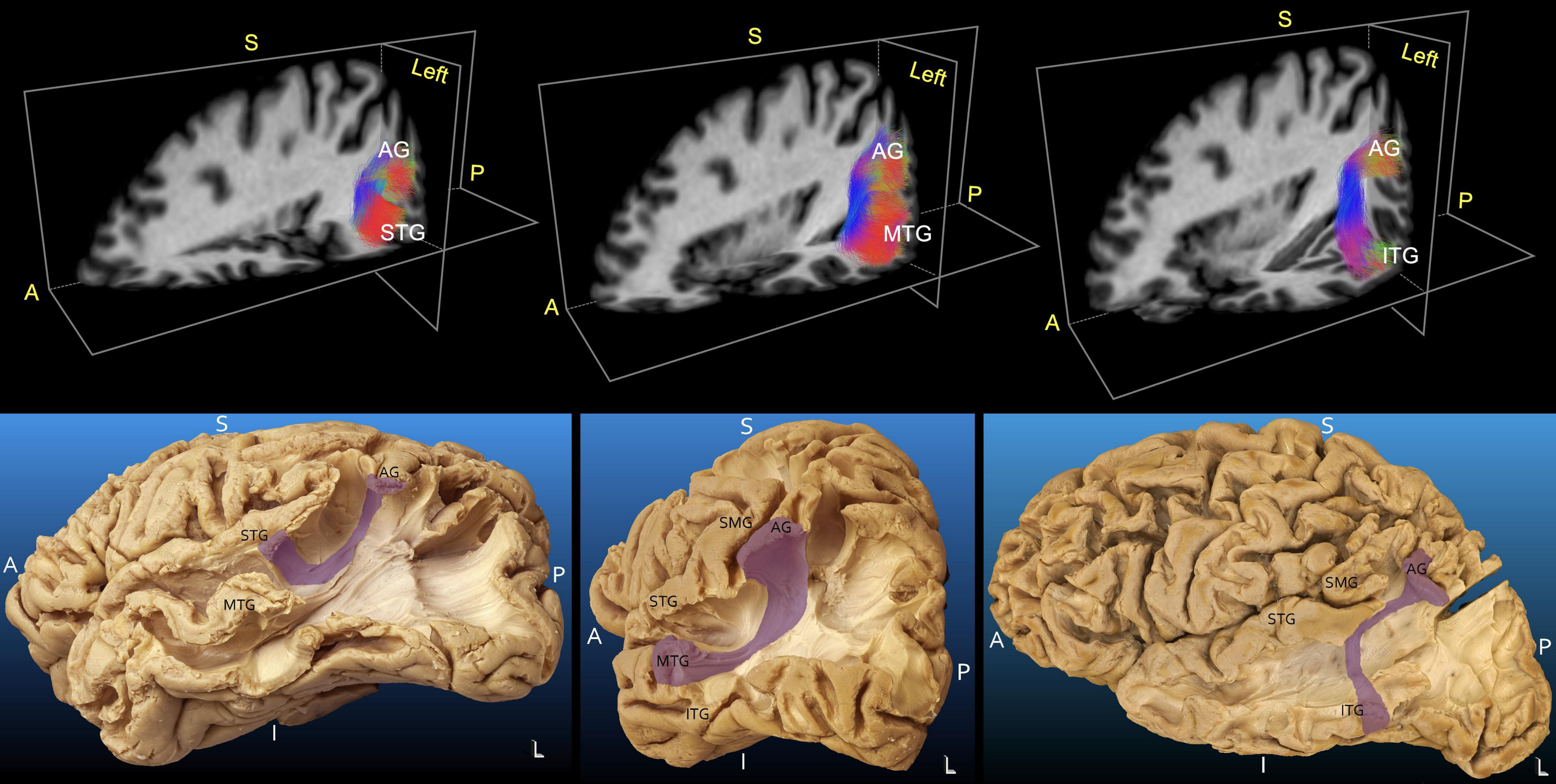
S
Left
AG
P
STG
A
S
Left
AG
P
MTG
A
S
Left
AG
P
ITG
A
S
AG
STG
A
P
MTG
I
L
S
SMG
AG
STG
A
P
MTG
ITG
I
L
S
AG
SMG
STG
A
P
ITG
I
L

Left

1. SMG
2. PoCg
3. SPG
4. PrCu

1. SOG
2. MOG
3. IOG

1. STG
2. MTG
3. ITG

Right

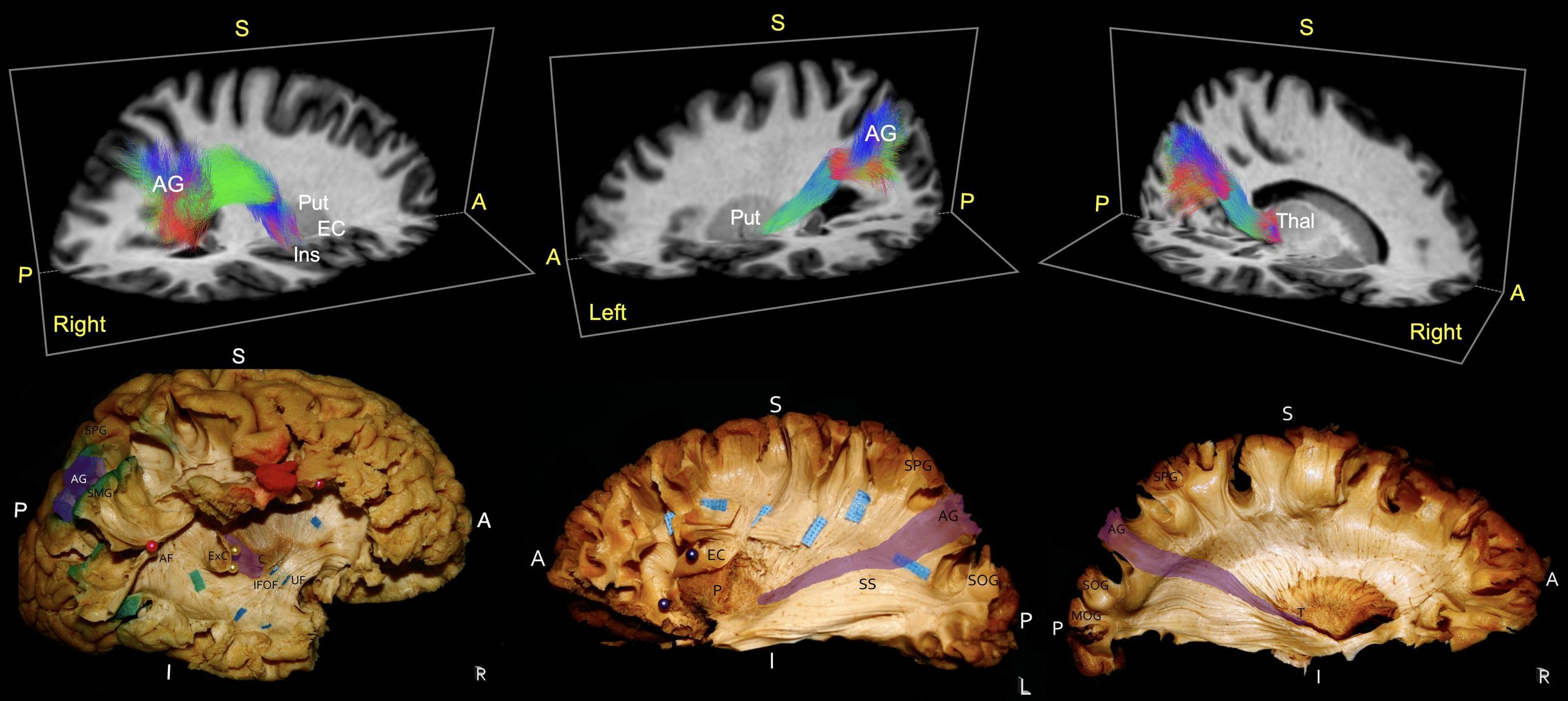
S
AG
Put
EC
Ins
A
P
Right
S
AG
Put
A
P
Left
S
P
Thal
A
Right
S
SPG
AG
SMG
P
A
AF
ExC
C
IFOF
UF
I
R
S
SPG
AG
EC
P
SS
SOG
A
P
I
L
S
SPG
AG
SOG
MOG
T
P
A
I
R

Figure 11

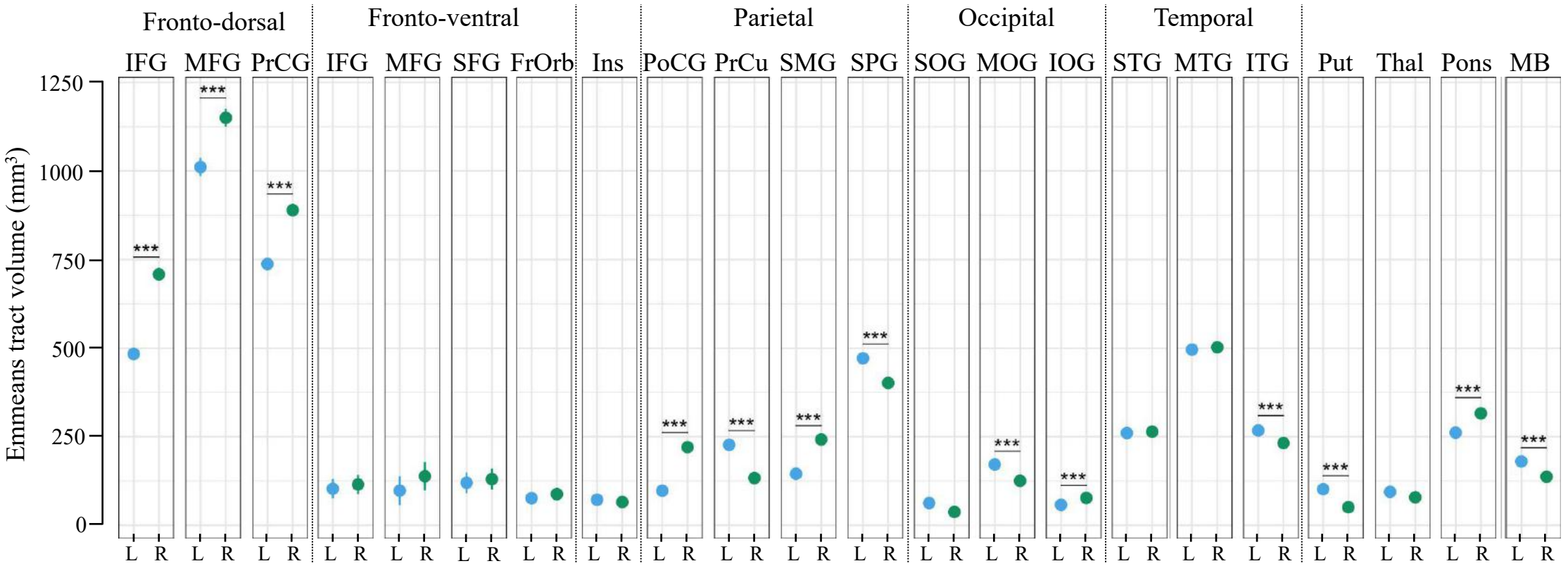
Fronto-dorsal
Fronto-ventral
Parietal
Occipital
Temporal
IFG
MFG
PrCG
IFG
MFG
SFG
FrOrb
Ins
PoCG
PrCu
SMG
SPG
SOG
MOG
IOG
STG
MTG
ITG
Put
Thal
Pons
MB
Emmeans tract volume (mm³)
1250
1000
750
500
250
0
***
L
R

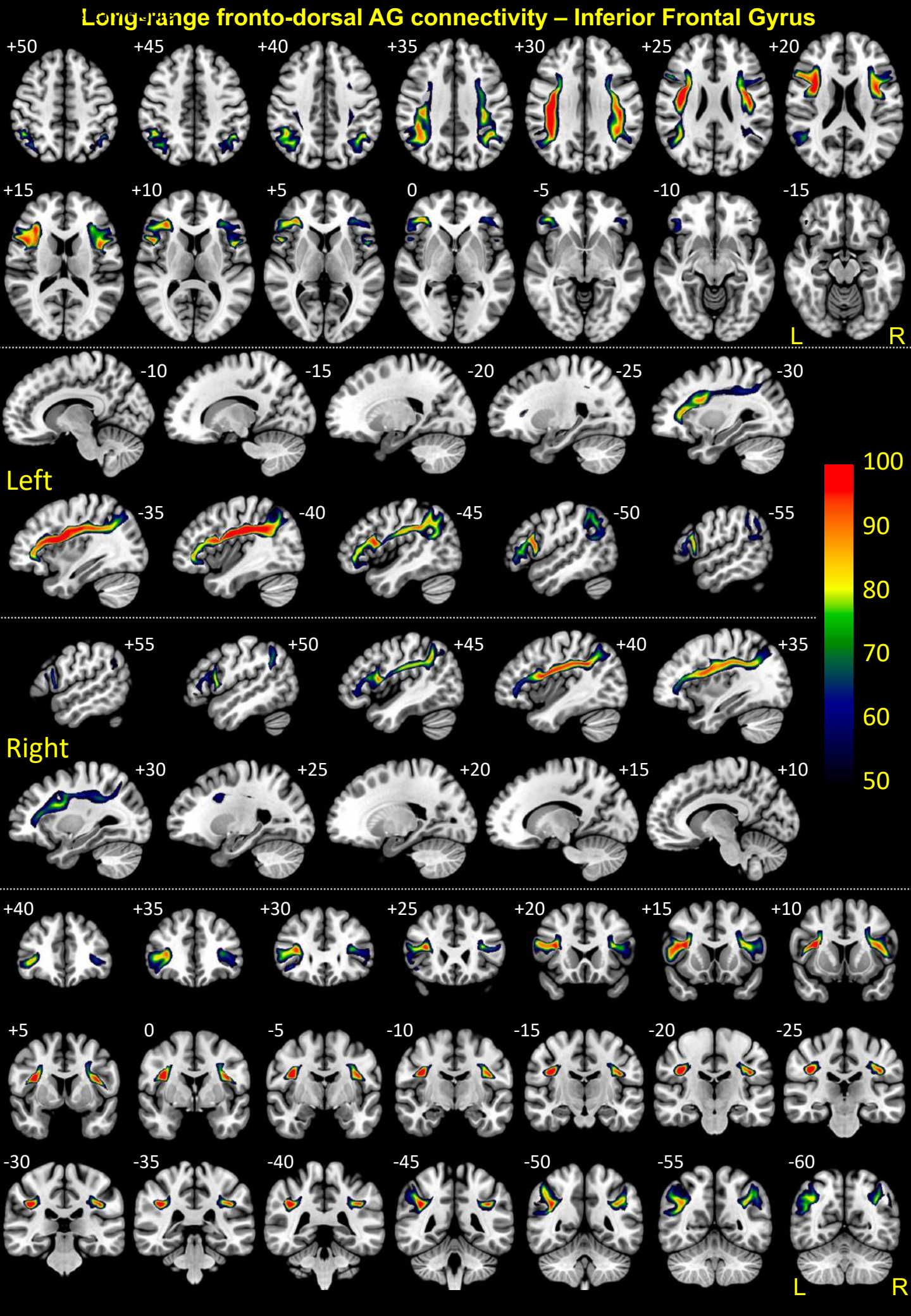
Long-range fronto-dorsal AG connectivity – Inferior Frontal Gyrus
+50
+45
+40
+35
+30
+25
+20
+15
+10
+5
0
-5
-10
-15
L
R
-10
-15
-20
-25
-30
Left
-35
-40
-45
-50
-55
+55
+50
+45
+40
+35
Right
+30
+25
+20
+15
+10
100
90
80
70
60
50
+40
+35
+30
+25
+20
+15
+10
+5
0
-5
-10
-15
-20
-25
-30
-35
-40
-45
-50
-55
-60
L
R

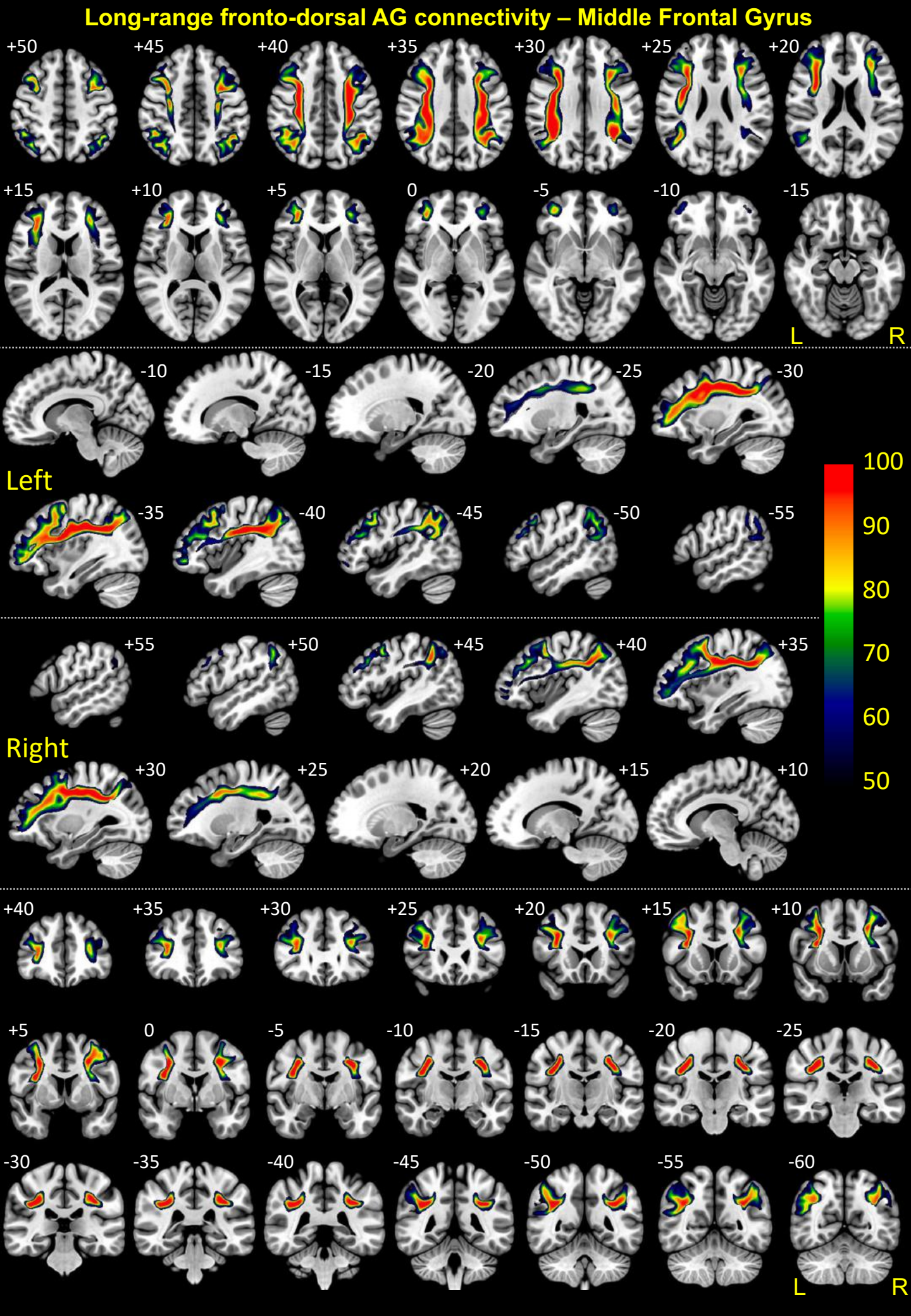
Long-range fronto-dorsal AG connectivity – Middle Frontal Gyrus
+50
+45
+40
+35
+30
+25
+20
+15
+10
+5
0
-5
-10
-15
L
R
-10
-15
-20
-25
-30
Left
-35
-40
-45
-50
-55
100
90
80
70
60
50
+55
+50
+45
+40
+35
Right
+30
+25
+20
+15
+10
+40
+35
+30
+25
+20
+15
+10
+5
0
-5
-10
-15
-20
-25
-30
-35
-40
-45
-50
-55
-60
L
R

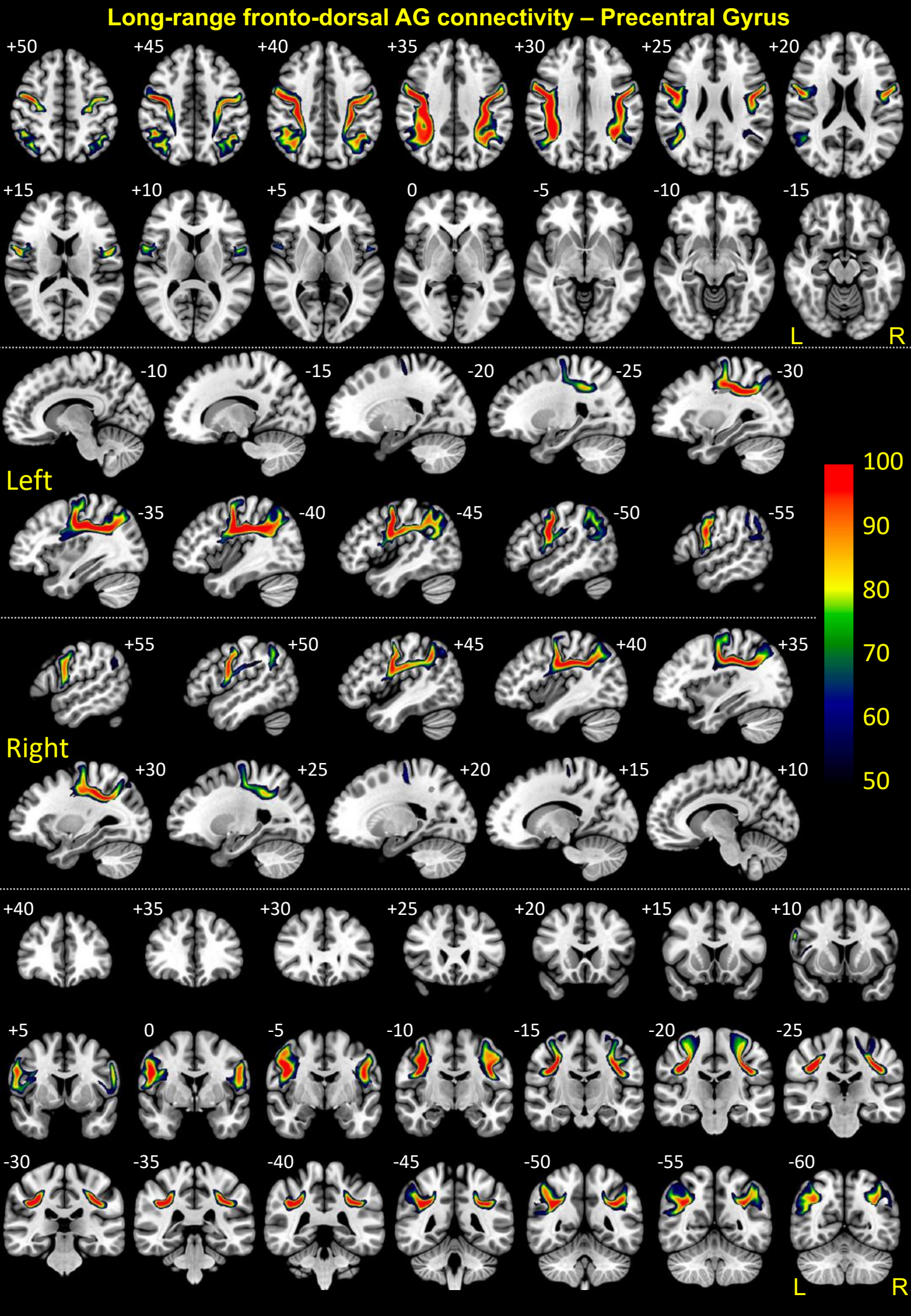
Long-range fronto-dorsal AG connectivity – Precentral Gyrus
+50
+45
+40
+35
+30
+25
+20
+15
+10
+5
0
-5
-10
-15
L
R
-10
-15
-20
-25
-30
Left
-35
-40
-45
-50
-55
+55
+50
+45
+40
+35
Right
+30
+25
+20
+15
+10
100
90
80
70
60
50
+40
+35
+30
+25
+20
+15
+10
+5
0
-5
-10
-15
-20
-25
-30
-35
-40
-45
-50
-55
-60
L
R

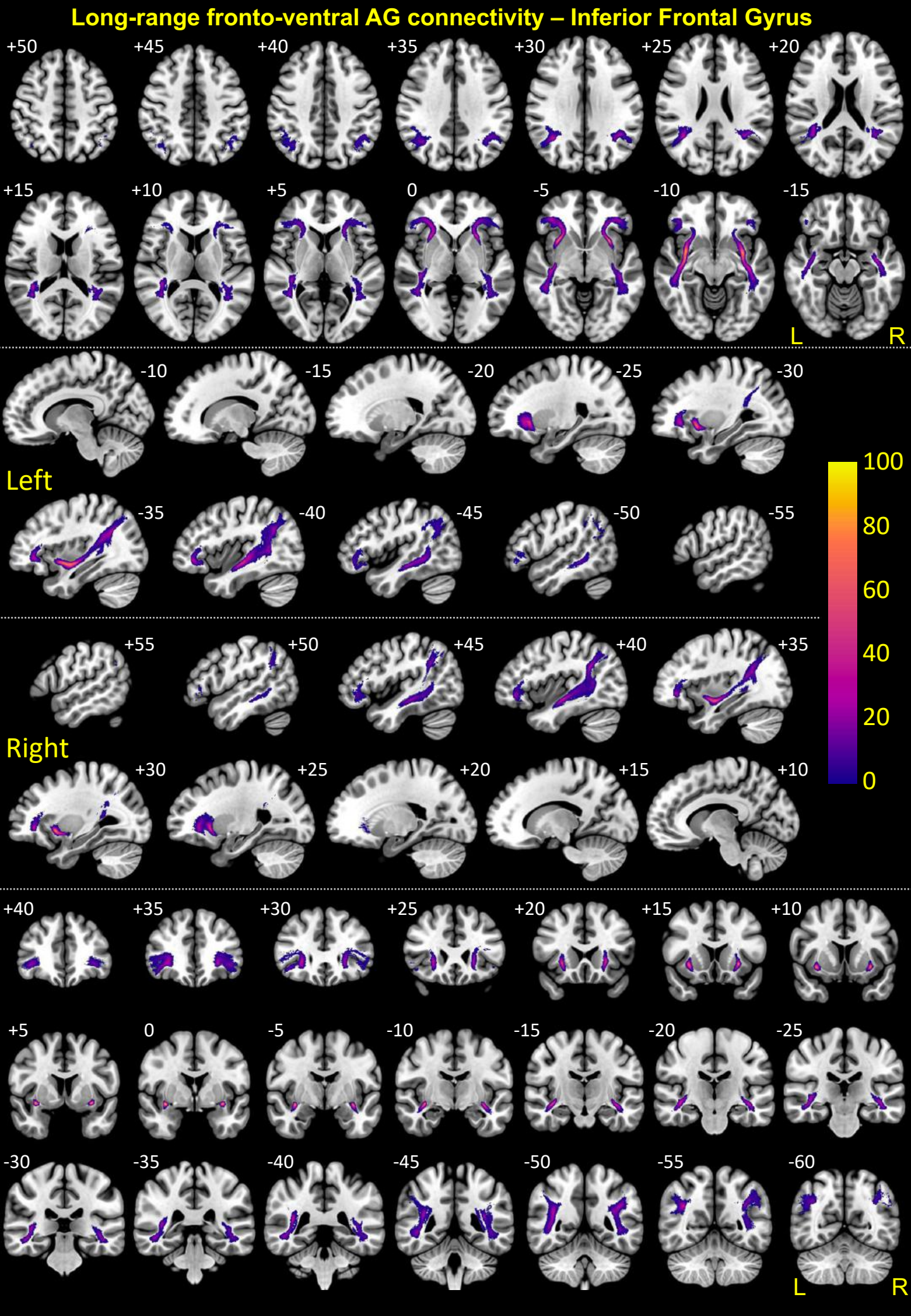
Long-range fronto-ventral AG connectivity – Inferior Frontal Gyrus
+50
+45
+40
+35
+30
+25
+20
+15
+10
+5
0
-5
-10
-15
L
R
-10
-15
-20
-25
-30
Left
-35
-40
-45
-50
-55
+55
+50
+45
+40
+35
Right
+30
+25
+20
+15
+10
100
80
60
40
20
0
+40
+35
+30
+25
+20
+15
+10
+5
0
-5
-10
-15
-20
-25
-30
-35
-40
-45
-50
-55
-60
L
R

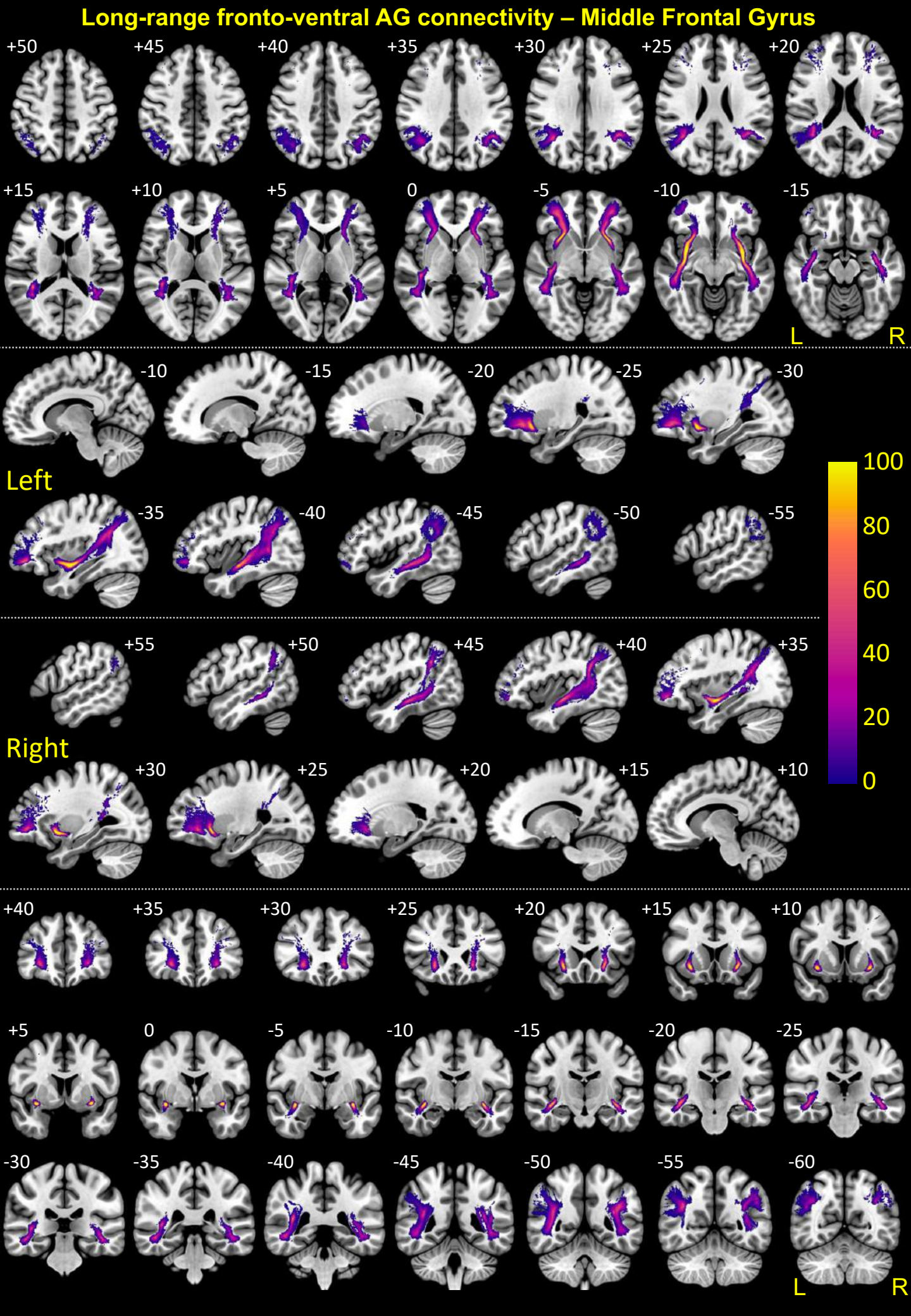
Long-range fronto-ventral AG connectivity – Middle Frontal Gyrus
+50
+45
+40
+35
+30
+25
+20
+15
+10
+5
0
-5
-10
-15
L
R
-10
-15
-20
-25
-30
Left
-35
-40
-45
-50
-55
+55
+50
+45
+40
+35
Right
+30
+25
+20
+15
+10
100
80
60
40
20
0
+40
+35
+30
+25
+20
+15
+10
+5
0
-5
-10
-15
-20
-25
-30
-35
-40
-45
-50
-55
-60
L
R

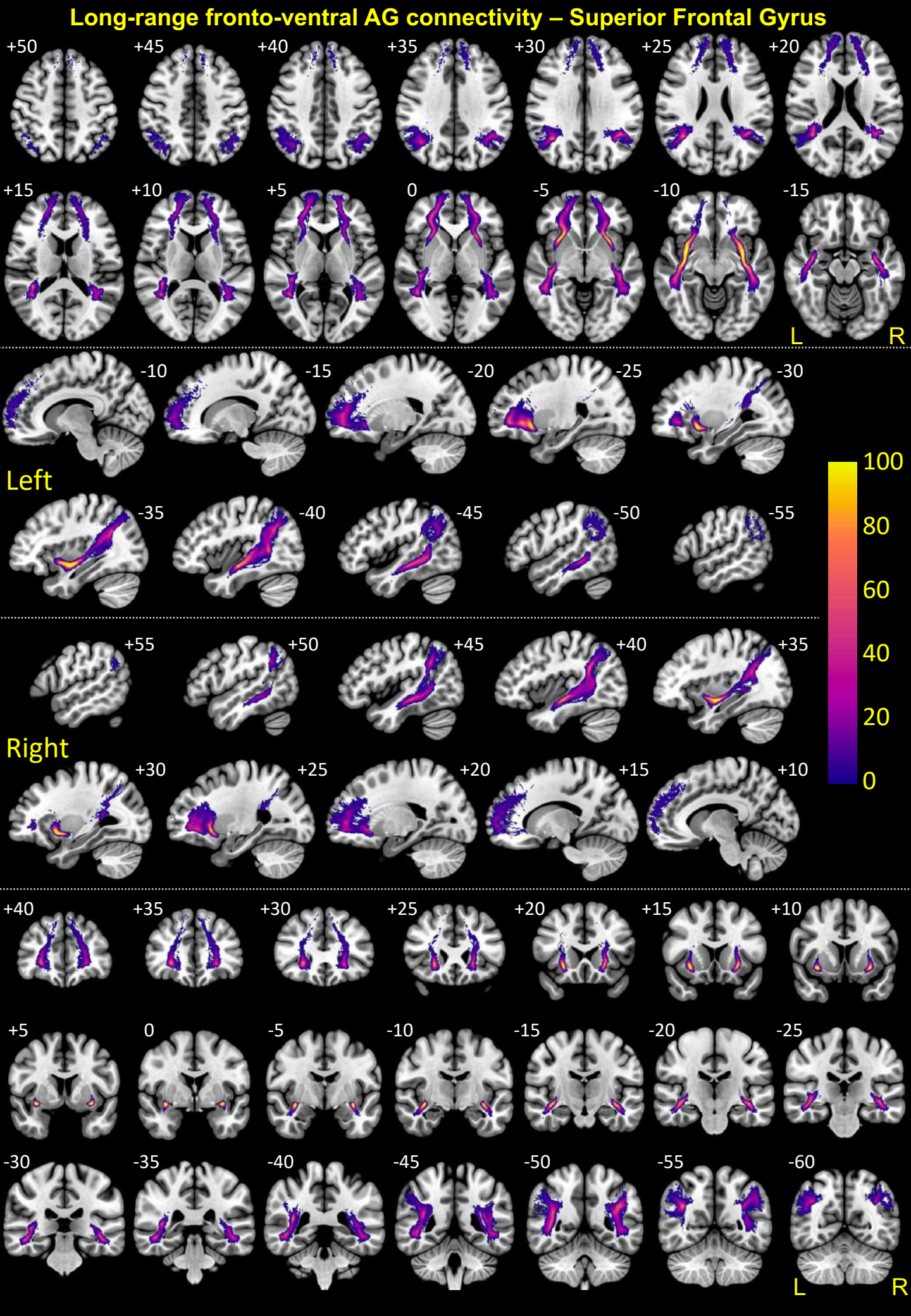
Long-range fronto-ventral AG connectivity – Superior Frontal Gyrus
+50
+45
+40
+35
+30
+25
+20
+15
+10
+5
0
-5
-10
-15
L
R
-10
-15
-20
-25
-30
Left
-35
-40
-45
-50
-55
+55
+50
+45
+40
+35
Right
+30
+25
+20
+15
+10
100
80
60
40
20
0
+40
+35
+30
+25
+20
+15
+10
+5
0
-5
-10
-15
-20
-25
-30
-35
-40
-45
-50
-55
-60
L
R

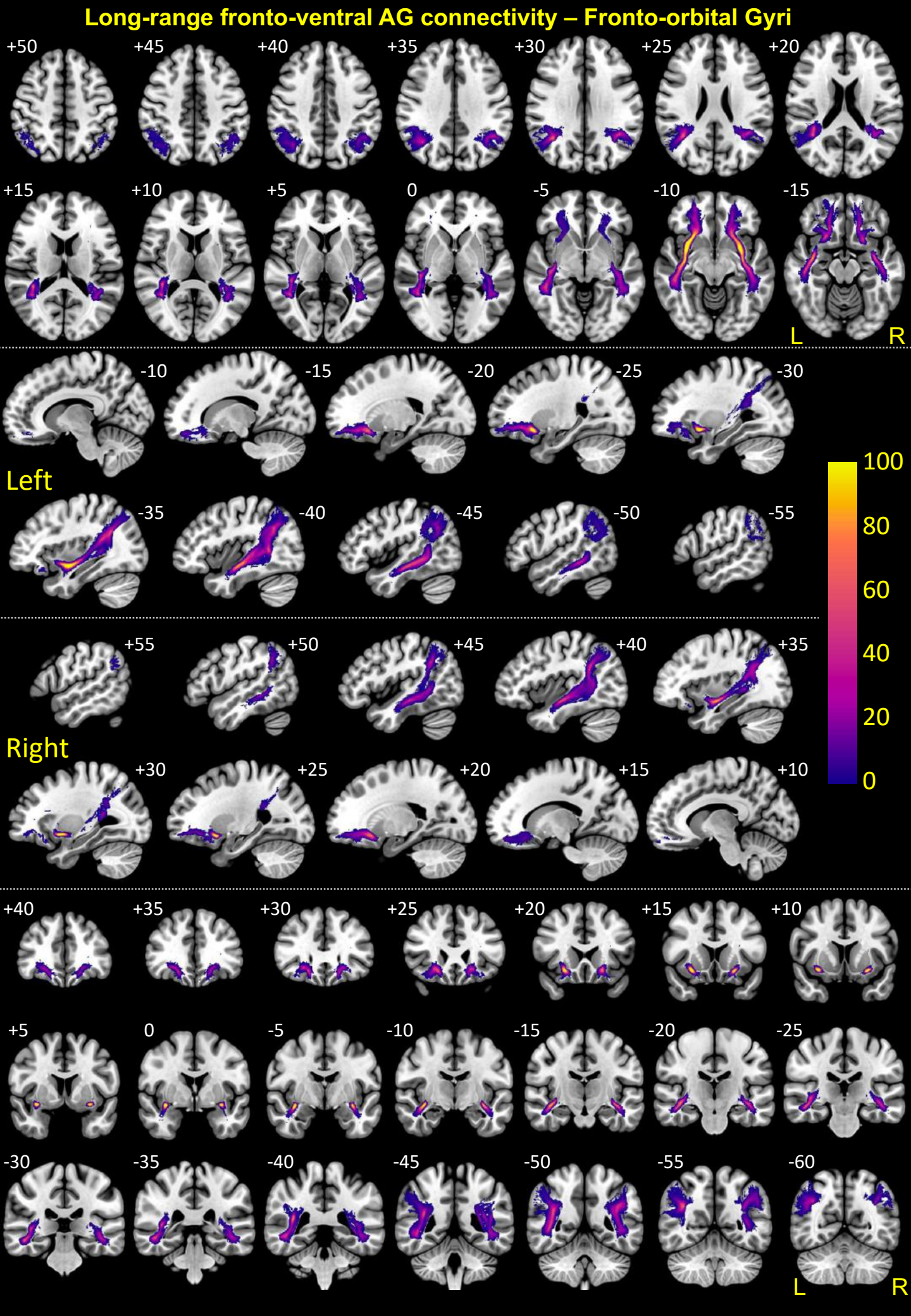
Long-range fronto-ventral AG connectivity – Fronto-orbital Gyri
+50
+45
+40
+35
+30
+25
+20
+15
+10
+5
0
-5
-10
-15
L
R
-10
-15
-20
-25
-30
Left
-35
-40
-45
-50
-55
+55
+50
+45
+40
+35
Right
+30
+25
+20
+15
+10
100
80
60
40
20
0
+40
+35
+30
+25
+20
+15
+10
+5
0
-5
-10
-15
-20
-25
-30
-35
-40
-45
-50
-55
-60
L
R

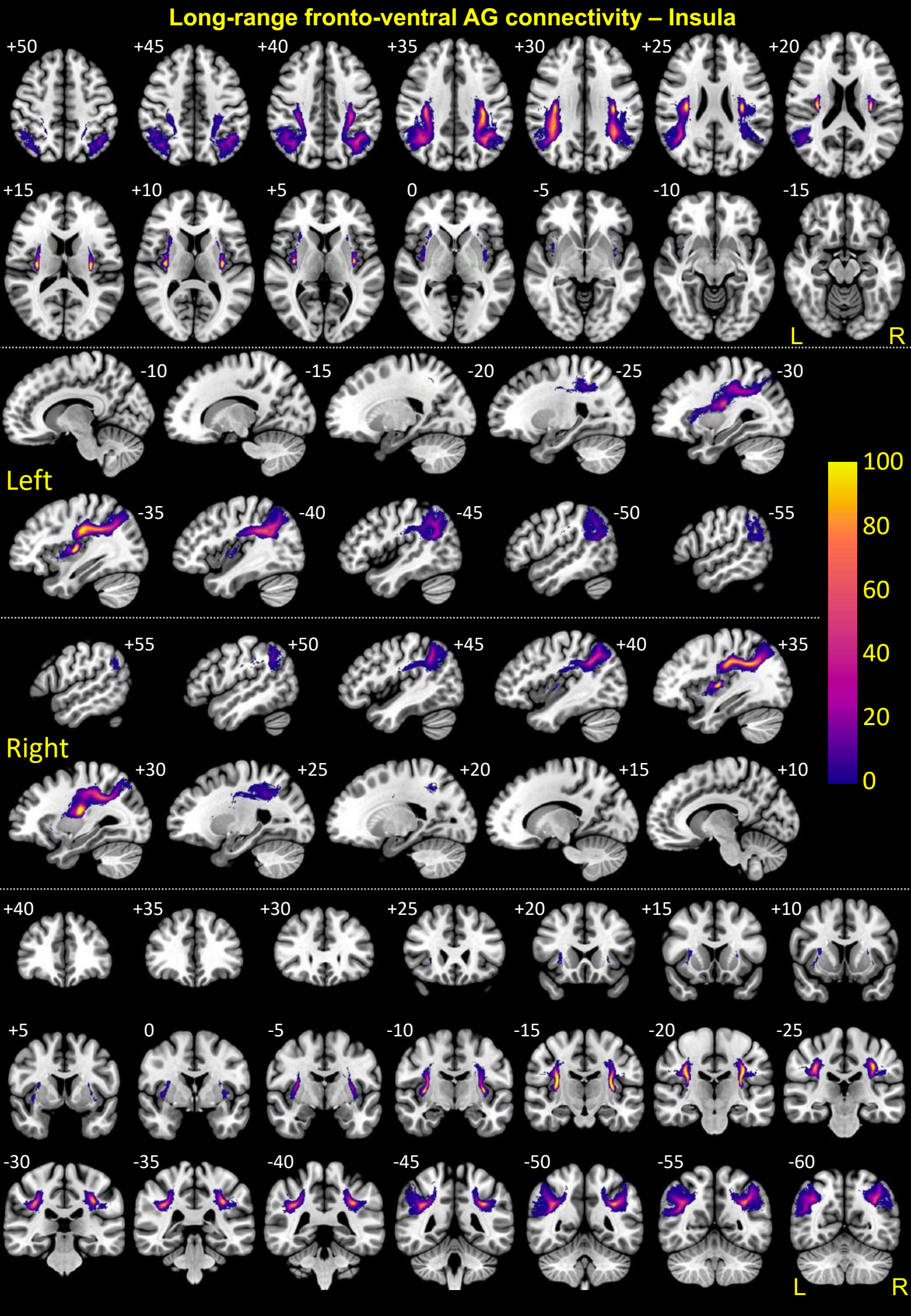
Long-range fronto-ventral AG connectivity – Insula
+50
+45
+40
+35
+30
+25
+20
+15
+10
+5
0
-5
-10
-15
L
R
-10
-15
-20
-25
-30
Left
-35
-40
-45
-50
-55
+55
+50
+45
+40
+35
Right
+30
+25
+20
+15
+10
100
80
60
40
20
0
+40
+35
+30
+25
+20
+15
+10
+5
0
-5
-10
-15
-20
-25
-30
-35
-40
-45
-50
-55
-60
L
R

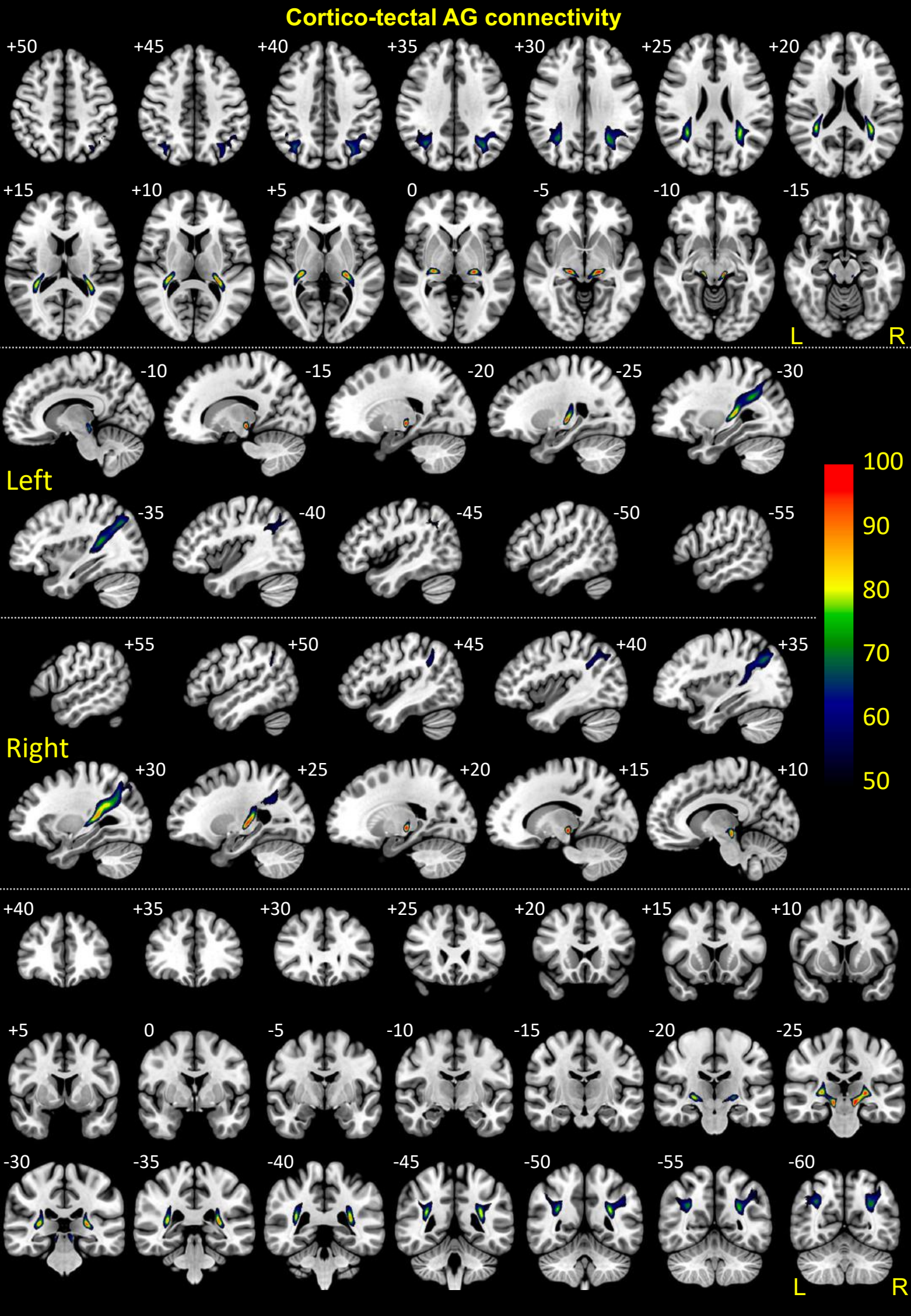
Cortico-tectal AG connectivity
+50
+45
+40
+35
+30
+25
+20
+15
+10
+5
0
-5
-10
-15
L
R
-10
-15
-20
-25
-30
Left
-35
-40
-45
-50
-55
+55
+50
+45
+40
+35
Right
+30
+25
+20
+15
+10
100
90
80
70
60
50
+40
+35
+30
+25
+20
+15
+10
+5
0
-5
-10
-15
-20
-25
-30
-35
-40
-45
-50
-55
-60
L
R

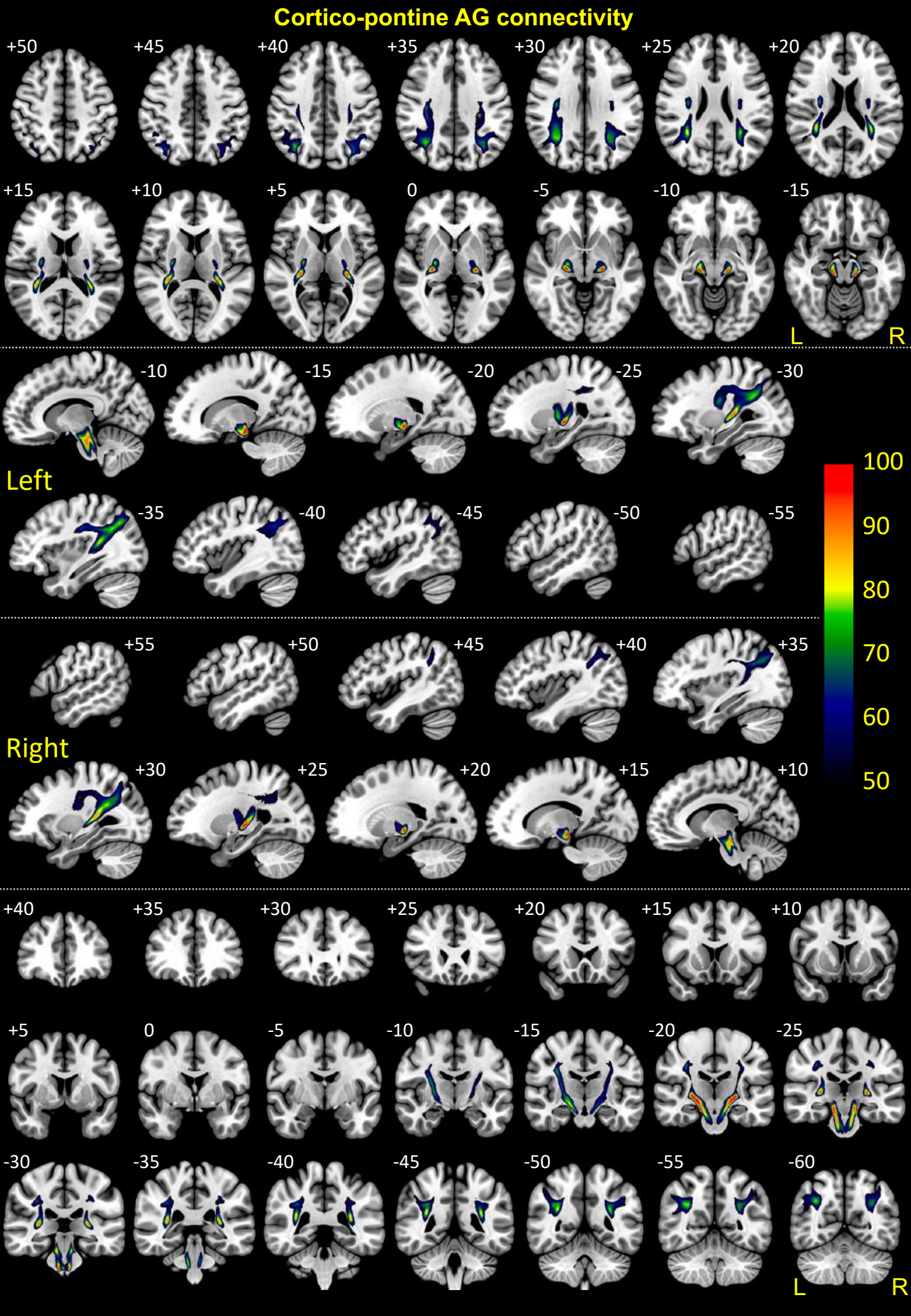
Cortico-pontine AG connectivity
+50
+45
+40
+35
+30
+25
+20
+15
+10
+5
0
-5
-10
-15
L
R
-10
-15
-20
-25
-30
Left
-35
-40
-45
-50
-55
+55
+50
+45
+40
+35
Right
+30
+25
+20
+15
+10
100
90
80
70
60
50
+40
+35
+30
+25
+20
+15
+10
+5
0
-5
-10
-15
-20
-25
-30
-35
-40
-45
-50
-55
-60
L
R

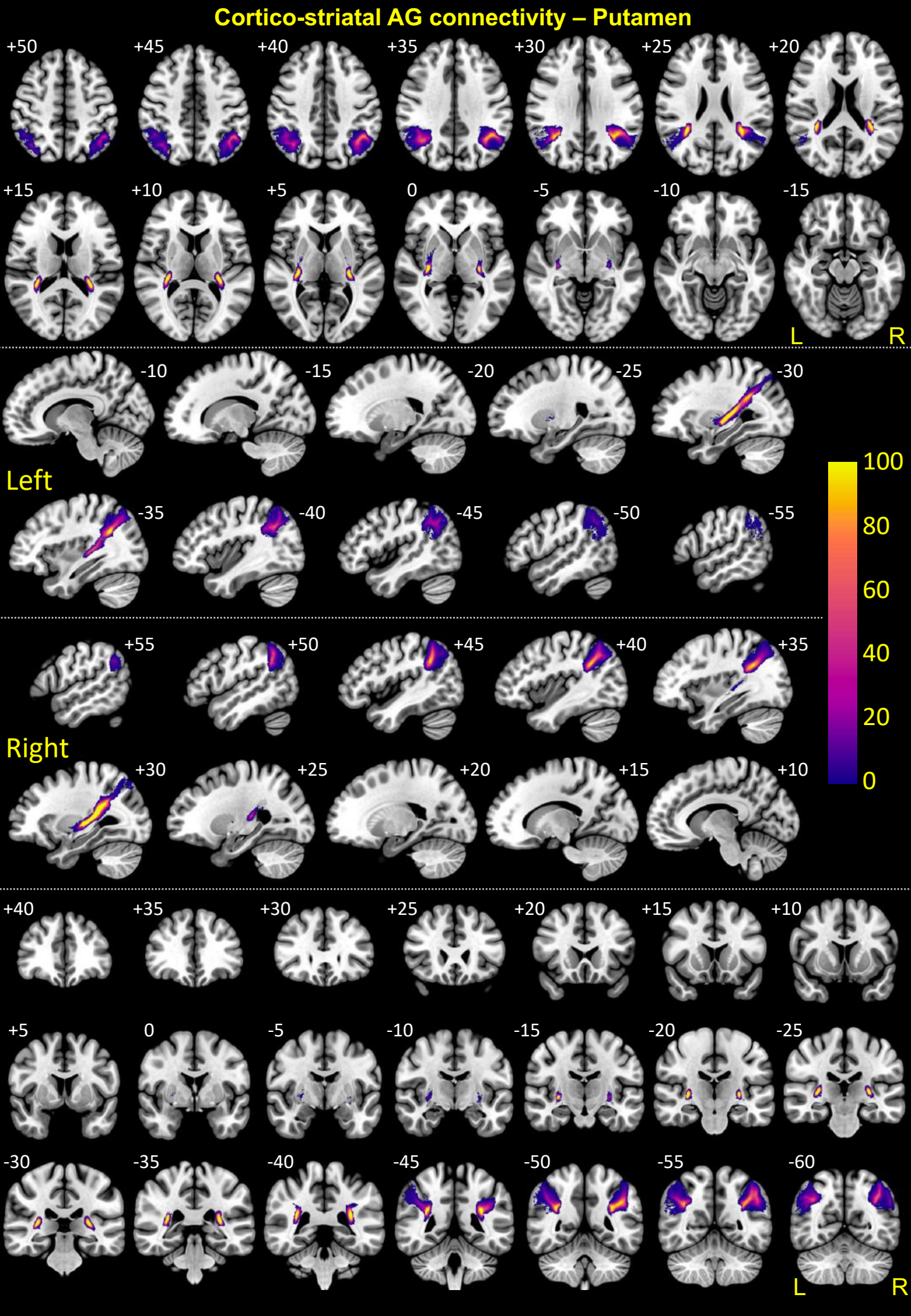
Cortico-striatal AG connectivity – Putamen
+50
+45
+40
+35
+30
+25
+20
+15
+10
+5
0
-5
-10
-15
L
R
-10
-15
-20
-25
-30
Left
-35
-40
-45
-50
-55
+55
+50
+45
+40
+35
Right
+30
+25
+20
+15
+10
100
80
60
40
20
0
+40
+35
+30
+25
+20
+15
+10
+5
0
-5
-10
-15
-20
-25
-30
-35
-40
-45
-50
-55
-60
L
R

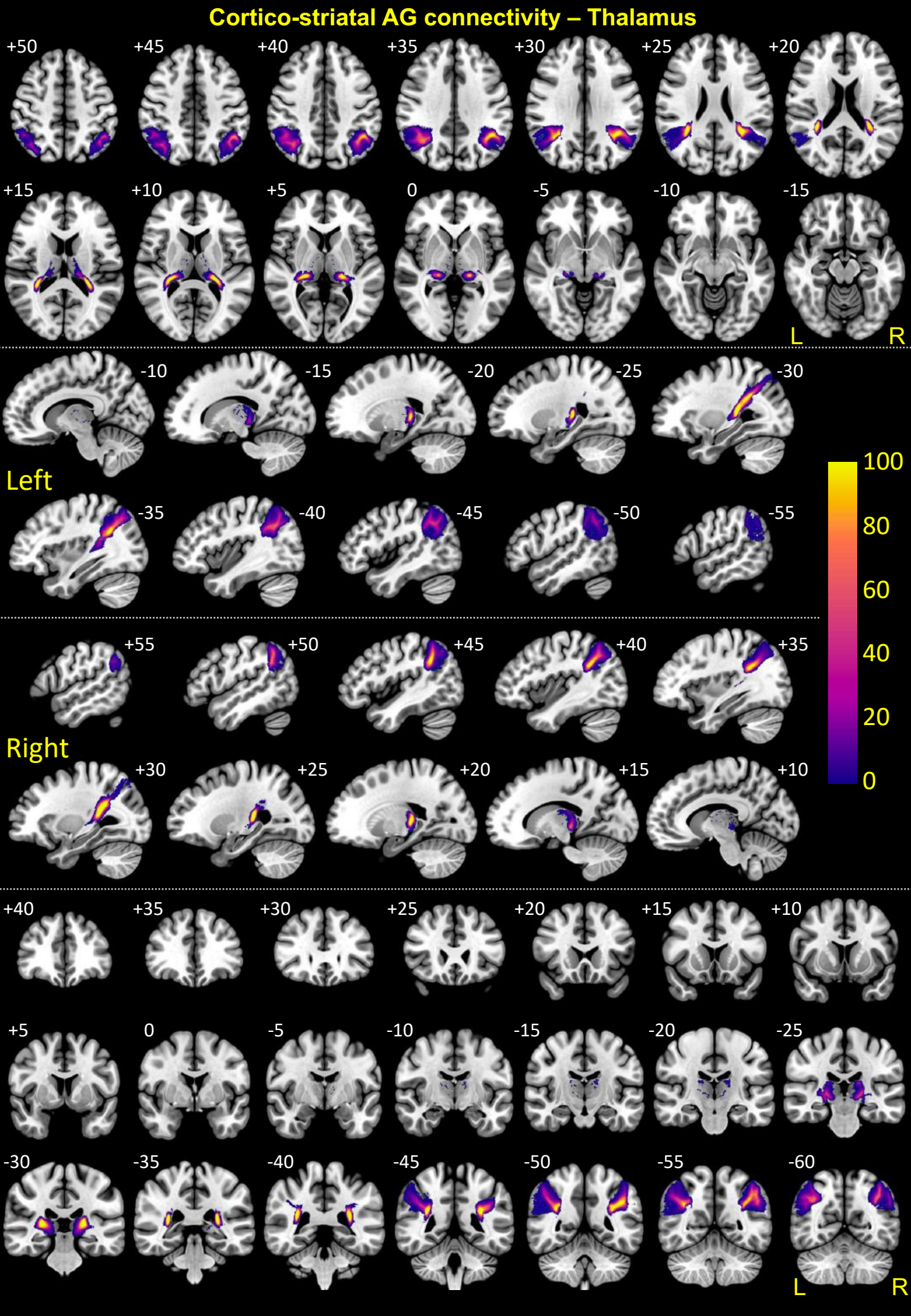
Cortico-striatal AG connectivity – Thalamus
+50
+45
+40
+35
+30
+25
+20
+15
+10
+5
0
-5
-10
-15
L
R
-10
-15
-20
-25
-30
Left
-35
-40
-45
-50
-55
+55
+50
+45
+40
+35
Right
+30
+25
+20
+15
+10
100
80
60
40
20
0
+40
+35
+30
+25
+20
+15
+10
+5
0
-5
-10
-15
-20
-25
-30
-35
-40
-45
-50
-55
-60
L
R

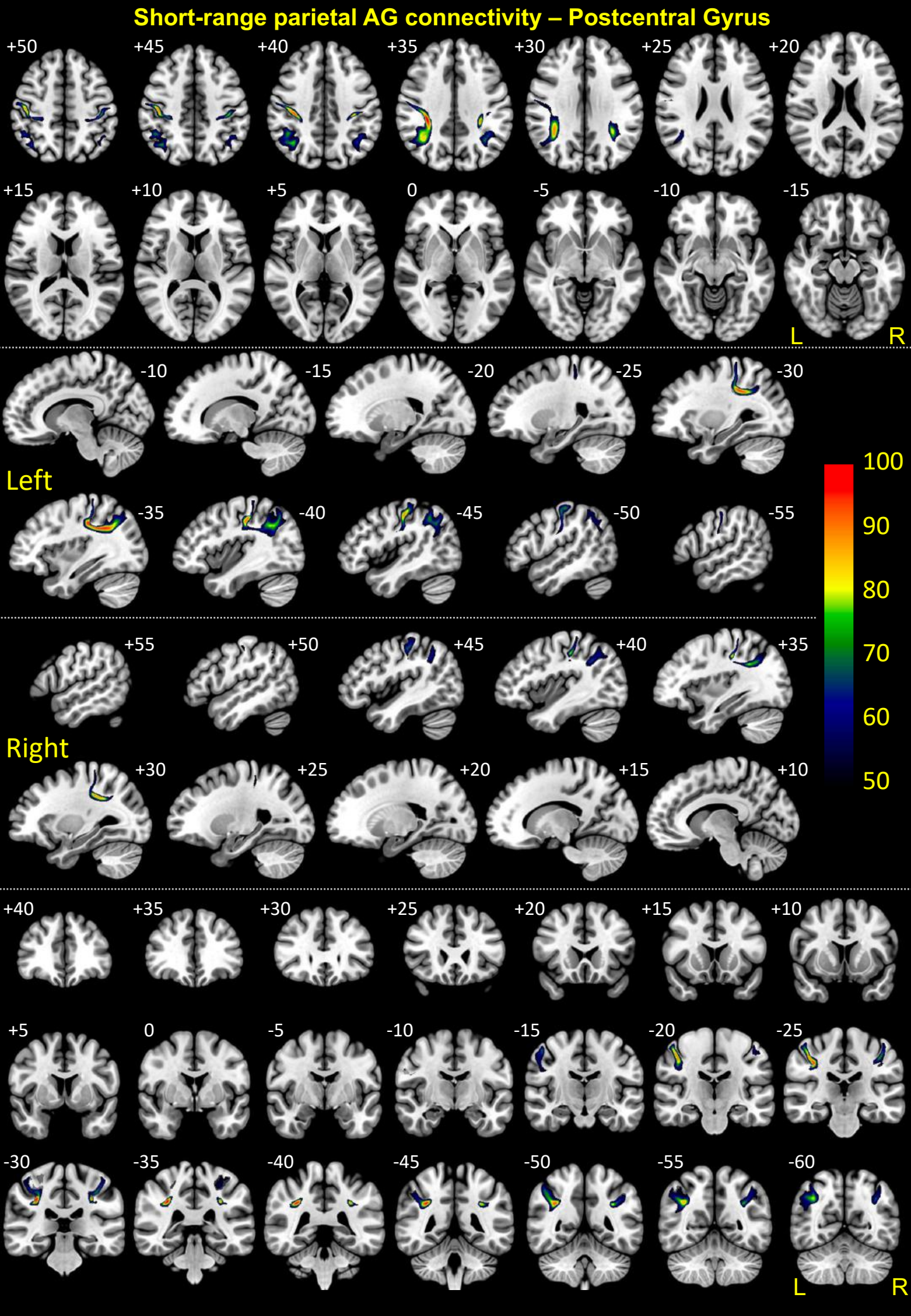
Short-range parietal AG connectivity – Postcentral Gyrus
+50
+45
+40
+35
+30
+25
+20
+15
+10
+5
0
-5
-10
-15
L
R
-10
-15
-20
-25
-30
Left
-35
-40
-45
-50
-55
100
90
80
70
60
50
+55
+50
+45
+40
+35
Right
+30
+25
+20
+15
+10
+40
+35
+30
+25
+20
+15
+10
+5
0
-5
-10
-15
-20
-25
-30
-35
-40
-45
-50
-55
-60
L
R

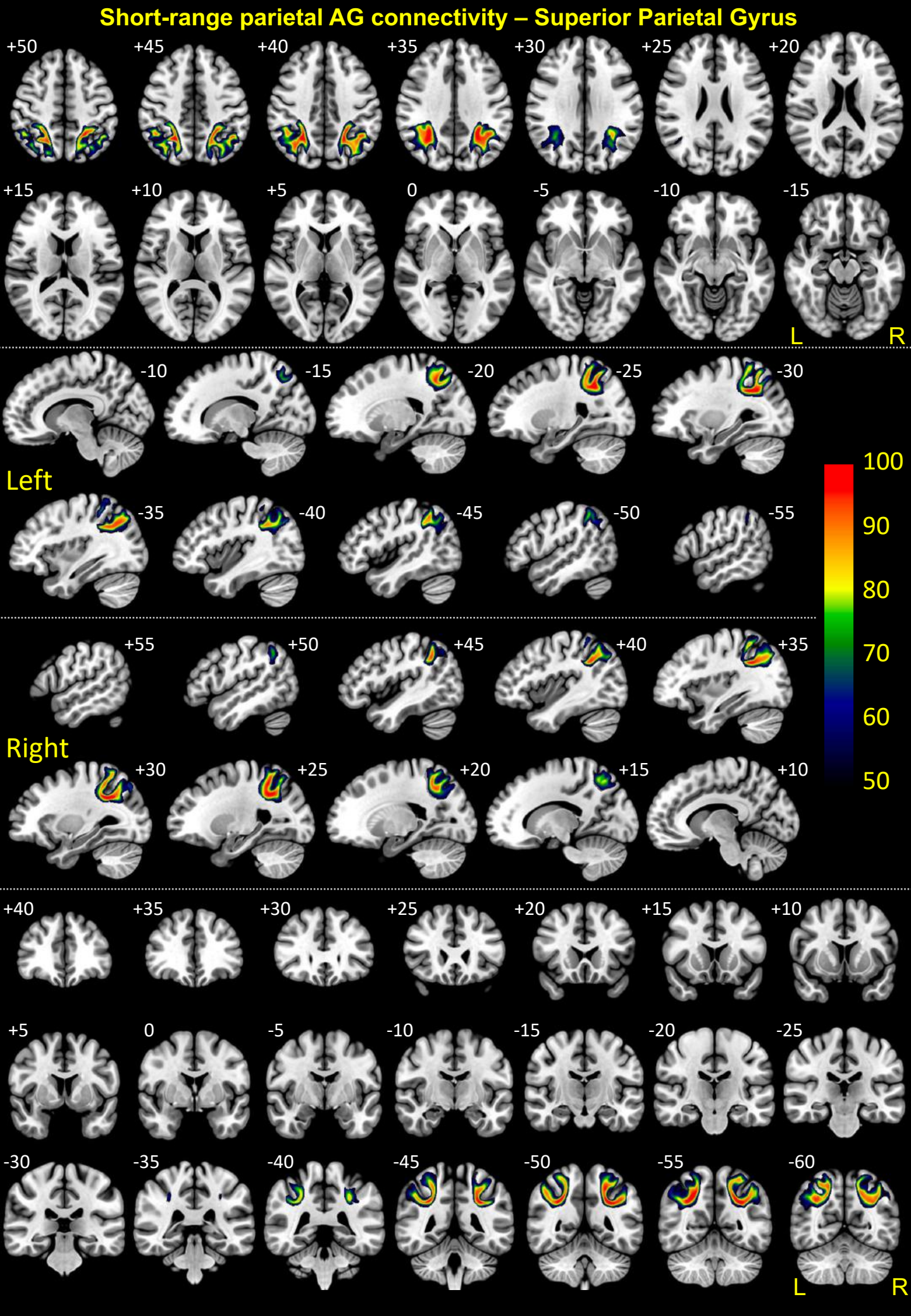
Short-range parietal AG connectivity – Superior Parietal Gyrus
+50
+45
+40
+35
+30
+25
+20
+15
+10
+5
0
-5
-10
-15
L
R
-10
-15
-20
-25
-30
Left
-35
-40
-45
-50
-55
100
90
80
70
60
50
+55
+50
+45
+40
+35
Right
+30
+25
+20
+15
+10
+40
+35
+30
+25
+20
+15
+10
+5
0
-5
-10
-15
-20
-25
-30
-35
-40
-45
-50
-55
-60
L
R

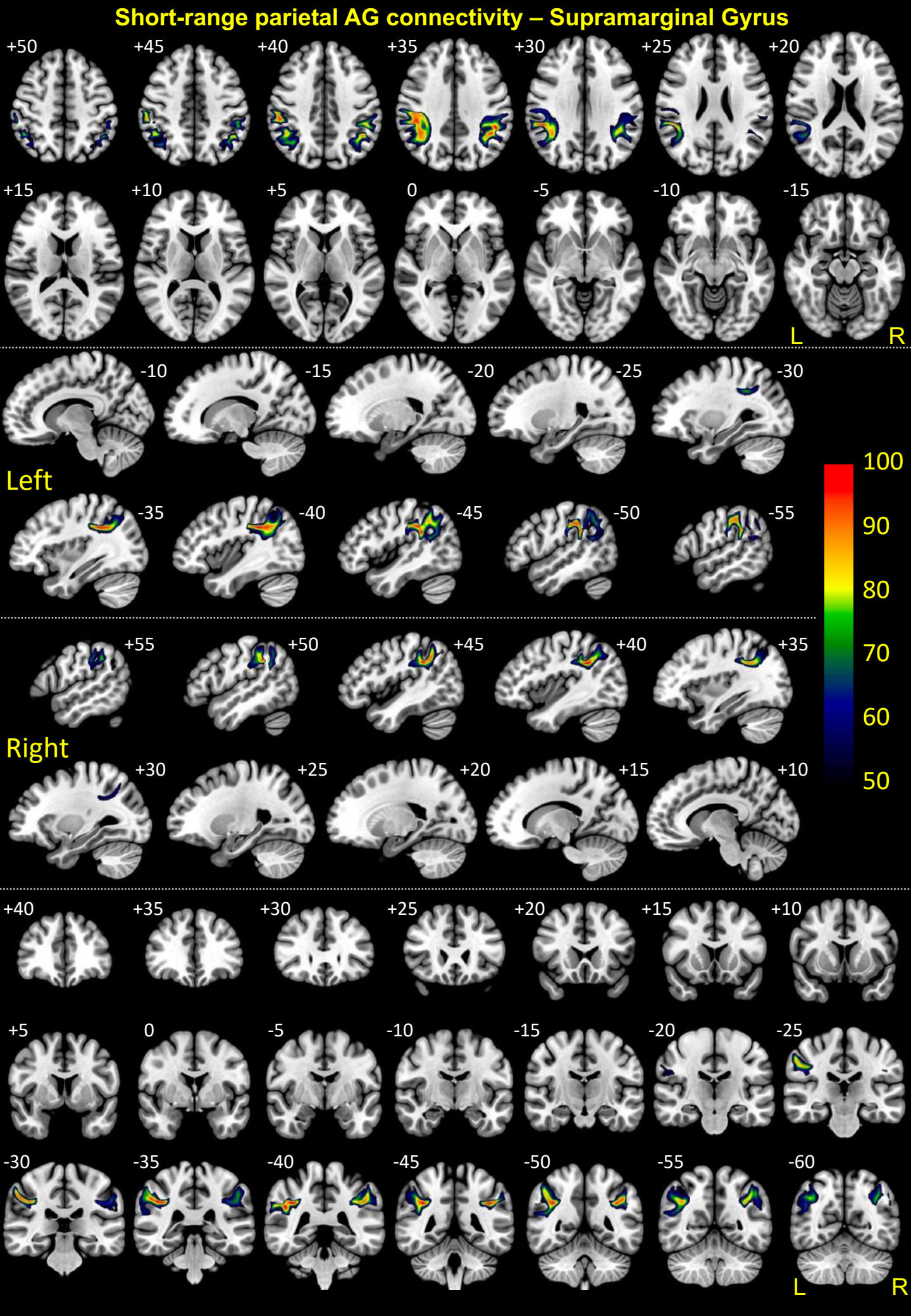
Short-range parietal AG connectivity – Supramarginal Gyrus
+50
+45
+40
+35
+30
+25
+20
+15
+10
+5
0
-5
-10
-15
L
R
-10
-15
-20
-25
-30
Left
-35
-40
-45
-50
-55
100
90
80
70
60
50
+55
+50
+45
+40
+35
Right
+30
+25
+20
+15
+10
+40
+35
+30
+25
+20
+15
+10
+5
0
-5
-10
-15
-20
-25
-30
-35
-40
-45
-50
-55
-60
L
R

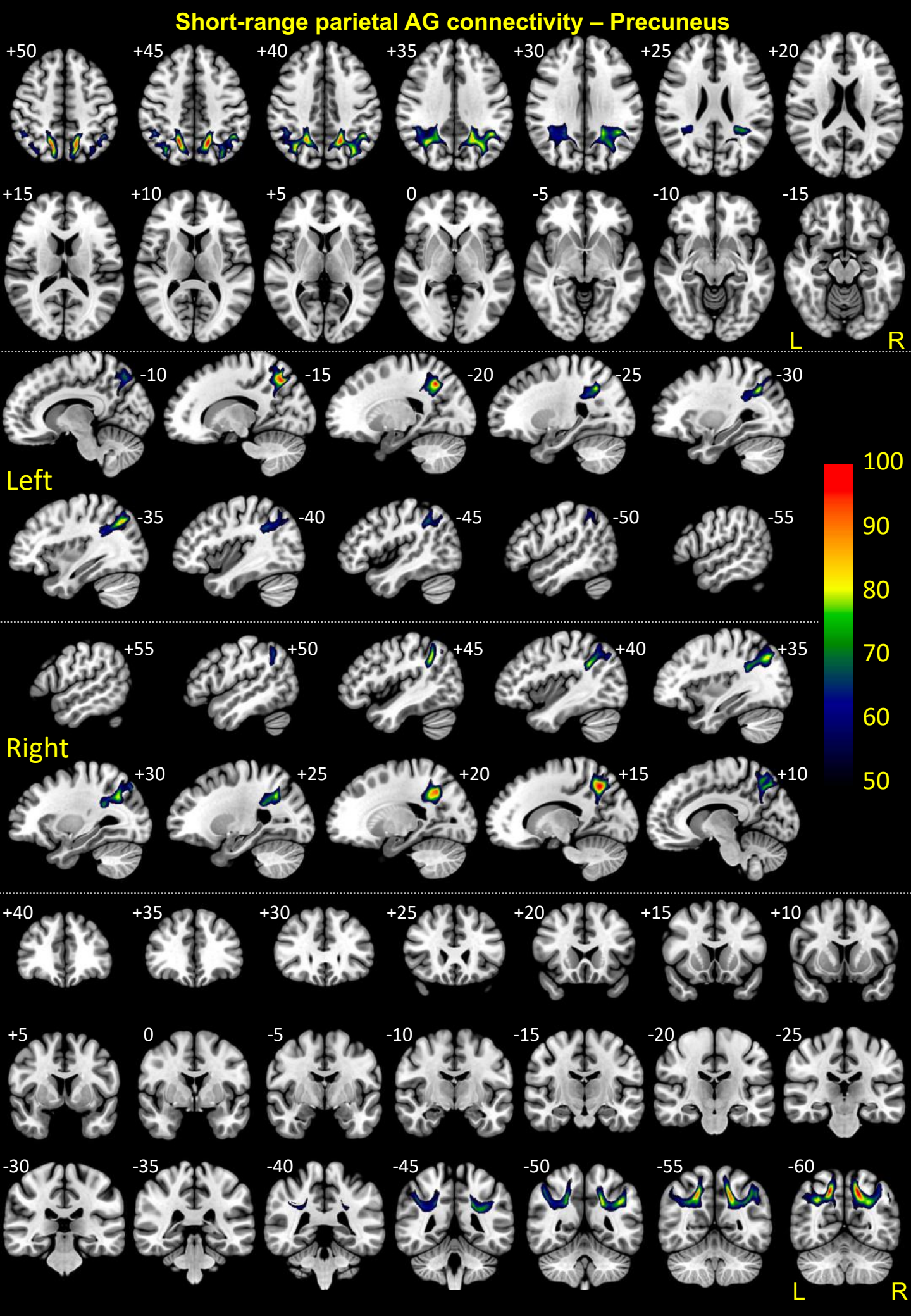
Short-range parietal AG connectivity – Precuneus
+50
+45
+40
+35
+30
+25
+20
+15
+10
+5
0
-5
-10
-15
L
R
-10
-15
-20
-25
-30
Left
-35
-40
-45
-50
-55
+55
+50
+45
+40
+35
Right
+30
+25
+20
+15
+10
100
90
80
70
60
50
+40
+35
+30
+25
+20
+15
+10
+5
0
-5
-10
-15
-20
-25
-30
-35
-40
-45
-50
-55
-60
L
R

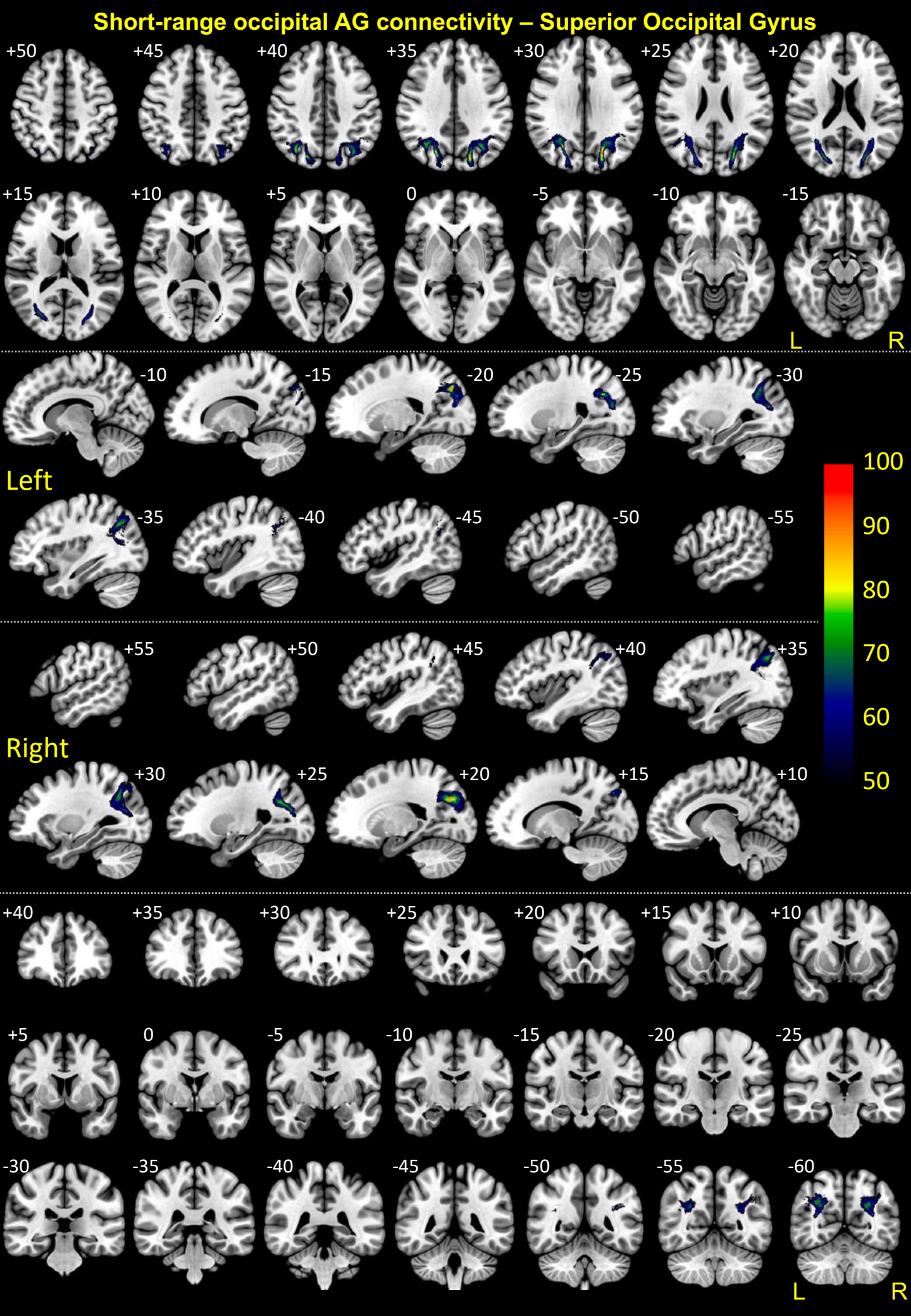
Short-range occipital AG connectivity – Superior Occipital Gyrus
+50
+45
+40
+35
+30
+25
+20
+15
+10
+5
0
-5
-10
-15
L
R
-10
-15
-20
-25
-30
Left
-35
-40
-45
-50
-55
+55
+50
+45
+40
+35
Right
+30
+25
+20
+15
+10
100
90
80
70
60
50
+40
+35
+30
+25
+20
+15
+10
+5
0
-5
-10
-15
-20
-25
-30
-35
-40
-45
-50
-55
-60
L
R

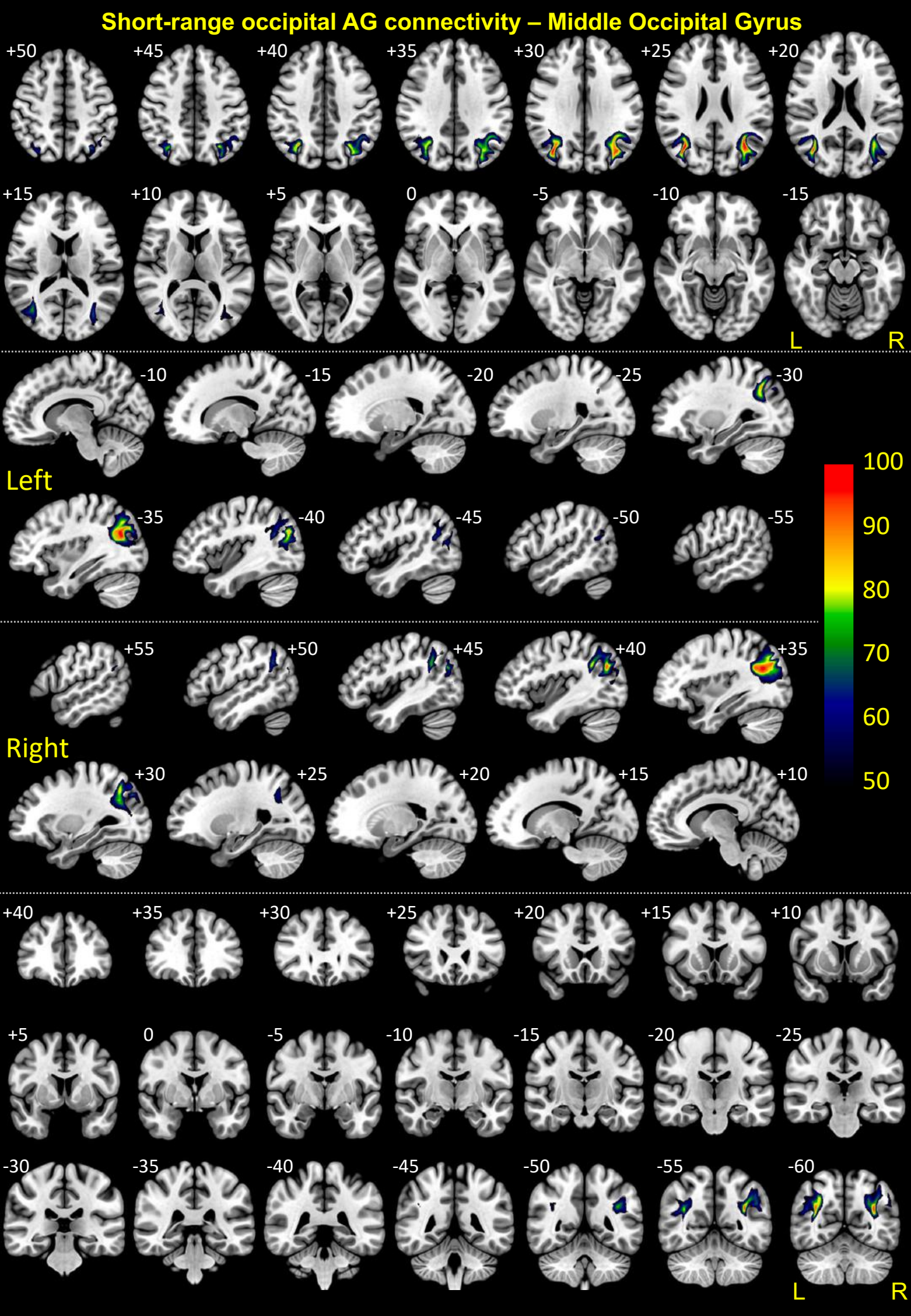
Short-range occipital AG connectivity – Middle Occipital Gyrus
+50
+45
+40
+35
+30
+25
+20
+15
+10
+5
0
-5
-10
-15
L
R
-10
-15
-20
-25
-30
Left
-35
-40
-45
-50
-55
+55
+50
+45
+40
+35
Right
+30
+25
+20
+15
+10
100
90
80
70
60
50
+40
+35
+30
+25
+20
+15
+10
+5
0
-5
-10
-15
-20
-25
-30
-35
-40
-45
-50
-55
-60
L
R

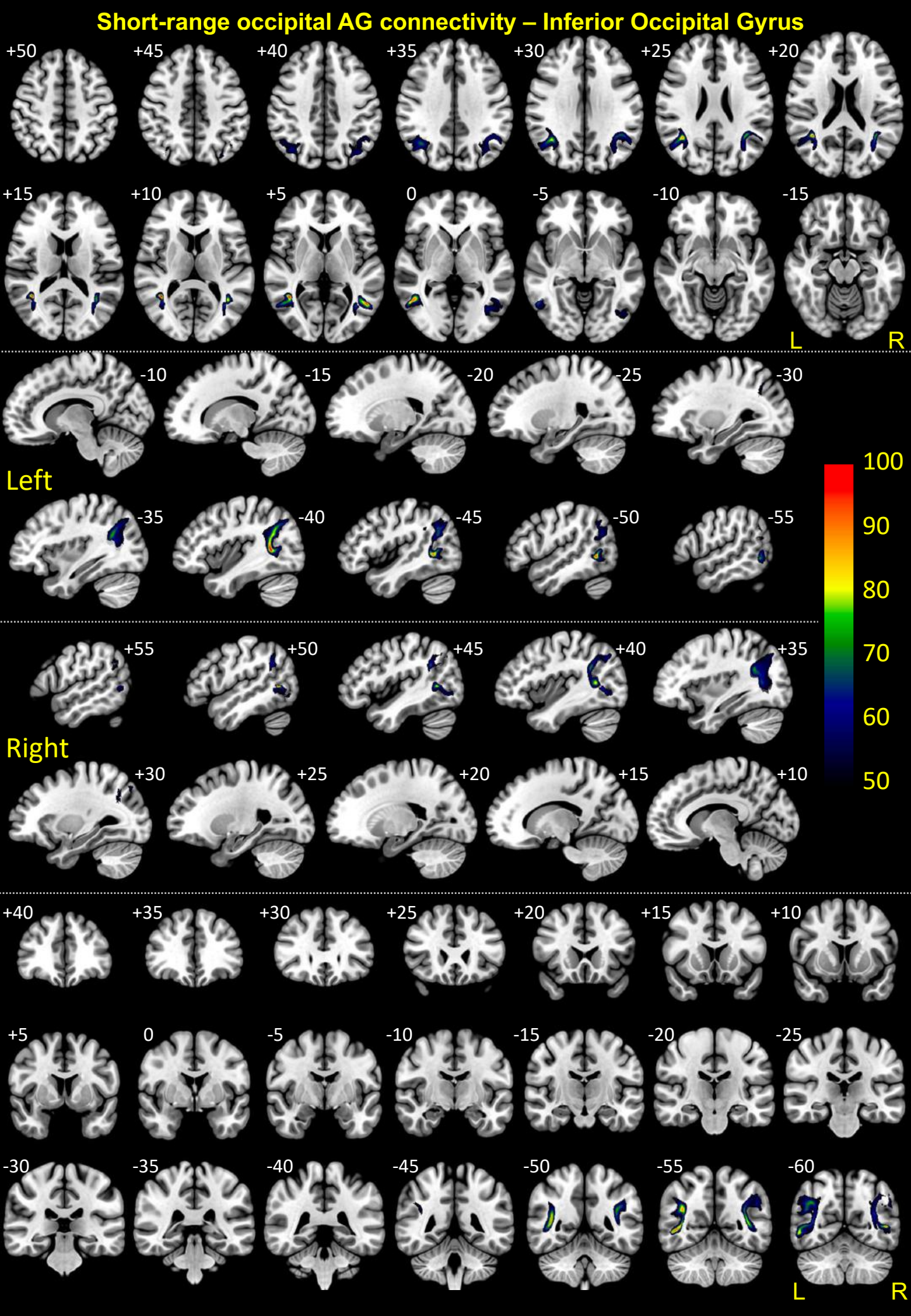
Short-range occipital AG connectivity – Inferior Occipital Gyrus
+50
+45
+40
+35
+30
+25
+20
+15
+10
+5
0
-5
-10
-15
L
R
-10
-15
-20
-25
-30
Left
-35
-40
-45
-50
-55
+55
+50
+45
+40
+35
Right
+30
+25
+20
+15
+10
100
90
80
70
60
50
+40
+35
+30
+25
+20
+15
+10
+5
0
-5
-10
-15
-20
-25
-30
-35
-40
-45
-50
-55
-60
L
R

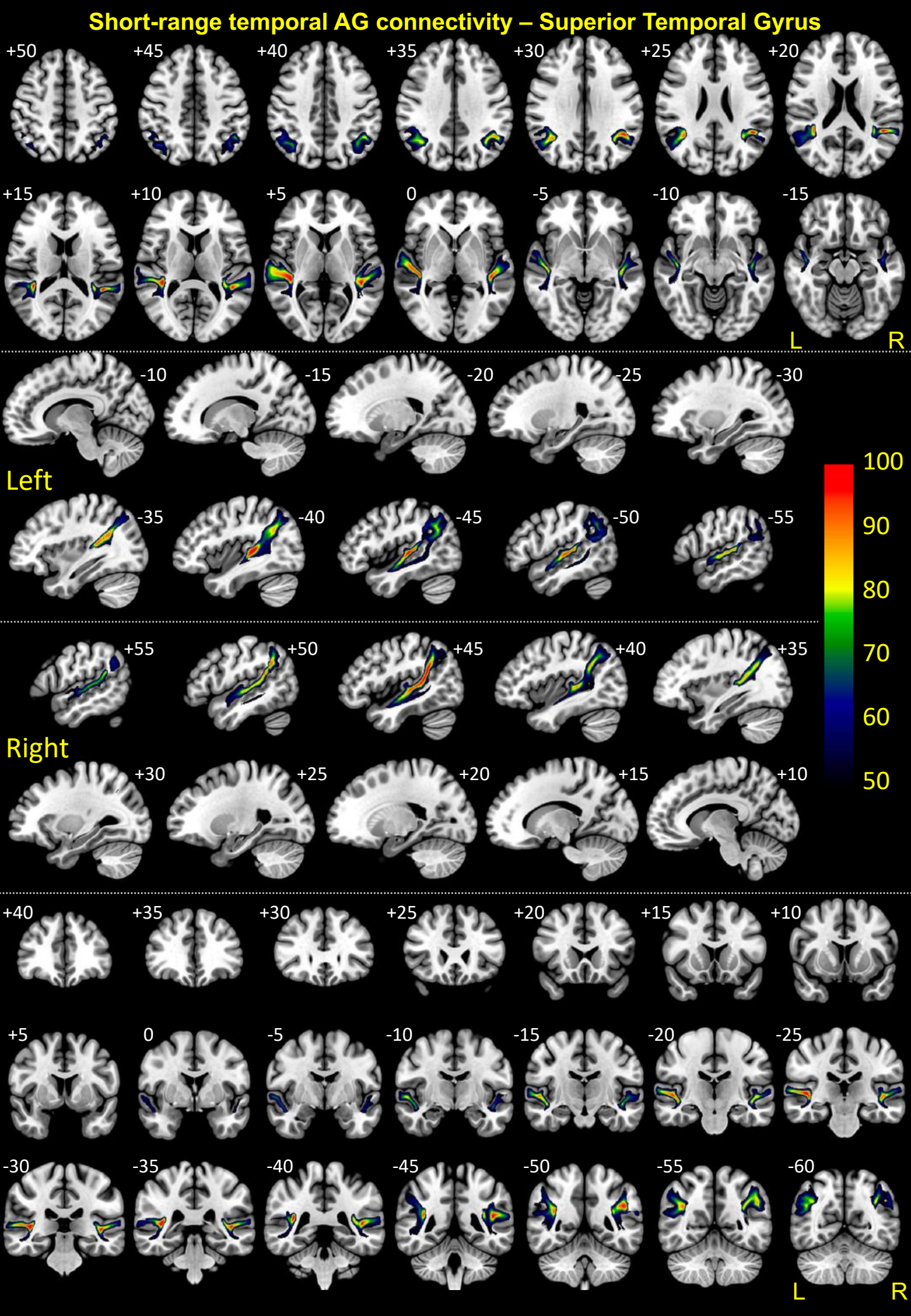
Short-range temporal AG connectivity – Superior Temporal Gyrus
+50
+45
+40
+35
+30
+25
+20
+15
+10
+5
0
-5
-10
-15
L
R
-10
-15
-20
-25
-30
Left
-35
-40
-45
-50
-55
+55
+50
+45
+40
+35
Right
+30
+25
+20
+15
+10
100
90
80
70
60
50
+40
+35
+30
+25
+20
+15
+10
+5
0
-5
-10
-15
-20
-25
-30
-35
-40
-45
-50
-55
-60
L
R

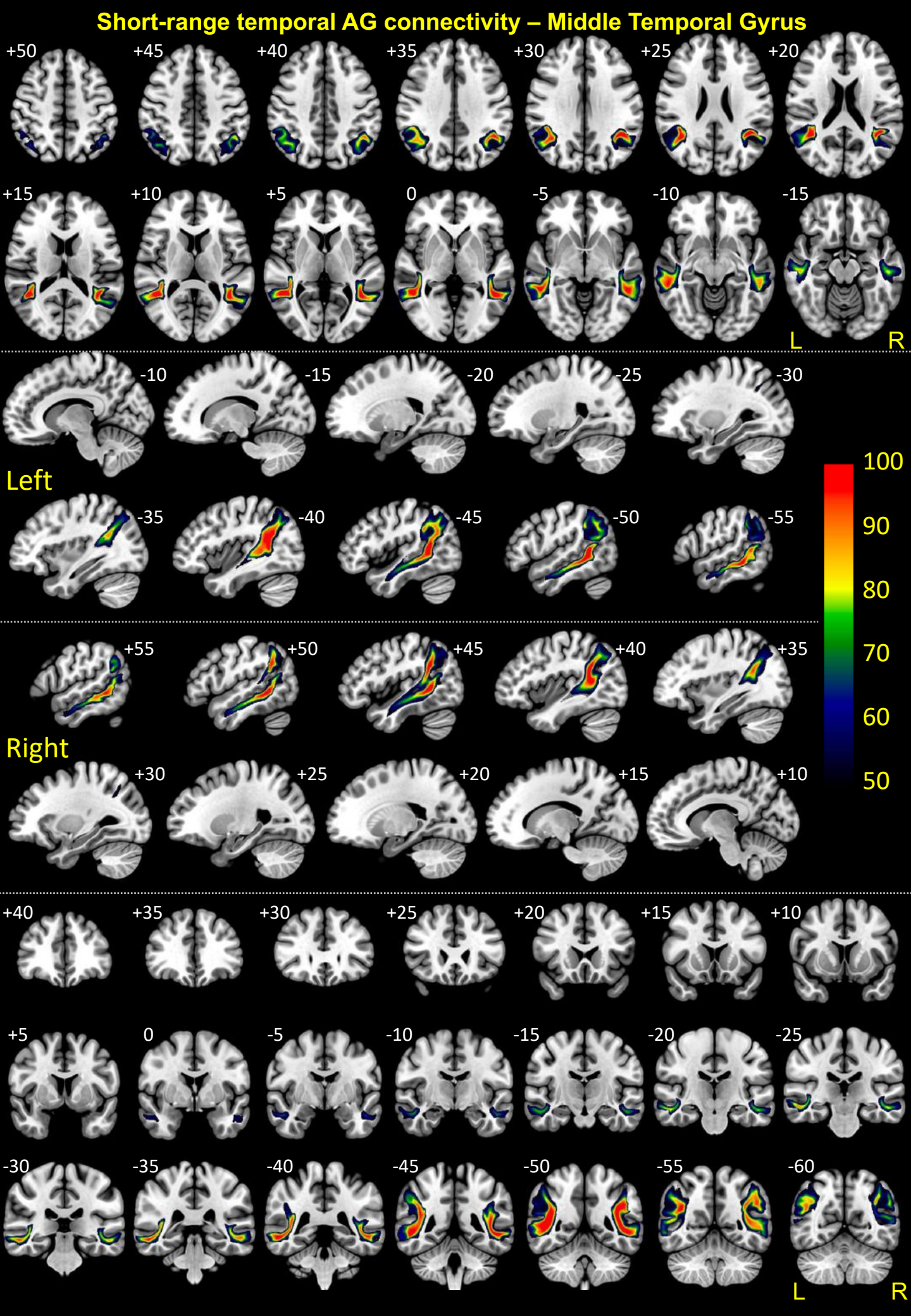
Short-range temporal AG connectivity – Middle Temporal Gyrus
+50
+45
+40
+35
+30
+25
+20
+15
+10
+5
0
-5
-10
-15
L
R
-10
-15
-20
-25
-30
Left
-35
-40
-45
-50
-55
+55
+50
+45
+40
+35
Right
+30
+25
+20
+15
+10
100
90
80
70
60
50
+40
+35
+30
+25
+20
+15
+10
+5
0
-5
-10
-15
-20
-25
-30
-35
-40
-45
-50
-55
-60
L
R

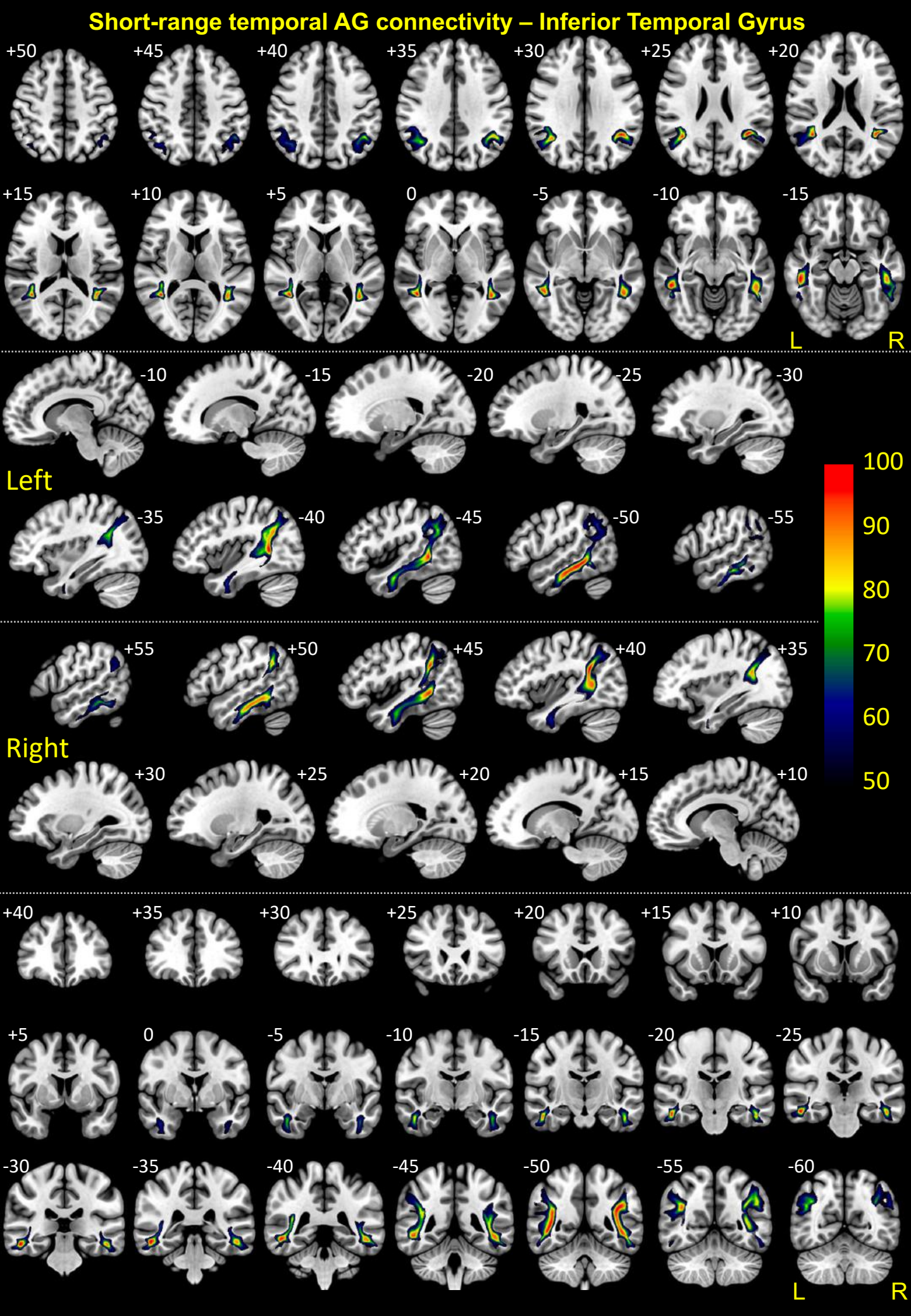
Short-range temporal AG connectivity – Inferior Temporal Gyrus
+50
+45
+40
+35
+30
+25
+20
+15
+10
+5
0
-5
-10
-15
L
R
-10
-15
-20
-25
-30
Left
-35
-40
-45
-50
-55
+55
+50
+45
+40
+35
Right
+30
+25
+20
+15
+10
100
90
80
70
60
50
+40
+35
+30
+25
+20
+15
+10
+5
0
-5
-10
-15
-20
-25
-30
-35
-40
-45
-50
-55
-60
L
R

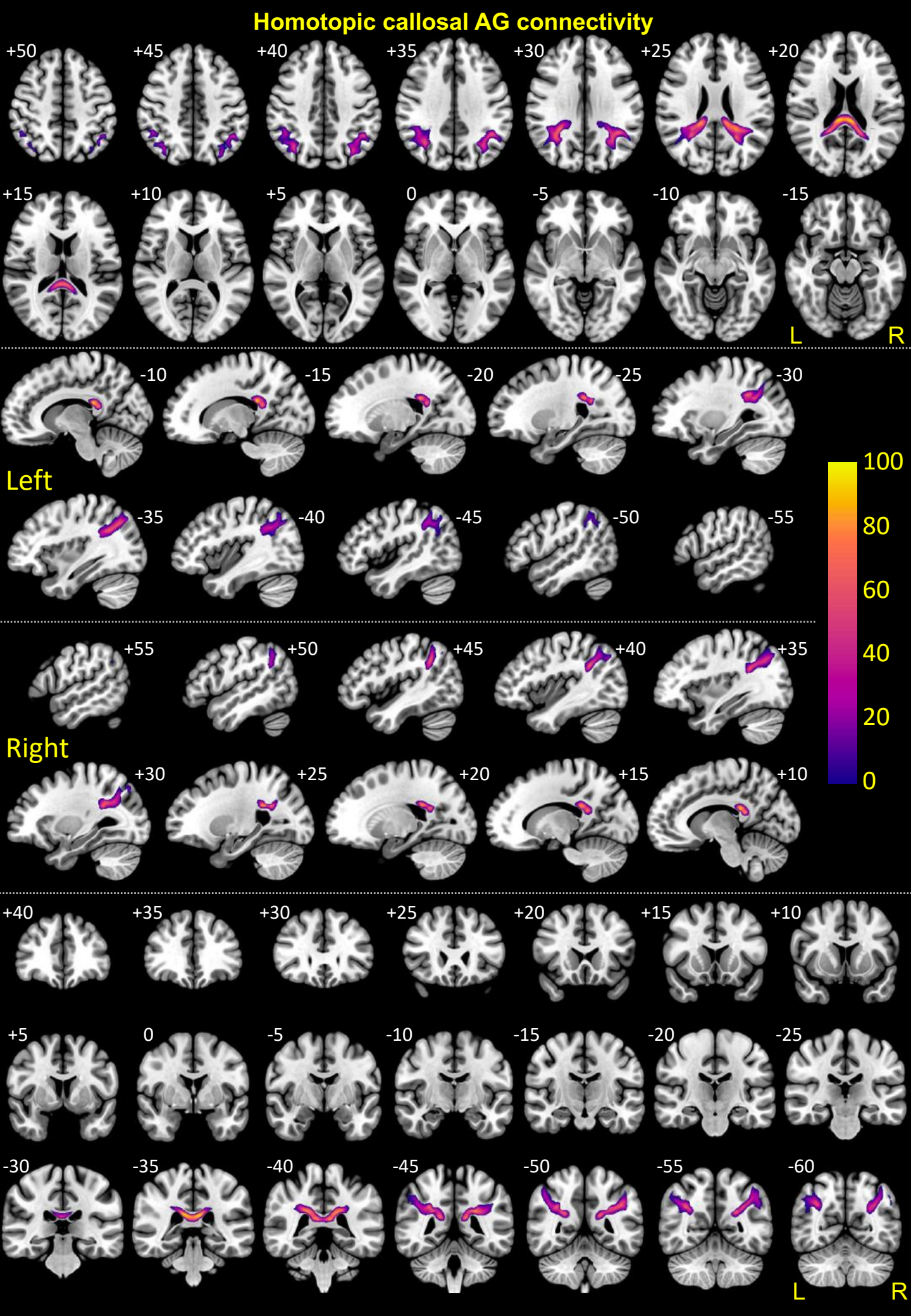
Homotopic callosal AG connectivity
+50
+45
+40
+35
+30
+25
+20
+15
+10
+5
0
-5
-10
-15
L
R
-10
-15
-20
-25
-30
Left
-35
-40
-45
-50
-55
+55
+50
+45
+40
+35
Right
+30
+25
+20
+15
+10
100
80
60
40
20
0
+40
+35
+30
+25
+20
+15
+10
+5
0
-5
-10
-15
-20
-25
-30
-35
-40
-45
-50
-55
-60
L
R

Table 1. Mean (± standard deviation) of MNI coordinates of the AG tracts

			Angular gyrus			Opposite termination		
			X	Y	Z	X	Y	Z
Long-range fronto-dorsal	IFG	L	-45.0 ± 3.2	-58.7 ± 3.0	+43.5 ± 3.4	-49.3 ± 1.7	+18.0 ± 3.4	+11.7 ± 3.0
		R	+47.4 ± 2.6	-56.7 ± 2.8	+40.3 ± 3.9	+50.5 ± 2.0	+23.5 ± 3.9	+9.5 ± 3.8
	MFG	L	-41.7 ± 2.8	-60.7 ± 2.9	+45.9 ± 2.5	-38.7 ± 2.0	+17.6 ± 6.8	+41.0 ± 7.5
		R	+44.7 ± 2.8	-59.4 ± 2.9	+41.7 ± 3.9	+40.1 ± 1.9	+25.5 ± 7.5	+33.3 ± 8.5
	PrCG	L	-42.5 ± 2.7	-59.9 ± 2.8	+45.3 ± 2.5	-47.8 ± 5.1	-6.1 ± 3.9	+40.1 ± 8.2
		R	+44.1 ± 2.5	-58.7 ± 2.8	+43.1 ± 3.2	+50.4 ± 3.3	-2.1 ± 2.7	+38.1 ± 5.7
Long-range fronto-ventral	IFG	L	-47.1 ± 3.4	-59.5 ± 3.2	+41.3 ± 4.5	-45.4 ± 1.6	+32.9 ± 2.0	-4.7 ± 2.6
		R	+46.3 ± 3.5	-61.4 ± 3.2	+38.1 ± 4.9	+45.6 ± 2.5	+32.9 ± 2.2	-5.7 ± 3.1
	MFG	L	-47.2 ± 3.2	-59.8 ± 2.3	+39.9 ± 4.2	-36.3 ± 2.0	+50.9 ± 2.9	+2.5 ± 7.1
		R	+47.4 ± 3.4	-60.2 ± 3.6	+37.6 ± 4.4	+38.0 ± 2.2	+52.3 ± 2.2	-3.4 ± 4.8
	SFG	L	-46.6 ± 2.9	-59.6 ± 2.7	+41.4 ± 3.8	-12.6 ± 2.2	+59.6 ± 4.0	+14.2 ± 8.9
		R	+47.0 ± 3.6	-60.8 ± 3.3	+37.4 ± 5.3	+13.9 ± 2.1	+62.3 ± 2.8	+9.4 ± 7.0
	FrOrb	L	-47.1 ± 3.3	-59.3 ± 2.6	+40.8 ± 4.2	-20.6 ± 2.0	+36.7 ± 6.1	-14.9 ± 1.5
		R	+46.8 ± 3.5	-60.7 ± 3.6	+38.0 ± 5.1	+22.6 ± 2.8	+37.3 ± 5.0	-14.4 ± 1.6
	Insula	L	-41.6 ± 3.3	-59.9 ± 8.8	+44.6 ± 7.1	-35.1 ± 1.7	-12.0 ± 7.6	+7.9 ± 7.0
		R	+46.4 ± 3.8	-59.4 ± 4.7	+38.1 ± 5.9	+35.7 ± 1.2	-10.5 ± 3.9	+7.4 ± 3.3
Short-range Parietal	PoCG	L	-42.9 ± 3.3	-60.1 ± 4.0	+45.6 ± 3.5	-43.3 ± 6.2	-26.5 ± 4.2	+54.8 ± 6.2
		R	+43.9 ± 3.0	-58.9 ± 3.3	+44.5 ± 3.3	+45.8 ± 4.9	-22.5 ± 4.0	+51.6 ± 4.6
	PrCu	L	-38.7 ± 4.2	-66.4 ± 4.2	+46.7 ± 2.5	-9.9 ± 1.2	-67.6 ± 2.9	+52.4 ± 4.0
		R	+39.5 ± 4.5	-65.5 ± 5.0	+46.4 ± 2.8	+11.2 ± 0.9	-67.8 ± 3.6	+52.6 ± 4.7
	SMG	L	-45.8 ± 3.5	-57.1 ± 3.1	+43.5 ± 4.1	-53.6 ± 3.6	-38.1 ± 3.4	+41.4 ± 3.9
		R	+48.9 ± 3.5	-54.3 ± 3.3	+38.6 ± 6.1	+58.1 ± 2.2	-34.0 ± 3.4	+36.9 ± 5.4
	SPG	L	-39.6 ± 2.9	-62.1 ± 3.4	+46.9 ± 2.0	-25.3 ± 2.6	-60.1 ± 3.8	+56.3 ± 2.0
		R	+41.4 ± 3.4	-59.9 ± 4.5	+45.7 ± 2.3	+25.6 ± 2.3	-59.5 ± 3.9	+56.5 ± 2.1
Short-range Occipital	SOG	L	-35.4 ± 4.4	-70.0 ± 3.7	+44.1 ± 2.4	-18.6 ± 1.6	-82.9 ± 2.2	+35.4 ± 2.8
		R	+36.5 ± 4.9	-69.3 ± 3.5	+43.3 ± 4.3	+17.8 ± 1.5	-81.6 ± 2.2	+37.3 ± 2.6
	MOG	L	-38.9 ± 5.3	-65.8 ± 4.2	+42.7 ± 3.8	-39.8 ± 2.8	-75.8 ± 2.8	+27.4 ± 3.2
		R	+37.9 ± 4.9	-66.2 ± 3.7	+40.4 ± 5.6	+39.9 ± 2.6	-74.9 ± 2.5	+24.8 ± 4.3
	IOG	L	-43.3 ± 4.6	-65.6 ± 4.7	+40.1 ± 3.4	-49.7 ± 2.2	-68.1 ± 2.5	-1.1 ± 2.0
		R	+43.0 ± 3.8	-66.2 ± 3.2	+36.2 ± 5.0	+51.3 ± 2.2	-62.0 ± 1.8	0.0 ± 3.0
Short-range Temporal	STG	L	-50.1 ± 2.6	-57.6 ± 2.3	+36.7 ± 3.5	-56.7 ± 2.4	-36.7 ± 4.7	+10.4 ± 3.5
		R	+51.0 ± 2.8	-57.5 ± 3.6	+30.5 ± 4.8	+56.2 ± 3.7	-27.1 ± 4.6	+4.9 ± 2.6
	MTG	L	-50.2 ± 2.2	-58.0 ± 1.8	+36.0 ± 3.3	-58.2 ± 1.1	-49.2 ± 4.0	+0.9 ± 3.5
		R	+50.5 ± 2.2	-58.4 ± 2.8	+33.3 ± 3.9	+58.6 ± 1.2	-47.2 ± 3.3	+0.2 ± 2.9
	ITG	L	-51.6 ± 2.3	-58.4 ± 2.3	+34.2 ± 3.6	-54.6 ± 2.0	-40.6 ± 6.6	-19.9 ± 2.9
		R	+50.0 ± 2.5	-62.0 ± 2.5	+30.9 ± 4.1	+53.2 ± 1.9	-39.1 ± 4.3	-20.6 ± 2.5
Projection fibers	Putamen	L	-45.7 ± 3.4	-59.0 ± 3.0	+44.1 ± 3.6	-29.2 ± 0.2	-19.3 ± 0.8	+0.7 ± 0.9
		R	+44.3 ± 3.9	-60.9 ± 3.9	+43.3 ± 4.5	+31.1 ± 0.4	-15.5 ± 0.8	-1.5 ± 1.3
	Thalamus	L	-46.5 ± 3.2	-58.3 ± 2.9	+43.8 ± 3.9	-18.1 ± 1.2	-28.6 ± 0.9	+5.7 ± 2.1
		R	+43.8 ± 4.6	-60.7 ± 4.2	+43.4 ± 4.3	+19.2 ± 1.2	-28.0 ± 0.6	+4.4 ± 1.8
	Pons	L	-38.4 ± 3.4	-65.8 ± 3.6	+45.3 ± 2.0	-6.1 ± 1.4	-30.7 ± 0.9	-39.1 ± 3.1
		R	+41.0 ± 3.6	-63.9 ± 3.3	+42.4 ± 3.4	+6.5 ± 1.3	-30.7 ± 0.8	-41.1 ± 2.6
	Midbrain	L	-38.3 ± 4.1	-65.5 ± 4	+44.7 ± 2.3	-10.1 ± 0.9	-27.1 ± 0.9	-9.3 ± 0.8
		R	+39.8 ± 4.2	-64.3 ± 4.4	+42.7 ± 4.1	+11.9 ± 1.9	-26.1 ± 2.3	-9.1 ± 2.3
Corpus Callosum			-41.8 ± 4.7	-63.4 ± 4.9	+44.1 ± 2.7	+42.9 ± 4.5	-61.6 ± 5.5	+42.7 ± 3.9

Supplementary Table 1. Mean (± standard deviation) values of shape descriptors for each AG pathway

A. Long-range fronto-dorsal AG connectivity

		Descriptors	Inf. Frontal Gyrus		Mid. Frontal Gyrus		Precentral Gyrus	
			L (404)	R (411)	L (411)	R (411)	L (411)	R (411)
LENGTH	(mm)	Length	110.6 ± 8.3	116.1 ± 7.1	109.6 ± 7.6	114.9 ± 7.4	82.8 ± 3.1	84.6 ± 3.0
		Span	84.1 ± 5.1	87.2 ± 5.5	80.4 ± 8.0	87.9 ± 8.6	57.7 ± 4.5	60.1 ± 3.9
		Diameter	11.5 ± 2.9	14.6 ± 1.7	17.0 ± 2.6	18.8 ± 2.1	16.8 ± 2.2	19.3 ± 1.6
		AG end radius	13.5 ± 2.4	17.0 ± 2.2	13.6 ± 1.7	17.5 ± 2.0	14.1 ± 1.8	17.2 ± 1.8
		Opposite end radius	16.7 ± 3.0	17.9 ± 2.8	28.4 ± 6.6	32.2 ± 5.3	25.6 ± 5.1	23.3 ± 3.6
AREA	(10^2 mm^2)	Whole area	176.4 ± 46.1	208.1 ± 24.1	257.2 ± 41.5	288.6 ± 24.4	197.4 ± 26.2	229.7 ± 21.2
		AG end area	14.0 ± 1.0	37.6 ± 14.9	37.9 ± 1.3	58.2 ± 18.4	34.5 ± 1.2	60.8 ± 14.4
		Other end area	15.1 ± 11	34.4 ± 13.3	59.2 ± 27.2	77 ± 30.5	45.5 ± 18.1	68.5 ± 17.5
		Volume (10^3 mm^3)	12.3 ± 5.6	19.7 ± 4.4	25.5 ± 7.2	32.2 ± 6.9	18.7 ± 4.5	24.8 ± 3.9
SHAPE		Curl	1.3 ± 0.1	1.3 ± 0.0	1.4 ± 0.1	1.3 ± 0.1	1.4 ± 0.1	1.4 ± 0.1
		Elongation	10.5 ± 4.4	8.1 ± 1.4	6.7 ± 2.2	6.2 ± 1.0	5.0 ± 0.8	4.4 ± 0.4
		Irregularity	4.4 ± 0.5	3.9 ± 0.3	4.4 ± 0.3	4.3 ± 0.4	4.5 ± 0.4	4.5 ± 0.3
		AG end irregularity	1.0 ± 2.2	0.3 ± 0.4	0.3 ± 1.7	0.2 ± 0.2	0.2 ± 0.2	0.2 ± 0.1
		Other end irregularity	1.4 ± 2.3	0.4 ± 0.4	0.7 ± 1.5	0.6 ± 0.5	0.6 ± 0.6	0.3 ± 0.1

B. Long-range fronto-ventral AG connectivity

	Descriptors	Inf. Frontal Gyrus		Mid. Frontal Gyrus		Sup. Frontal Gyrus		Fronto-Orbital Gyri		Insula	
		L (40)	R (93)	L (35)	R (93)	L (69)	R (102)	L (79)	R (166)	L (253)	R (246)
LENGTH (mm)	Length	171.7 ± 7.8	164.3 ± 7.7	174.5 ± 7.2	169 ± 6.0	185.5 ± 6.5	182.1 ± 6.6	153 ± 9.7	150.3 ± 7.8	87.1 ± 5.3	81.7 ± 6.1
	Span	103.8 ± 4.2	104.8 ± 4.8	118.4 ± 4.9	121 ± 4.2	128.2 ± 5.3	131.7 ± 4.3	114.9 ± 5.5	114.6 ± 5.3	64.7 ± 3.9	60.6 ± 4.6
	Diameter	3.9 ± 0.9	4.1 ± 1.1	3.8 ± 0.8	4.3 ± 1.1	4.2 ± 1.2	4.3 ± 1.3	3.8 ± 0.8	4.3 ± 1.1	4.7 ± 1.4	4.8 ± 1.6
	AG end radius	11.5 ± 3.1	14.4 ± 3.6	13.1 ± 3.2	14.8 ± 3.5	13.0 ± 3.1	14.0 ± 3.3	12.4 ± 3.0	14.2 ± 3.5	11.9 ± 2.8	15.7 ± 3.5
	Opposite end radius	11.7 ± 2.5	11.7 ± 2.4	15.1 ± 5.9	12.4 ± 4.9	18.9 ± 6.7	16.3 ± 5.0	15.4 ± 3.6	15.5 ± 3.2	6.0 ± 2.3	7.3 ± 3.7
AREA (10^2 mm^2)	Whole area	67 ± 26.2	71.1 ± 28.4	67.9 ± 25.8	78.8 ± 30.9	83.9 ± 38.3	84.9 ± 37.6	56.7 ± 19.4	68.4 ± 26.3	43.7 ± 17.7	44 ± 20.3
	AG end area	0.6 ± 0.0	0.7 ± 0.5	0.6 ± 0.0	0.8 ± 0.6	0.7 ± 0.1	0.8 ± 0.7	0.6 ± 0.0	0.8 ± 0.6	1.2 ± 0.1	1.3 ± 1.4
	Other end area	0.6 ± 0.3	0.7 ± 0.5	0.6 ± 0.4	0.8 ± 0.6	0.8 ± 0.6	0.8 ± 0.7	0.6 ± 0.4	0.8 ± 0.6	0.9 ± 0.6	0.9 ± 0.7
	Volume (10^3 mm^3)	2.1 ± 1	2.3 ± 1.3	2.1 ± 1.1	2.6 ± 1.4	2.7 ± 1.7	2.8 ± 1.8	1.8 ± 0.9	2.3 ± 1.2	1.7 ± 1.0	1.6 ± 1.1
SHAPE	Curl	1.7 ± 0.1	1.6 ± 0.1	1.5 ± 0.1	1.4 ± 0.1	1.4 ± 0.1	1.4 ± 0.1	1.3 ± 0.1	1.3 ± 0.1	1.3 ± 0.1	1.3 ± 0.1
	Elongation	46.5 ± 9.4	42.1 ± 9.3	47.5 ± 8.5	41.6 ± 9.7	47.4 ± 10.7	45.6 ± 11	42.0 ± 7.8	37.2 ± 9.0	19.9 ± 5.7	18.8 ± 5.8
	Irregularity	3.1 ± 0.5	3.2 ± 0.4	3.2 ± 0.4	3.3 ± 0.5	3.3 ± 0.5	3.3 ± 0.5	3.0 ± 0.3	3.3 ± 0.4	3.3 ± 0.4	3.4 ± 0.5
	AG end irregularity	8.9 ± 6.5	13.0 ± 9.8	12.2 ± 8.8	12.5 ± 8.4	11.0 ± 7.9	11.6 ± 8.3	10.8 ± 7.2	11.6 ± 9.3	6.5 ± 5.5	11.9 ± 10.5
	Other end irregularity	9.3 ± 6.0	8.2 ± 5.5	15.8 ± 11.6	9.7 ± 10.5	22.7 ± 19.4	16.7 ± 16.5	16.8 ± 11.6	13.7 ± 9.1	2.1 ± 3.0	3.5 ± 6.1

C. Short-range parietal AG connectivity

	Descriptors	Postcentral Gyrus		Precuneus		Supramarginal Gyrus		Sup. Parietal Gyrus	
		L (179)	R (407)	L (395)	R (367)	L (401)	R (411)	L (411)	R (411)
LENGTH (mm)	Length	73.5 ± 4.0	70.8 ± 3.5	64.4 ± 6.7	63.4 ± 7.0	47.6 ± 5.7	52.0 ± 5.5	56.0 ± 3.7	53.3 ± 4.3
	Span	37.2 ± 4.5	39.4 ± 4.2	31.5 ± 4.0	31.4 ± 4.5	23.3 ± 3.5	25.7 ± 3.4	21.9 ± 2.4	23.3 ± 2.8
	Diameter	6.0 ± 2.1	9.7 ± 2.4	8.0 ± 2.5	6.6 ± 2.3	7.6 ± 2.4	9.4 ± 2.4	13.4 ± 1.8	13.4 ± 2.1
	AG end radius	11.1 ± 2.3	13.6 ± 2.4	11.2 ± 3.1	10.4 ± 3.1	12.6 ± 3.0	15.8 ± 3.7	14.0 ± 2.1	14.2 ± 2.5
	Opposite end radius	13.0 ± 3.7	14.6 ± 4.3	10.4 ± 2.5	11.3 ± 3.8	11.5 ± 2.8	12.9 ± 3.1	14.6 ± 2.4	15.1 ± 2.5
AREA (10^3 mm^2)	Whole area	48.6 ± 21.6	87.7 ± 25.5	64.9 ± 24.2	51.9 ± 24.1	48.5 ± 20	72.6 ± 23	104.3 ± 15.2	104.2 ± 19.0
	AG end area	3.3 ± 0.4	11.6 ± 8.2	4.8 ± 0.4	2.8 ± 2.8	4.8 ± 0.4	9.1 ± 7.0	21.1 ± 0.9	20.5 ± 10.0
	Other end area	3.3 ± 3.8	10.5 ± 7.1	4.8 ± 4.2	3.0 ± 3.1	4.5 ± 4.0	7.4 ± 5.0	22.5 ± 9.7	21.1 ± 10.2
	Volume (10^3 mm^3)	2.4 ± 1.6	5.5 ± 2.4	3.6 ± 2.1	2.5 ± 1.7	2.5 ± 1.5	4.2 ± 2.0	8.2 ± 2.3	7.9 ± 2.6
SHAPE	Curl	2.0 ± 0.2	1.8 ± 0.2	2.1 ± 0.2	2.0 ± 0.2	2.1 ± 0.2	2.0 ± 0.2	2.6 ± 0.3	2.3 ± 0.2
	Elongation	13.7 ± 4.9	8.0 ± 3.0	9.0 ± 3.8	10.9 ± 4.3	7.1 ± 2.6	6.2 ± 2.1	4.3 ± 0.7	4.1 ± 0.9
	Irregularity	3.4 ± 0.5	4.0 ± 0.4	3.9 ± 0.6	3.8 ± 0.6	4.1 ± 0.6	4.5 ± 0.6	4.5 ± 0.4	4.7 ± 0.5
	AG end irregularity	3.3 ± 4.8	1.2 ± 2.1	2.1 ± 3.5	3.1 ± 4.5	3.1 ± 4.3	2.9 ± 4.0	0.5 ± 0.5	0.5 ± 0.7
	Other end irregularity	4.7 ± 6.2	2.0 ± 7.0	1.8 ± 2.6	3.7 ± 5.4	2.7 ± 4.2	2.2 ± 3.2	0.5 ± 0.7	0.6 ± 1.2

D. Short-range occipital AG connectivity

	Descriptors	Sup. Occipital Gyrus		Mid. Occipital Gyrus		Inf. Occipital Gyrus	
		L (79)	R (67)	L (405)	R (405)	L (185)	R (316)
LENGTH (mm)	Length	59.6 ± 7.0	60.7 ± 7.5	45.3 ± 5.8	43.7 ± 5.3	64.2 ± 4.0	59.2 ± 5.5
	Span	24.5 ± 4.7	25.0 ± 5.2	22.9 ± 2.8	23.3 ± 3.4	43.0 ± 3.8	38.5 ± 6.2
	Diameter	4.2 ± 1.3	3.9 ± 0.9	8.7 ± 2.7	8.0 ± 2.3	4.5 ± 1.5	5.4 ± 1.6
	AG end radius	8.5 ± 3.1	6.8 ± 2.0	13.9 ± 3.8	13.5 ± 4.6	10.6 ± 3.8	10.6 ± 3.6
	Opposite end radius	6.9 ± 2.3	8.4 ± 3.3	12.8 ± 3.0	12.7 ± 2.9	5.7 ± 1.8	7.0 ± 1.8
AREA (10^3 mm^2)	Whole area	24.8 ± 12.0	22.0 ± 8.5	59.8 ± 24.8	49.3 ± 20.1	26.7 ± 11.5	30.6 ± 11.9
	AG end area	0.9 ± 0.1	0.6 ± 0.4	5.1 ± 4.2	3.9 ± 3.2	1.3 ± 1.6	2.4 ± 2.3
	Other end area	0.8 ± 0.8	0.7 ± 0.5	5.4 ± 0.5	4.7 ± 4.1	1.1 ± 0.1	1.9 ± 1.7
	Volume (10^3 mm^3)	0.9 ± 0.7	0.8 ± 0.4	3.0 ± 1.8	2.4 ± 1.4	1.1 ± 0.8	1.5 ± 0.9
SHAPE	Curl	2.5 ± 0.4	2.5 ± 0.4	2.0 ± 0.3	1.9 ± 0.2	1.5 ± 0.1	1.6 ± 0.2
	Elongation	15.2 ± 4.2	16.4 ± 4.1	6.0 ± 2.5	6.0 ± 2.1	15.6 ± 4.7	12.4 ± 4.0
	Irregularity	3.0 ± 0.5	2.9 ± 0.4	4.7 ± 0.8	4.4 ± 0.6	2.9 ± 0.4	3.0 ± 0.4
	AG end irregularity	4.8 ± 4.8	3.5 ± 2.8	2.9 ± 3.6	3.3 ± 4.7	6.5 ± 7.6	4.3 ± 5.3
	Other end irregularity	3.2 ± 3.5	5.2 ± 5.8	2.2 ± 2.7	2.4 ± 3.3	1.9 ± 2.1	1.9 ± 1.9

E. Short-range temporal AG connectivity

	Descriptors	Sup. Temporal Gyrus		Mid. Temporal Gyrus		Inf. Temporal Gyrus	
		L (411)	**R (408)**	**L (411)**	**R (411)**	**L (408)**	**R (402)**
LENGTH (mm)	**Length**	54.1 ± 7.9	64.2 ± 7.8	62.7 ± 4.5	60.6 ± 4.6	82.3 ± 6.1	81.2 ± 6.3
	Span	36.0 ± 5.9	42.2 ± 6.8	38.4 ± 5.1	37.5 ± 4.5	58.7 ± 5.6	58.2 ± 5.5
	Diameter	8.6 ± 2.0	7.8 ± 2.0	12.9 ± 1.7	14.0 ± 1.6	6.6 ± 1.7	6.2 ± 1.5
	AG end radius	14.9 ± 3.8	12.7 ± 3.3	12.5 ± 2.0	14.8 ± 2.0	9.9 ± 2.2	12.0 ± 2.5
	Opposite end radius	12.1 ± 3.7	14.2 ± 2.9	16.3 ± 2.9	15.6 ± 2.6	14.9 ± 3.9	12.9 ± 3.1
AREA (10^3 mm^2)	**Whole area**	71.3 ± 21.9	72.2 ± 23.4	113.2 ± 17.7	124.1 ± 16.8	67.0 ± 19.7	64 ± 18.4
	AG end area	7.1 ± 0.5	8.1 ± 5.9	17.2 ± 6.4	23.9 ± 8.3	4.6 ± 3.9	4.5 ± 4.0
	Other end area	6.4 ± 4.2	8.9 ± 6.6	18.6 ± 0.7	21.6 ± 7.0	4.3 ± 0.4	3.9 ± 3.2
	Volume (10^3 mm^3)	3.8 ± 1.7	4.2 ± 2.0	8.7 ± 2.3	9.8 ± 2.2	3.8 ± 1.9	3.5 ± 1.7
SHAPE	**Curl**	1.6 ± 0.1	1.6 ± 0.2	1.7 ± 0.2	1.7 ± 0.2	1.4 ± 0.1	1.4 ± 0.1
	Elongation	7.1 ± 2.3	9.8 ± 3.2	5.0 ± 0.9	4.5 ± 0.7	15.4 ± 4.4	16.1 ± 4.1
	Irregularity	4.3 ± 0.6	3.9 ± 0.5	4.4 ± 0.3	4.6 ± 0.4	3.4 ± 0.4	3.3 ± 0.3
	AG end irregularity	2.1 ± 2.5	3.0 ± 3.7	0.4 ± 0.3	0.4 ± 0.3	2.5 ± 2.8	4.6 ± 4.4
	Other end irregularity	1.8 ± 2.4	3.3 ± 4.0	0.6 ± 0.6	0.4 ± 0.3	4.6 ± 7.2	3.3 ± 4.2

F. Cortico-striatal, cortico-thalamic and commissural pathways

	Descriptors	Putamen		Thalamus		Pons		Midbrain		Corpus Callosum
		L (302)	R (185)	L (287)	R (297)	L (399)	R (406)	L (390)	R (381)	(326)
LENGTH	Length	69.9 ± 2.8	74.2 ± 2.6	64.9 ± 3.4	67.3 ± 3.2	129.5 ± 8.8	131.5 ± 8.5	90.4 ± 2.1	89.0 ± 2.3	134.4 ± 3.9
	Span	61.8 ± 3.0	66.0 ± 3.3	57.0 ± 2.7	57.8 ± 2.8	97.8 ± 3.1	97.2 ± 2.8	73.1 ± 1.5	71.6 ± 1.9	85.8 ± 8.0
	Diameter	6.0 ± 2.0	4.6 ± 1.4	6.3 ± 2.1	5.9 ± 2.0	7.8 ± 2.2	8.9 ± 2.4	7.6 ± 2.3	7.0 ± 2.1	7.2 ± 2.6
	AG end radius	12.0 ± 2.4	13.2 ± 3.0	11.8 ± 2.4	13.3 ± 3.3	13.9 ± 2.8	15.9 ± 3.2	13.5 ± 3.2	14.5 ± 3.7	14.4 ± 3.4
	Opposite end radius	3.7 ± 0.7	4.0 ± 1.1	6.9 ± 1.4	6.0 ± 1.4	15.3 ± 3.1	13.3 ± 3.4	6.2 ± 1.7	6.2 ± 1.6	14.6 ± 3.7
AREA	Whole area	41.2 ± 16.4	33.5 ± 14.2	43.2 ± 17.5	42.8 ± 19.1	140.4 ± 50.6	163.7 ± 52	81.5 ± 28.9	76.1 ± 28.2	116.2 ± 50.6
	AG end area	3.9 ± 0.5	1.2 ± 1.3	3.9 ± 0.4	3.0 ± 3.5	4.0 ± 3.3	6.0 ± 5.0	4.8 ± 4.2	3.7 ± 3.7	4.7 ± 0.5
	Opposite end area	1.2 ± 0.7	0.7 ± 0.5	2.7 ± 2.2	2.0 ± 1.7	1.9 ± 0.1	2.5 ± 1.2	2.2 ± 0.1	1.8 ± 1.0	4.9 ± 5.6
	Volume (10^3 mm^3)	2.2 ± 1.4	1.3 ± 0.9	2.3 ± 1.5	2.1 ± 1.4	6.6 ± 3.6	8.7 ± 4.4	4.4 ± 2.4	3.8 ± 2.2	6.2 ± 4.3
SHAPE	Curl	1.1 ± 0.0	1.1 ± 0.0	1.1 ± 0.0	1.2 ± 0.0	1.3 ± 0.1	1.4 ± 0.1	1.2 ± 0.0	1.2 ± 0.0	1.6 ± 0.1
	Elongation	13.0 ± 4.7	17.6 ± 4.7	11.6 ± 4.5	12.9 ± 4.7	18.6 ± 7.2	16.2 ± 5.8	13.4 ± 5.1	13.9 ± 4.7	21.7 ± 9.3
	Irregularity	3.0 ± 0.4	3.0 ± 0.4	3.3 ± 0.4	3.3 ± 0.5	4.4 ± 0.6	4.4 ± 0.5	3.7 ± 0.5	3.8 ± 0.5	3.7 ± 0.5
	AG end irregularity	3.3 ± 3.8	8.3 ± 6.8	3.3 ± 4.2	5.1 ± 6.4	3.2 ± 3.5	3.0 ± 4.8	3.1 ± 4.2	4.2 ± 5.4	4.7 ± 6.7
	Opposite end irregularity	0.5 ± 0.4	1.0 ± 1.0	1.3 ± 1.7	1.2 ± 1.5	5.4 ± 4.5	3.0 ± 3.0	0.9 ± 1.2	1.0 ± 1.2	4.9 ± 7.7